The solid molecular hydrogens in the condensed phase: Fundamentals and static properties

Isaac F. Silvera

Natuurkundig Laboratorium, Universiteit van Amsterdam, Valckenierstraat 65, 1018 XE Amsterdam, The Netherlands

The molecular hydrogens (H_2, D_2, HD, etc.) form the simplest of all molecular solids. The combination of the light mass, small moment of inertia, weak interactions, and the quasi-metastable ortho-para species result in a fascinating low-temperature behavior that can be understood to a large extent from considerations of first principles. After discussing single molecule properties and intermolecular interactions we discuss in detail the ortho–para properties, conversion and diffusion. This is followed by a description of the crystal structures and the orientational ordering phenomena. The thermodynamic properties are reviewed. The article is concluded with a discussion of the translational ground state of the solid and the effect of the large zero-point motion on the solid state properties. A large number of data are collected in tables and graphs to provide a reference source.

CONTENTS

GLOSSARY OF SYMBOLS

Most symbols used are listed here with an indication of the approximate location in the text (indicated by equation number) where more complete definitions are usually given.

AAA	Alcoa activated alumina	(5.7)
$B(R)$	Anisotropic potential parameter	(3.14)
B, B_v	Rotational constant	(2.16)
B_m	Bulk modulus	(7.2)
BD	Body diagonal	Table VI
$C(l_1 l_2 j;\ n, -n)$	Clebsch-Gordan coefficient	(3.14)
c_1	Molar concentration of $J=1$ molecules	
c_e	Molar concentration of even rotational states	(5.2)
cg	Correlated Gaussian	(8.4), (8.7)
c_k	Parameters in inverse power series expansion of intermolecular potential	(3.6)
c_0	Molar concentration of odd rotational states	(5.2)
C_{VL}	Lattice specific heat	(7.1)
C_{VQ}	Quadrupolar specific heat	(7.7)
D	Diffusion constant	(5.17)
D	Dissociation energy	After (2.12), Table I
D_2	Molecular deuterium	
$D^{(2)}_{mn}$	Rotation matrix	(2.23)
D_v	Rotational energy distortion constant	(2.16a)
E_{HL}	Heitler-London energy	(3.3)
E_J	Rotational energy	(5.1)
E^0_n	Electronic energy	(2.6)
EQ	Electric quadrupole	(2.17)
EQQ	Electric quadrupole-quadrupole	
EOS	Equation of state	
F	Free energy	(7.1)
$F(R)$	Potential cutoff function	(3.9)
$f(R)$	Potential cutoff function	(3.12)
$F_v(J)$	Rotational energy of diatomic molecule	(2.16a)

fcc	Face centered cubic	
$g(r)$	Pair distribution function	(8.9), (8.11)
g_I	Nuclear spin degeneracy	(5.1)
$\mathcal{H}$	Hamiltonian operator	(2.1)
H	Hydrogen	
H_v	Rotational energy distortion constant	(2.16a)
HD	Hydrogen deuteride molecule	
hcp	Hexagonal close packed	
I	Moment of inertia	
I	Light intensity	
i_6	Nuclear spin	(5.14)
in–out	Neighboring molecules in and out of basal plane of a hcp lattice	
$\underline{J}$	Molecular rotational angular momentum operator	(2.16b)
$J(R)$	Exchange energy	(2.13)
K	Thermal conductivity	
K, K', K_1	Rate constants	(5.2), (5.10), (5.12)
k_B	Boltzmann constant	
M	Molecular mass	
m	Electronic mass	
m, M	Angular momentum projection quantum numbers	
P	Pressure	
P_L	Lattice pressure	(7.4)
P_Q	Quadrupolar pressure	(7.4)
P^*	Thermal pressure	(7.5)
$Q(R)$	Molecular electric quadrupole moment	(2.17)
Q	Matrix element of $Q(R)$	(2.20)
$\overline{Q}$	Matrix element of $Q(R)$	(2.20)
$Q^{(2)}_{vJ,v'J'}$	Radial matrix element of $Q(R)$	(2.10)
$Q^{20}_{vJM,vJ'M'}$	Rotational matrix element of $Q(R)$	(2.20)
R	Interatomic or intermolecular separation	(2.13), (3.5)
R_0	Rigid lattice nearest neighbor separation	(3.18)
$R_m, R_{\min}$	Position of well minimum in interatomic or intermolecular potential	(3.6), (3.8), (3.12)
RL	Rigid lattice	
S	Separation coefficient	(5.7)
s	Singlet	(2.13)
$S(i \rightarrow f)$	Raman scattering efficiency	(5.3)
scp	Self-consistent phonon approximation	(8.6)
srcg	Short-range-correlated Gaussian	(8.10)
t	Triplet	(2.13)
T_2	Molecular tritium	
T_c	Critical temperature	
T_{hc}	Critical temperature for hcp → fcc transition	
U_i	Molecular field	(6.3), (8.3)
U_n	Effective potential for nuclear motion	(2.10)
u_s	Displacement from equilibrium	(5.15)
V	Volume	
V_0	Zero-pressure molar volume	
V_c	Crystal field parameter	(3.22d)
V_{cp}	Crystal field of a pair of molecules	(3.23)
$V_{\Delta B}$	Crystal field parameter	(3.22)
W	Thermal resistance	(7.13)
$w_h^{\alpha\beta}$	Harmonic force constants	(8.3)
$Y_L^M(\theta, \phi)$	Spherical harmonic	(2.19), (3.13)
$\alpha(R)$	Isotropic polarizability	(2.21)
$\boldsymbol{\alpha}_{\text{crystal}}$	Polarizability tensor of a crystal	(4.7)
α_j	Anisotropic potential coefficient	(3.14)
$\alpha_\parallel$	Polarizability parallel to internuclear axis	(2.21)
$\alpha_\perp$	Polarizability perpendicular to internuclear axis	(2.21)
$\alpha_{vJ,v'J'}$	Matrix element of polarizability	(2.22)
α_1^{2m}	Polarizability in the laboratory frame	(2.23), (2.25)
α_b^{2m}	Polarizability in the body fixed frame	(2.23)
α_{xy}	Cartesian components of polarizability	(2.24)
$\overline{\alpha}$	Matrix element of polarizability	(2.25)
$\Gamma(R)$	EQQ coupling constant	(3.17)
Γ_0	Rigid lattice value of $\Gamma(R)$	
$\overline{\Gamma}$	Experimental value of $\Gamma(R)$	
$\gamma(R)$	Anisotropy in polarizability	(2.21)
γ_α	Grüneisen constant	(7.6)
Δ_i	Energy splitting of rotational states	(5.8)
ε	Depth of potential well	(3.7), (3.8)
$\varepsilon_i(R)$	Anisotropic potential parameters	(3.14)
ε_μ^i	Molecular field energy levels	(6.4)
$\varepsilon_{l_1 l_2}$	Anisotropic potential parameter	(3.13)
ε_i^v	Valence interaction parameter	(3.20)
$\varepsilon_i^{\text{di}}$	Dispersion interaction parameter	
θ_D	Debye temperature	(7.7)
κ	Matrix element of normalized anisotropy in polarizability	(2.25)
λ	de Boer quantum parameter	(8.2)
μ_p	Nuclear magnetic moment	(5.14)
$\nu(v)$	Vibrational transition frequency	Table IX
ξ	Solid effective EQQ reduction factor	(3.18)
ξ_{54}	EQQ reduction factor	(3.19), (8.13)
ξ_{mn}	Generalized reduction factor	(8.14)
ρ	Density	
ρ_0	Equilibrium concentration of odd rotational states	(5.1)
ρ_e	Equilibrium concentration of even rotational states	(5.1)
ρ_{eq}	Equilibrium rotational concentration	(5.2)
$^1\Sigma_g^+$	H_2 ground state	(2.11)
$^3\Sigma_u^+$	Excited electronic state	(2.11)
σ	Lennard-Jones potential parameter	(3.7)
$\sigma(T)$	Orientational order parameter	(6.8)
τ	Time between diffusional jumps	(5.16)
$\phi(R)$	H–H binding energy	(2.13)
$\phi_A(R_{ij}, \Omega_i, \Omega_j)$	Anisotropic intermolecular potential	(3.1)
ϕ_c	Crystal field	(3.22)
ϕ_{EQQ}	EQQ interaction	(3.15)
$\phi_I(R_{ij})$	Isotropic intermolecular potential	(3.1)
χ_n	Nuclear wave function	(2.5)
ψ_{HL}	Heitler–London wave function	(3.2)

ψ_n	Electronic wave function	(2.5)
Ω_i	Set of spherical polar angles θ_i, ϕ_i	Fig. 5
ω	Angular frequency of light	(5.3)
ω_D	Debye frequency	
ω_i	Set of spherical polar angles θ_i, ϕ_i	Fig. 5

I. INTRODUCTION

The hydrogen atom (H) is the simplest atomic species that exists. As such, it has been extensively studied and its electronic excitation spectra were fundamental to the establishment of quantum mechanics in the early part of the twentieth century. Atomic hydrogen, however, is unstable under normal conditions on earth, forming molecular hydrogen (H_2), the simplest of all molecular species. The instability of H has retarded studies of its behavior in a condensed state.

Note added in proof: A gas of atomic hydrogen has recently been stabilized, Silvera, I. F. and J. T. M. Walraven 1980, Phys. Rev. Lett. 44, 164. Thus, until recently, almost all experimental studies on pure condensed hydrogen and its isotopes have been on the molecular species. It is a rather remarkable situation in physics that such a fascinating and fundamental system as condensed H_2 resisted intensive theoretical and experimental studies until about the early 1960s. By contrast, the properties of condensed helium have undergone such a study since the 1930s, although even in this case thirty years passed between its liquefaction and the discovery of superfluidity.

In the solid state, molecular hydrogen has a number of features which distinguish it from other (molecular) solids. Most important and simplifying is that, even in the solid, the free rotor states that describe the rotational motions of an isolated molecule are almost undistorted by the interactions with neighbors. Thus the solid can be visualized as an assembly of molecules all translationally localized at lattice sites but freely rotating even at $T = 0$ K! This remarkable state is a consequence of the large molecular rotational constant (small moment of inertia) and the weak anisotropic forces which are a result of the almost spherical molecular charge distribution and the relatively large intermolecular nearest neighbor distances (~3.79 Å) in the zero-pressure solid. To demonstrate this we show the radial distribution of the electronic charge density of the hydrogen molecule in the ground electronic state. In Fig. 1(a) we plot[1] the contours of equal charge density. The proton–proton separation is 0.74 Å. At the distance corresponding to nearest neighbor separation in the solid, the charge density is $\sim 3 \times 10^{-4}$ that at the nuclei, while the ratio of the minor to the major axis of the distribution is ~0.94. Thus for low densities, the molecule must be visualized as being almost spherical rather than dumbbell shaped. The plots in Fig. 1 use a density function of Stewart *et al.* (1965) based on a wave function of Kolos and Roothan (1960).

Due to requirements on the symmetry of the wave

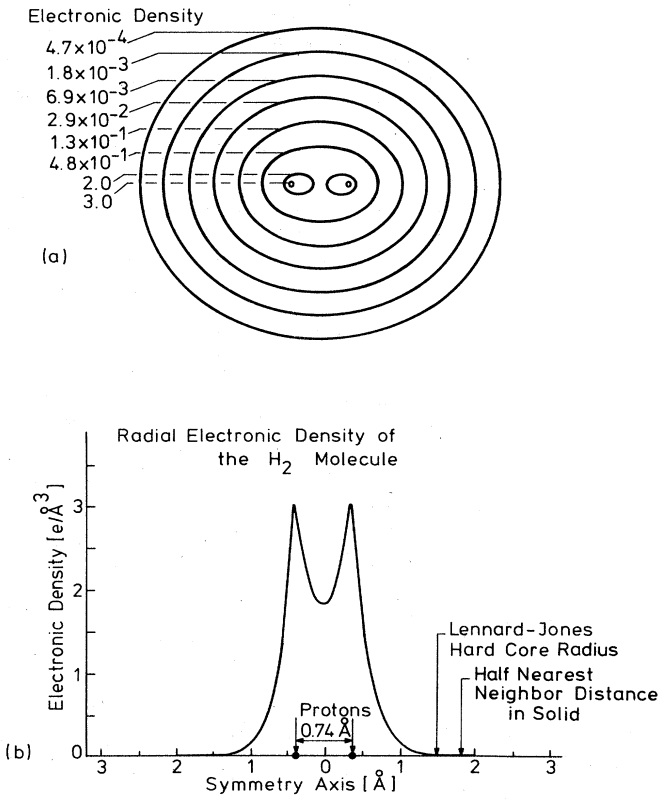

FIG. 1. The electronic charge density of the hydrogen molecule. (a) Contours of equal density. (b) Density along the symmetry axis.

function, molecular hydrogen has two species: para and ortho. The former is characterized by an even rotational quantum number, the latter by odd. Transitions between these states are forbidden and as a result samples of almost pure para or ortho species can be prepared. The ground-state para species are spherical whereas the ortho are anisotropic in charge distribution. By varying the concentration of these species one can easily "turn the anisotropic interactions on and off." The same properties apply to the isotope deuterium. These molecules interact almost identically to H_2 but have a mass greater by a factor of 2. This provides experimentalists with an enormous isotope effect, which is extremely useful in sorting out observations.

Another distinction, which hydrogen shares with helium, is that it is a translational quantum solid. In such solids, at $T = 0$, the particles are not sharply localized at lattice sites due to the large zero point motion (ZPM); in H_2 the rms width of the single particle distribution function is ~18% of the nearest neighbor distance. This large ZPM is a result of the weak isotropic intermolecular potential and the light mass. Due to the large ZPM and the accompanying large anharmonicities the usual quasiharmonic theory of lattice dynamics is not applicable. Instead one must use the "theory of quantum solids" in which interactions are renormalized by performing certain averages over the molecular motions. So treated, one recovers the usual phonon dispersion relations of solids; however, the phonon spec-

[1] I thank E. Hartman for programming the density function.

tral functions are no longer sharp, as for a harmonic solid, but rather spread out in frequency.

At zero pressure hydrogen is highly compressible: a pressure of ~10 kbar results in a 100% reduction in volume, whereas with a nonquantum solid volume changes of but a few percent would be obtained. This large compressibility is a characteristic of quantum solids. The lattice is expanded so that the particles do not sit in the minimum of the attractive potential wells of their neighbor. Without this expansion the ground state energy would be raised substantially since the large ZPM results in an overlap of the molecular hard cores. This large compressibility makes studies of the radial dependence of interactions easily accessible by performing measurements as a function of pressure.

Indeed, the equation of state (EOS) of hydrogen is of interest, not only because it provides the density as a function of pressure, but because it is also an excellent testing ground for the isotropic intermolecular potential. The EOS of hydrogen is known to ~25 kbar: One of the more exciting ideas concerning H_2 is the prediction that at sufficiently high pressures it will exhibit an insulator–metal transition. Moreover, it has been speculated that the atomic metallic phase will be a high-temperature superconductor. The pressure at which the transition takes place is expected to be in the $(1-5)\times 10^6$ bar region; however, a sharper prediction requires a better knowledge of the high-pressure EOS.

Central to all of the condensed phase properties is the intermolecular interaction. In spite of the fact that the theory of quantum mechanics has been in existence for over 50 years, it is only very recently that reasonably accurate calculations of the potential over a broad range of molecular separations have been performed. The solid has provided an almost ideal experimental testing ground for both the isotropic and anisotropic interactions.

At low temperatures hydrogen has a disorder–order phase transition in which the molecules align along certain crystalline directions. This orientationally ordered state has been the area of intense study for the past decade in an attempt to understand the ground state and its low-lying excitations. This state has been studied by an assortment of techniques: x-ray and neutron diffraction, NMR, Raman and infrared absorption, etc. Currently it is considered to be reasonably well understood, both experimentally and theoretically.

A more recent area of interest takes us back to the beginning of this introduction: atomic hydrogen. Neutral H is a composite boson with a total spin of 1 or 0. Attempts to stabilize H are currently being carried out with the hope of observing Bose–Einstein condensation and superfluidity in this magnetic gas.

This article is not the first to review hydrogen in the condensed phase. An earlier review of the thermal properties was given by Woolley, Scott, and Brickwedde (1948); Van Kranendonk and Karl reviewed the rotational and vibrational properties of solid parahydrogen (1968); most recently Souers (1979) has reviewed cryogenic data of hydrogen. A general review of the excitations in solid molecular hydrogen was given by Silvera (1975); to a certain extent this article can be considered to be a more detailed expansion and extension of the latter.

Originally, it was my intention to review all of the important properties of both molecular and atomic hydrogen in one article. A combination of the size and scope of this project and the many recent developments has resulted in a change in this plan. In this first article I consider the single molecule properties, intermolecular interactions, the rotational state in the solid, ortho–para preparation and related phenomena, the various structural and orientational states of the solid, thermodynamic properties, and the translational ground state of the solid. In a second article, the excitations of the molecular solids will be discussed. The third article will be devoted to atomic hydrogen in the condensed state.

II. ATOM-ATOM POTENTIALS AND SINGLE MOLECULE PROPERTIES

In this section we begin by considering the interactions between two neutral hydrogen atoms. The bound states are the excited states of the hydrogen molecule. The properties of the ground state and the low-lying excited states of the H_2 molecule are of importance because they are almost unchanged in the condensed state.

A. H-H interactions

Perhaps the most extensive and accurate first-principles calculations carried out on a molecular system are those of Kolos and Wolniewicz (KW) on H_2 and its isotopes in a series of papers starting in 1964. One begins by writing the exact nonrelativistic Hamiltonian of the two electrons denoted $\boldsymbol{r}_1$ and $\boldsymbol{r}_2$ and the two nucleii, R_1 and R_2, in which the center of mass of the system is at rest

$$\mathcal{H}\psi = (\mathcal{H}_0 + \mathcal{H}_1 + \mathcal{H}_2)\psi = E\psi \tag{2.1}$$

with

$$\mathcal{H}_0 = -\hbar^2/2m\,(\nabla_1^2 + \nabla_2^2) + V, \tag{2.2}$$

$$\mathcal{H}_1 = -\hbar^2/2\mu\,\nabla_R^2, \tag{2.3}$$

$$\mathcal{H}_2 = -\hbar^2/8\mu\,(\nabla_1^2 + \nabla_2^2 + 2\nabla_1\nabla_2). \tag{2.4}$$

Here m is the electron mass, $\mu = M/2$ the reduced nuclear mass, R the internuclear separation, and V the Coulomb potential between all four particles. $\mathcal{H}_0$ is the Hamiltonian in the clamped nucleii approximation. $\mathcal{H}_1$ describes the relative kinetic energy of the nucleii, and $\mathcal{H}_2$ the motion of the center of mass in the coordinate system fixed to the nucleii; this term couples the electronic and nuclear motions. The procedure is then to write

$$\psi(\boldsymbol{r}, R) = \sum_n \chi_n(R)\,\Psi_n(\boldsymbol{r}, R) \tag{2.5}$$

where $\Psi_n(\boldsymbol{r}, R)$ are the solutions of the electronic problem:

$$\mathcal{H}_0\Psi_n(\boldsymbol{r}, R) = E_n^0(R)\,\Psi_n(\boldsymbol{r}, R), \tag{2.6}$$

and $\boldsymbol{r}$ represents the electronic coordinates. Assuming Eq. (2.6) to be solved, one gets the equation for $\chi_n(R)$:

TABLE I. Properties of $^1\Sigma_g^+$ ground state. Values for HT and DT are also given in Kolos and Wolniewicz (1968). ϕ is the binding energy and D the dissociation energy.

	Units	H_2	HD	D_2	T_2	Ref.
$\phi(R_{min})$-theor.	cm^{-1}	−38 297.1	−38 295.5	−38 294.7		Kolos and Wolniewicz (1964a, b)
$\phi(R_{min})$-expt.	cm^{-1}	−38 292.9 ± 0.5	−38 290.9 ± 1.5	−38 291.4 ± 0.7		Herzberg and Monfils (1960)
R_{min} (theor)	Å	0.741 4	0.7414	0.7414		
R_{min} (expt.)	Å	0.741 16				Herzberg and Howe (1959)
D(theor)	cm^{-1}	−36 118.09	−36 405.92	−36 748.69	−37 028.89	Kolos and Wolniewicz (1968), Poll and Karl (1966)
D(expt.)		−36 113.6 ± 0.3		−36 744.2 ± 0.5		Herzberg and Monfils (1960)

$$[-(1/2\mu)\nabla_R^2 + E_n^0(R) + (\mathcal{H}_1 + \mathcal{H}_2)_{nn} - E]\chi_n(R) = \sum_{m \neq n} (\mathcal{H}_1 + \mathcal{H}_2)_{mn}\chi_m(R)\,, \quad (2.7)$$

where

$$(\mathcal{H}_1 + \mathcal{H}_2)_{mn} = \int \psi_m^*(r, R)(\mathcal{H}_1 + \mathcal{H}_2)\psi_n(r, R)\,dr\,. \quad (2.8)$$

The adiabatic approximation corresponds to setting Eq. (2.8) to zero for $m \neq n$, which reduces Eq. (2.7) to a Schrödinger equation for the nuclear motion and total energy:

$$[-(1/2\mu)\nabla_R^2 + U_n(R) - E]\chi_n(R) = 0 \quad (2.9)$$

with

$$U_n(R) = E_n^0(R) + (\mathcal{H}_1 + \mathcal{H}_2)_{nn}\,. \quad (2.10)$$

$U_n(R)$ is the effective potential for the nuclear motion in the nth electronic state. The nuclear wave function $\chi_n(R)$ is composed of a product of oscillator functions that describe the vibrational motions and spherical harmonics, Y_{JM}, that describe the rotational motions.

Kolos and Wolniewicz (1964a, b) used a James–Coolidge type of wave function of the form

$$\psi_{rs\bar{r}\bar{s}} = \frac{1}{2\pi}\exp[-\alpha(\epsilon_1 + \epsilon_2)]\zeta_1^r \eta_1^s \zeta_2^{\bar{r}} \eta_2^{\bar{s}} \rho^t \quad (2.11)$$

where ζ and η denote elliptic coordinates, and $\rho = 2r_{12}/R$, where r_{12} is the interelectronic distance. They used 54-, 67-, and 80-term wave functions to solve the clamped nucleii problem, Eq. (2.6), finding adequate results for the 54-term expansion. Diagonal corrections for the nuclear motion, as well as relativistic corrections, were calculated for $R = 0.2$ Å to 1.96 Å (1 a.u. = 0.529 177 Å) for the $^1\Sigma_g^+$ ground state. Later they (KW, 1968) used a 100-term wave function and double precision computer calculations to get a slight increase in accuracy. The binding energy $\phi(R)$ (the reduction in energy with respect to neutral atoms at $R = \infty$) is given in Table I for the minimum of ϕ at $R = R_{min}$, as well as the experimental values (Herzberg, 1960) for H_2, HD, and D_2. At R_{min} for H_2, the contribution due to the diagonal nuclear correction and the relativistic corrections are 4.9 cm^{-1} and −0.5 cm^{-1}, respectively. They then calculated (KW, 1964a, b) the ground vibrational state using the variational method on a 154-term wave function of the form

$$\psi = \sum c_{mn}\psi_m\chi_n \quad (2.12)$$

in which they used the 54-term electronic wave function ψ_m and functions built up of Hermite polynomials for the χ_n. The dissociation energies, D, are also given in Table I. Poll and Karl (1966) also calculated D, using the effective potentials of KW and obtained values differing by a few cm^{-1}. Kolos and Wolniewicz (1968) improved their accuracy in a later publication; these are the values given in Table I. Nonadiabatic corrections [off-diagonal terms in Eq. (2.2)] have been shown to be quite small (Poll and Karl, 1966; Orlikowski and Wolniewicz, 1974). A discrepancy between theory and experiment of a few cm^{-1} out of ~36 000 still remains an unresolved problem.

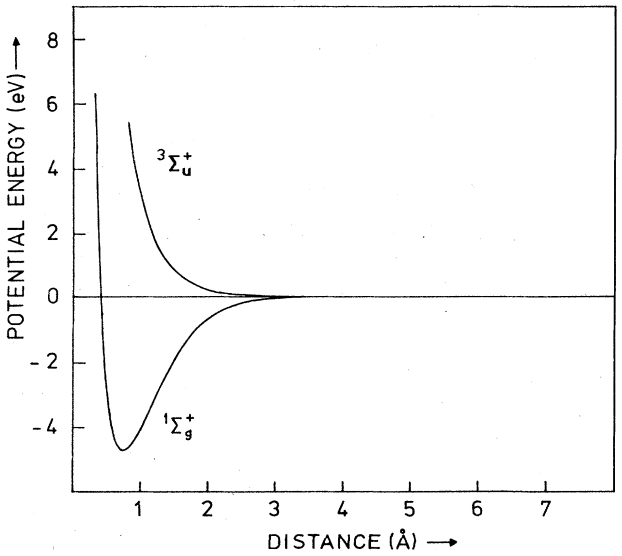

FIG. 2. The interaction potentials of two neutral hydrogen atoms with electron spins in a singlet state ($^1\Sigma_g^+$) and a triplet state ($^3\Sigma_u^+$).

Later, KW calculated properties of H_2 for R out to ~5 Å. These calculations were performed for the $^1\Sigma_g$, $^3\Sigma_u^+$, and $^1\pi_u$ states (KW, 1965, 1974) and for the $^1\Sigma_u^+$ state (Kolos and Wolniewicz, 1966a). The atomic dissociation energies for the most important of these, the ground state $^1\Sigma_g^+$ and the first excited state $^3\Sigma_u^+$, are plotted in Fig. 2. In Fig. 3 we plot the long-range part on an expanded scale to show the van der Waals well of $^3\Sigma_u$; a comparison is made to the He–He potential. These two potentials for atomic hydrogen provide two extremes for atomic interactions. The ground $^1\Sigma_g^+$ state with antiparallel electronic spins has a tightly

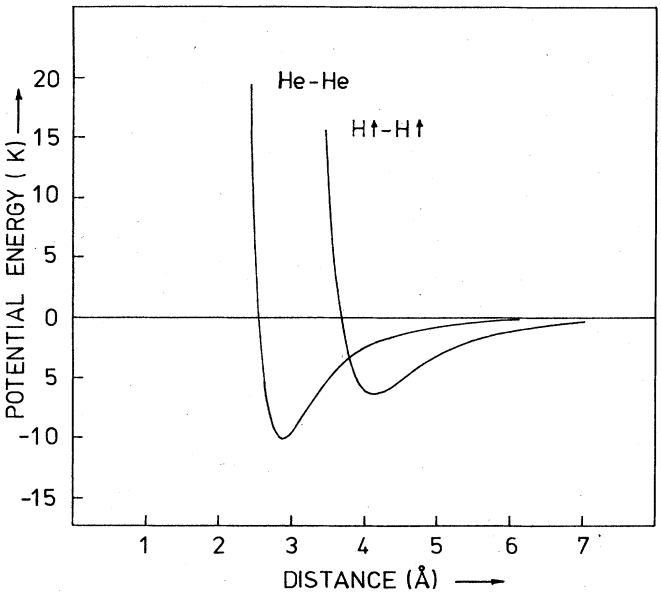

FIG. 3. The weak triplet interaction between two hydrogen atoms on an expanded scale. The He–He interaction is also shown for comparison.

bound molecular ground state with equilibrium atomic separation of 0.74 Å. By contrast, the essentially repulsive spin-aligned state, $^3\Sigma_u^+$, has a well minimum at ~4.15 Å with a well depth of only 4.49 cm^{-1}. Due to the light mass and large zero-point energy there are no bound molecular states for hydrogen in the $^3\Sigma_u^+$ state.

The spin-dependent H–H potentials can be written as

$$\phi(R) = \tfrac{1}{4}[\phi_s(R) + 3\phi_t(R)] + J(R)\mathbf{s}_1 \cdot \mathbf{s}_2 , \tag{2.13}$$

where ϕ_t and ϕ_s are the singlet and triplet potentials, the exchange J is $\phi_t - \phi_s$, and $\mathbf{s}_1$ and $\mathbf{s}_2$ are the electronic spins ($\mathbf{s}_i = \frac{1}{2}$) on the two atoms. We have fit the KW triplet potential to a rather accurate analytical form, useful for calculations:

$$\phi_t(R) = \exp(0.096\,78 - 1.101\,73R - 0.039\,45R^2) + \exp\left[-\left(\frac{10.04}{R} - 1\right)^2\right]\left\{-\frac{6.5}{R^6} - \frac{124}{R^8} - \frac{3285}{R^{10}}\right\} \tag{2.14}$$

with ϕ and R in atomic units (1 hartree = 219,474.6 cm^{-1}, 1 a.u. = 0.529 177 Å). The fit is based on approximating the potential by an exponential repulsive part (first term) plus a long-range attractive part (second term) which is exponentially attenuated at short range as proposed by Ahlrichs *et al.* (1976). The constants for the long-range potential are taken from Deal (1972). Such a fit has the proper long-range asymptotic behavior as well as at intermediate ranges. The exchange can be fit from ~1 to 12 a.u. by

$$J(R) = \exp(-0.288 - 0.275R - 0.176R^2 + 0.0068R^3) \tag{2.15}$$

also with J and R in atomic units. To provide a point at $R = 0$ we have appended to the KW results the singlet–triplet energy of the helium atom which is the equivalent of two H atoms with $R = 0$.

Equations (2.14) and (2.15) are useful analytic forms for calculating properties in the triplet state as the fit has focused upon the long-range values ($R \gtrsim 1.5$ Å). Although combining these equations provides $\phi_s(R)$, the fits are not adequate to represent the potential in the well region of 0.75 Å. This problem arises because values of the $^3\Sigma_u$ potential were only calculated by KW to 1 a.u. and the exchange had to be interpolated in the manner discussed in the previous paragraph. For precision calculations, in particular for the ground-state $^1\Sigma_g^+$ potential, it is recommended that the numerical results of KW be used, with interpolation for intermediate points.

B. Single molecule properties

The success of the KW $^1\Sigma_g^+$ potential for the H_2 molecule is manifested by the accurate comparison to a number of experimentally accessible quantities. Kolos and Wolniewicz (1964b) calculated the first excited vibronic state and later (KW, 1966) the vibrational and rotational excited states for H_2, HD, and D_2. They had numerical convergence problems for the highest excited states. Poll and Karl (1966) also calculated the vibrational states for H_2, D_2, and T_2 using the KW potential; however, they did not encounter convergence problems. They found agreement with experimental

TABLE II. Vibrational quanta of some hydrogen isotopes: $\nu(v) = E_0(v+1) - E_0(v)$ in units of cm^{-1}, after Kolos and Wolniewicz (1968).

	H_2	HD	D_2	T_2
v	$\nu(v)$	$\nu(v)$	$\nu(v)$	$\nu(v)$
0	4162.06	3632.84	2993.96	2743.63
1	3926.65	3455.33	2874.82	2644.02
2	3696.14	3281.33	2757.79	2546.09
3	3468.68	3109.80	2642.40	2449.48

values to about one part in 4000 for the 15 vibrational levels of H_2. Kolos and Wolniewicz (1968) overcame their convergence problem and determined vibrational and rotational energies for H_2 and all of the isotopic combinations. They found the highest bound vibrational levels to be $v = 14$, 21, 25, 17, 18, and 23 for H_2, D_2, T_2, HD, HT, and DT, respectively (v is the vibrational quantum number). The 14th vibrational level of H_2 has four bound rotational states. A sampling of results is given in Tables II and III. Most values agree with experiment to better than 1 cm^{-1} for the vibrational quanta and 0.1 cm^{-1} for rotational quanta. Waech and Bernstein (1967) have calculated the spectrum of all bound and quasibound states for H_2 using the KW potential and LeRoy (1971) has done this for H_2, HD, and D_2.

The rotational energies of a diatomic molecule are given by

$$F_v(J) = B_v J(J+1) - D_v J^2(J+1)^2 + H_v J^3(J+1)^3 , \qquad (2.16a)$$

where $B_v = \hbar^2/2\mu c R_v^2$ is the rotational constant in cm^{-1} and μ is the reduced mass. Experimental values of the constants are given in Table IV for the $v = 0$ ground vibrational state. In the solid, only the lowest rotational states usually come into consideration, and the rotational kinetic energy operator for the ith molecule is often approximated by

$$\mathcal{H}_i = B\mathbf{J}_i^2 . \qquad (2.16b)$$

Due to the fact that nucleons of H_2 (and D_2 and T_2) are identical, special symmetry restrictions are placed upon the wave functions, which result in two symmetry species. These species are designated ortho (the species with the largest spin degeneracy) and para. Although the distinguishing feature for the statistics is the nuclear spin state, one also finds a distinct separation of rotational states according to their parity. Molecular hydrogen is a homonuclear diatomic molecule with nuclear spin $I_N = \frac{1}{2}$ on each proton. Because

TABLE III. Rotational quanta $S_0(J) = E_{0,J+2} - E_{0,J}$ in the ground vibrational state (0). Units: cm^{-1}, reference Kolos and Wolniewicz, 1966a, b 1968).

	H_2		HD		D_2	
J	Expt.	Theory	Expt.	Theory	Exp.	Theory
0	354.38	354.39	267.09	267.12	179.06	179.12
1	587.06	587.07	443.08	443.17	297.52	297.63
2	814.41	814.48	616.09	616.21	414.66	414.78
3	1034.65	1034.75	784.99	785.15	529.91	530.07

TABLE IV. Experimental values of the rotational constants in the vibrational ground state. Units: $cm^{-1} \cdot H_2$, HD Stoicheff (1957) D_2, McKellar and Oka (1978).

	H_2	HD	D_2
B_0	59.339	44.667	29.913 2
D_0	0.0459	0.0259	0.011 51
H_0	5.2×10^{-5}	2.2×10^{-5}	0.69×10^{-6}

the protons are indistinguishable and fermions, the total molecular wave function involving the nuclear coordinates must be antisymmetric with respect to particle permutation. The relevant part of the wave function can be written as a product of vibrational, rotational, and nuclear wave functions. Inversion symmetry provides parity as a good quantum number; the vibrational ground state is manifestly symmetric, whereas the easily accessible nuclear spin and rotational wave functions are either symmetric (S) or antisymmetric (AS). The allowed combinations for an AS total wave function require consideration of only the latter two, and are given in Table V, along with the nuclear weight and ortho–para designation. We also give the combinations for tritium, which is similar to H_2 (i.e., $I_N = \frac{1}{2}$), and deuterium, for which the total wave function must be symmetric because the deuterons have spin 1 and are bosons. The nonhomonuclear molecules such as HD do not have the ortho–para distinction since the two nucleons are distinguishable. The classification of states is of great physical importance as ortho–para transitions (conversion) are forbidden for isolated molecules and the two species have different properties, as we shall see. The crystal structure of the solid will be most strongly influenced by the angular distributions of the molecules characterized by the rotational quantum number. This will be discussed in Sec. IV. From Table I, we would expect similar behavior amongst the isotopes for the even-J species, p-H_2 and o-D_2, or odd-J species, o-H_2 and p-D_2.

The reason for the large physical distinction between the species can be seen from considering the rotational energy levels given by Eq. (2.16) and shown in Fig. 4 for H_2. Due to the very large splittings of the rotational levels, at the low temperatures of the solid hydrogens ($\lesssim$20 K), only the $J = 0$ and 1 levels are thermally populated (a $J = 1$ molecule will remain metastably in that level, as conversion to the $J = 0$ level is very slow in the solid). This brings about a great simplification. Since the single molecule rotational wave functions are the spherical harmonics, $Y_{Jm}(\theta, \phi)$, all para-H_2 molecules will be in the spherically symmetric Y_{00} states, and all ortho-H_2 molecules will be in the p-like states, Y_{1m}.[2] One would expect solid p-H_2 to behave somewhat like solid helium, interacting isotropically, whereas anisotropic interactions between molecules should be important in solid o-H_2.

Other interesting single molecule properties of hydro-

[2]Note that the rotational wavefunctions depicted in Fig. 4 give the orientational distribution of the molecular axis. One should be careful to distinguish between this and the charge density distribution in the molecular frame, shown in Fig. 1.

TABLE V. Allowed combinations of nuclear-spin states and rotational states for hydrogen, deuterium, and tritium, and the ortho–para designations. Antisymmetric is abreviated by AS and symmetric by S; I_{mol} is the total molecular nuclear spin and J the rotational quantum number.

Molecule and spin of nucleon		I_{mol}	J	$\Psi(I_{mol})\Psi(J)$	Nuclear weight g_I	Designation
Hydrogen	State	0	Even			para
Tritium	Symmetry	AS	S	AS	1	
$I_N=\frac{1}{2}$	State	1	Odd			ortho
	Symmetry	S	AS	AS	3	
Deuterium	State	1	Odd			para
$I_N=1$	Symmetry	AS	AS	S	3	
	State	0, 2	Even			ortho
	Symmetry	S	S	S	6	

gen are its multipole moments and polarizability. The first nonzero multipole moment of H_2 is the electric quadrupole (EQ) moment which is defined by

$$Q(R)=\tfrac{1}{2}R^2-\langle 3z^2-r^2\rangle \tag{2.17}$$

for fixed nucleii of separation R, in a coordinate system with z along the internuclear axis. Kolos and Wolniewicz (1965) evaluated $Q(R)$ as a function of R. Karl and Poll (1967) then determined $Q(R)$ in a given nuclear state by evaluating the matrix elements of the vibrational and rotational states:

$$Q^{(2)}_{vJ,v'J'}=\int Q(R)\psi^*_{vJ}(R)\psi_{v'J'}(R)R^2dR\,, \tag{2.18}$$

where $\psi_{vJ}(R)$ represents the radial part of the molecular wave function in the vJ vibrational–rotational state. Some of their results for the quadrupole moment in the body fixed frame are tabulated in Table VI.

To obtain the quadrupole moment in a given rotational state, $|Jm\rangle$, represented by the spherical harmonic $Y_{Jm}(\theta,\phi)$, the quadrupole moment must be expressed in a laboratory frame. Since $Q(R)$ has axial symmetry and is a second rank tensor one has (see Gray, 1967),

$$Q^{20}_{vJ,v'J'}=Q^{(2)}_{vJ,v'J'}Y_{20}(\theta,\phi)\,, \tag{2.19}$$

where θ,ϕ are the polar angles of the symmetry axis of the molecule with respect to the z axis of the laboratory frame. We shall collectively define $\theta,\phi=\Omega$. The rotationally averaged moment is

$$Q^{20}_{vJm,vJ'm'}=\langle Jm|Q^{20}_{vJ,v'J'}|J'm'\rangle\,. \tag{2.20}$$

Matrix elements of spherical harmonics are easily evaluated (Rotenberg *et al.*, 1959). At the low temperatures of the condensed phase the most important matrix elements are the diagonal $v=0$, $J=0$, and $J=1$. In the spherically symmetric ground state $Q^{20}_{000,000}=0$; in the $J=1$ state $Q^{20}_{01m,01m}=(\frac{2}{5})Q^{20}_{01,01}$. This latter quantity arises frequently and we shall define $Q=Q^{(2)}_{01,01}$ and $\overline{Q}$

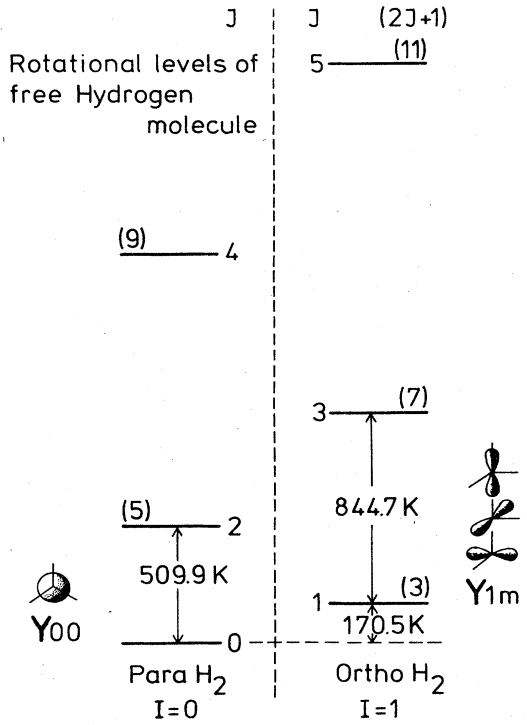

FIG. 4. The molecular rotational energy levels for an isolated H_2 molecule. The same diagram applies to D_2 but scaled down by about a factor of 2 due to the larger moment of inertia. The angular distribution of the two lowest rotational states are also indicated (Y_{10} and $Y_{11}\pm Y_{1-1}$ are actually shown). I is the total nuclear spin. Numbers in parenthesis are the m degeneracies.

TABLE VI. The electric quadrupole moment in the body fixed frame of the hydrogen molecule in various vibrational and rotational states in atomic units. ($ea_0^2=1.3449\times10^{26}$cgs, $a_0=0.529\,177\times10^{-8}$ cm). References: Karl and Poll (1967), Birnbaum and Poll (1968).

		H_2		D_2	
v	J	$Q_{vJ,vJ}$	$Q_{vJ,vJ+2}$	$Q_{vJ,vJ}$	$Q_{vJ,vJ+2}$
0	0	0.484 14	0.485 77	0.476 45	0.477 28
0	1	0.485 29	0.487 90	0.477 02	0.478 36
0	2	0.487 59	0.491 08	0.478 17	0.479 99
0	3	0.491 02	0.495 30	0.479 88	0.482 16
1	0	0.535 8	0.537 2		
1	1	0.537 0	0.539 1		
1	2	0.539 7	0.541 8		
1	3	0.542 8	0.545 4		

$= Q^{20}_{01m,01m}$ so that $\overline{Q} = \frac{2}{5}Q$. These abbreviated definitions will be used in later sections.

The static electric dipole polarizabilities have been calculated by KW (1967) as a function of nuclear separation R. Polarizabilities parallel ($\alpha_\parallel \equiv \alpha_z$) and perpendicular ($\alpha_\perp \equiv \alpha_x = \alpha_y$) to the internuclear axis were determined to provide

$$\alpha(R) = \tfrac{1}{3}(\alpha_\parallel + 2\alpha_\perp)\,,$$
$$\gamma(R) = \alpha_\parallel - \alpha_\perp\,. \tag{2.21}$$

These were averaged over nuclear states to give quantities such as

$$\alpha^{(2)}_{vJ,v'J'} = \int \alpha(R)\psi^*_{vJ}\psi_{v'J'}R^2dR \tag{2.22}$$

for H_2, HD, and D_2, as well as matrix elements of $\gamma(R)$. A few of the calculated matrix elements are given in Table VII for H_2. A more extensive tabulation, including values for H_2 and D_2, can be found in KW (1967). Values are in close agreement with experiment [see, for example, MacAdams and Ramsey (1972)]. At optical frequencies the dynamic polarizabilities are about 5% higher than those given in Table VI (Victor and Dalgarno, 1969; Kelly, 1970).

Matrix elements of the polarizability between rotational states must be evaluated frequently, particularly for the interpretation of optical measurements. Analogous to the handling of the quadrupole moment, we first express the polarizability, which is also a second rank tensor, in the laboratory frame [see, for example, Coll and Harris (1970)]. It is easiest to work with spherical tensors. The transformation between the body fixed frame b and the laboratory frame l is

$$\alpha^{2m}_l = \sum_n D^{(2)*}_{mn}(\alpha,\beta,\gamma)\,\alpha^{2n}_b\,, \tag{2.23}$$

where $D^{(2)}_{mn}(\alpha\beta\gamma)$ is a rotation matrix and $\alpha\beta\gamma$ are the Euler angles (Rose, 1957). The relationship between the spherical components and Cartesian components, in an arbitrary coordinate system, is given by

$$\alpha^{2,\pm2} = \tfrac{1}{2}(\alpha_{xx} - \alpha_{yy} \pm 2i\alpha_{xy})\,, \tag{2.24a}$$
$$\alpha^{2,\pm1} = \mp(\alpha_{xz} \pm i\alpha_{yz})\,, \tag{2.24b}$$
$$\alpha^{2,0} = (6)^{-1/2}(2\alpha_{zz} - \alpha_{xx} - \alpha_{yy})\,, \tag{2.24c}$$
$$\overline{\alpha} = \tfrac{1}{3}(\alpha_{xx} + \alpha_{yy} + \alpha_{zz})\,. \tag{2.24d}$$

For the body fixed frame, due to the axial symmetry, the only nonvanishing components are $\overline{\alpha}_b \equiv \overline{\alpha} = \overline{\alpha}^2_{vJv'J'}$ and $\alpha^{20}_b = (\frac{2}{3})^{1/2}\gamma^{(2)}_{vJv'J'} \equiv (\frac{2}{3})^{1/2}\kappa\overline{\alpha}$ (note that we have suppressed the vJ indexing in the spherical components, for simplification). Eq. (2.23) then becomes

$$\alpha^{2m}_l = (8\pi/15)^{1/2}3\kappa\overline{\alpha}Y_{2m}(\Omega)\,, \tag{2.25}$$

TABLE VII. Dipole polarizabilities in the body fixed framed of the hydrogen molecule (Kolos and Wolniewicz, 1967). Units: a_0^3.

v	J	$\alpha_{vJ,vJ}$	$\gamma_{vJ,vJ}$	$\alpha_{vJ,vJ+2}$	$\gamma_{vJ,vJ+2}$
0	0	5.4139	2.0239	5.4255	2.0338
0	1	5.4235	2.0317	5.4429	2.0488

where Ω is the same set of angles defined for Eq. (2.19), and a relationship from Rose (1957) between the rotation matrices and spherical harmonics has been used. Since the rotational wave functions in the laboratory frame are $Y_{Jm}(\Omega)$, matrix elements of Eq. (2.25) are easily evaluated. Cartesian components in the laboratory frame can be found from the transformations in Eqs. (2.24). These are also given by Silvera *et al.* (1971).

III. INTERMOLECULAR INTERACTIONS

One of the central problems in the study of the molecular hydrogen in the condensed state is the intermolecular interactions. In part, the interactions are of interest because they ultimately determine the equation of state, crystal structures, excitation spectra, etc., but most attention is focused here because they are fundamental, and in principle calculable to high precision from *ab initio* approaches. *The low density solid is an almost ideal testing ground* for theoretical interaction potentials. The problem is highly simplified in that, at least to moderate densities, the interactions can be fairly well described by a sum of pair interactions between molecules. Since the gas phase single molecule properties are almost undistorted when condensed into the solid state, the pair interactions in the solid can be represented by the interaction between an isolated pair with very small corrections for the environmental effects.

In this section we shall first discuss *ab initio* calculations of the intermolecular interaction energy of two H_2 molecules. We shall then discuss semiempirical determinations of the isotropic interaction with a comparison to experiment. Finally the anisotropic part of the potential will be considered both from the theoretical and experimental point of view.

A. *Ab initio* calculations

A precision *ab initio* calculation of the potential for four interacting hydrogen atoms is a formidable task and has recently been reviewed by McMahan *et al.* (1974); a general treatment can be found in Margenau and Kestner (1971). The four-atom Hamiltonian is given by Eq. (2.1), which must be extended to include the four protons and four electrons. Calculations are usually carried out in the Born–Oppenheimer approximation; the energies at short ranges are determined by variational treatments which give upper bounds, whereas at long ranges, perturbation treatments can be used. The quality of the results depends strongly on the complexity of the variational wave function. Energies are calculated as a function of interactomic distances and are found to be minimum when the atoms are paired as molecules, except for the closest ranges.

The anisotropic interaction energy depends on the mutual orientation of the axes of the H_2 molecules. An arbitrary orientation in which a number of useful angles are defined is shown in Fig. 5. In general an energy surface, or the energy as a function of molecular orientation and separation, must be determined. Efforts are usually confined to calculating the energies, ϕ^ρ, for four or five different geometries, ρ, as shown in Fig.

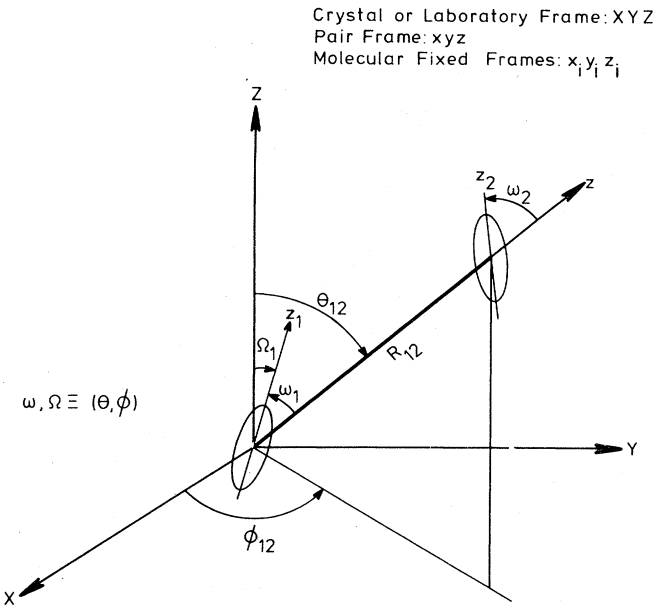

FIG. 5. Two H_2 molecules with arbitrary orientation and with a separation R_{12} between molecular centers. The letters Ω_i or ω_i refer collectively to the polar angles θ_i, ϕ_i, shown only for the orientation of the vector R_{12}. The orientation of the molecules with respect to a quantization axis (R_{12} here) is specified by angles ω_i. Orientations with respect to the crystal frame XYZ are specified by Ω_i. The molecular fixed frames are $x_i y_i z_i$.

6. It is then useful to fit the resulting energies to an isotropic part ϕ_I and an anisotropic part ϕ_A:

$$\phi(R_{ij}, \Omega_i, \Omega_j) = \phi_I(R_{ij}) + \phi_A(R_{ij}, \Omega_i, \Omega_j) . \tag{3.1}$$

By definition ϕ_I is the spherical average of ϕ, i.e., $\langle \phi \rangle = \phi_I$ and $\langle \phi_A \rangle = 0$; the isotropic part is obtained from the spherical average of the ϕ^ρ.

Even for the simplest wave functions, calculation of the energy involves a large number of electron–nucleus attraction terms and three- and four-center integrals. High precision is required as substantial cancellation amongst terms reduces the energy by an order of magnitude or more than the value of an individual term. Finally, the intermolecular interaction energy is found by subtracting off the energy of two isolated molecules. For intermolecular ranges of 3–4 Å the interaction energy is in the fifth or sixth decimal place of a term energy placing stringent demands on precision. For this and other reasons the short-range repulsive interaction is easiest to evaluate.

Calculations have in general been carried out by three techniques: self-consistent field (SCF), Heitler–London (HL), configuration interaction (CI). SCF and HL are special cases of CI. In the HL calculations for the wave function, one takes

$$\psi_{HL} = \tfrac{1}{2}[(a\bar{b}c\bar{d}) - (\bar{a}bc\bar{d}) - (a\bar{b}\bar{c}d) + (\bar{a}b\bar{c}d)] . \tag{3.2}$$

The letters a, b, c, d designate the four nuclear centers and each $(a\bar{b}c\bar{d})$ represents an antisymmetric product of single atom functions, including spin. Hydrogenic $1s$ state functions, localized on the four nuclei, are used; the bars over a letter indicate that the spin is opposite that of an unbarred letter and are chosen such that the molecules are in singlet spin states. The energy is determined by evaluating

$$E_{HL} = \langle \psi_{HL} | \mathcal{H} | \psi_{HL} \rangle / \langle \psi_{HL} | \psi_{HL} \rangle \tag{3.3}$$

which has no variational parameters.

An improvement over HL can be obtained by including ionized states such as

$$\Psi' = (a\bar{a}c\bar{c}) \tag{3.4}$$

in which two electrons are located on centers a and two on c, still restricted to total spin $S = 0$. Wave functions such as Eqs. (3.2) and (3.4) are called configurations.

A calculation in which the wave function consists of a sum of configurations, each multiplied by a variational parameter, is a CI calculation. For an arbitrary geometry of four atoms there are 20 possible configurations for the $S = 0$, $1s$ states. If all configurations consistent with the geometry are used, one has a *full* CI calculation. This can still be improved upon by enlarging the basis to include different $1s$ functions or $2p$ functions. To obtain an appreciation of the complexity of the problem, a single configuration can involve the calculation of ~10^2 integrals; a full CI calculation for the linear geometry involves 12 configurations for a $1s$ basis; for a $1s, 1s', 2p_x, 2p_y, 2pz$ basis 2172 configurations are involved.

The SCF technique is essentially a Hartree–Fock calculation in which an incomplete basis set is used. The trial wave function is determined self-consistently. It has the advantage of being less laborious, with shorter computing time, than a CI calculation. The disadvantage is lower accuracy and insufficient spatial correlation of the electrons. This means that SCF calculations are totally inadequate for interaction energies at medium and long range where attractive dispersion (induced dipole–induced dipole) forces due to electron correlation are important. In an appendix to their book, Margenau and Kestner (1971) argue that SCF calculations do not include dispersion energies. (However, they are unable to prove that an SCF calculation cannot give an attractive potential.) An SCF calculation *does* include attractive interactions due to permanent multipole moments, as do the HF and CI calculations.

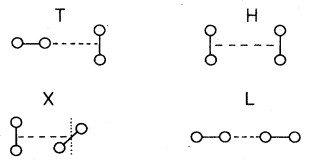

FIG. 6. Four orientational geometries commonly used in calculations of the intermolecular interaction energy. Only the X geometry is noncoplanar.

1. Short range

The results of a number of CI and CI+SCF calculations of the potential ϕ^ρ for various molecular geometries, ρ, are shown in Fig. 7 (after the review of McMahan *et al.*) for short ranges. The interactions, which are essentially exponential in this region, begin

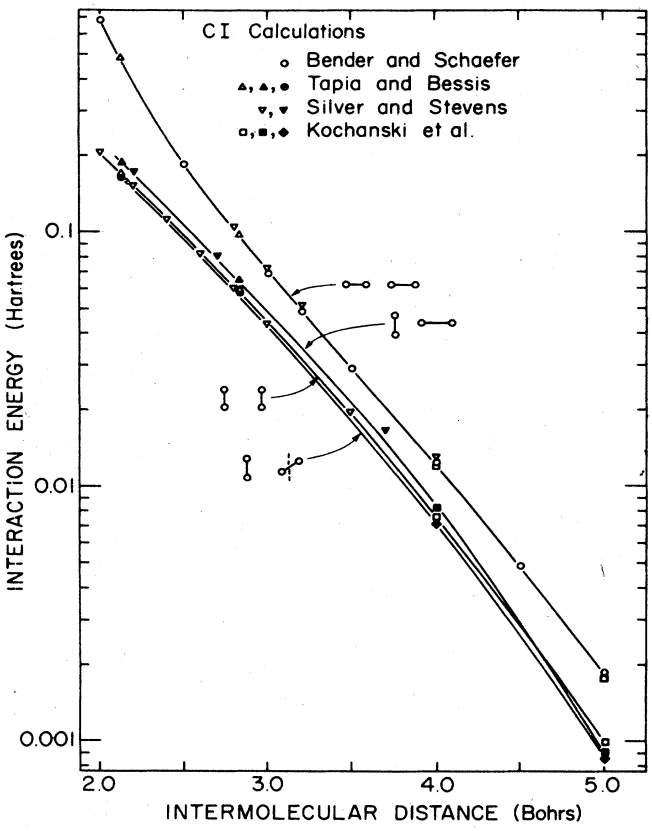

FIG. CI calculations of the H_2–H_2 intermolecular interaction energy at short ranges (after McMahan *et al.*, 1974). Results of Bender and Schaefer (1972), Tapia and Bessis (1972), Silver and Steven (1973), and Kochanski *et al.* (1974) are shown.

to fall off much faster with increasing intermolecular separations greater than ~4.5 bohr, reflecting the growing importance of the attractive dispersion forces. For a geometry, ρ, these potentials can be analytically represented by the repulsive form

$$\phi_{\text{rep}}^{\rho} = \exp(\alpha_\rho + \beta_\rho R - \gamma_\rho R^2) . \tag{3.5}$$

2. Long range

At long ranges, when the molecules are sufficiently far apart so that the overlap of their charge distribution may be considered to be negligible, it is well known (Margeneau and Kestner, 1971) that the potential arises from the interaction of electronic multipole moments and may be expanded in powers of the interatomic separation

$$\phi(R_{ij}, \Omega_i, \Omega_j) = \sum_k C_k(\Omega_i, \Omega_j)/R^k , \tag{3.6}$$

where we set $\phi(\infty, \Omega_i, \Omega_j) = 0$. Just as in Eq. (3.1), this can be separated into an isotropic and anisotropic part. The most important anisotropic term is for $k = 5$ and arises from the interaction of the permanent electric quadrupoles of the two molecules; this and other anisotropic terms will be treated in greater detail later. The leading isotropic terms are for $k = 6$ and 8 and arise from induced dipole–dipole and dipole–quadrupole interactions. These coefficients have been determined by direct calculations using perturbation theory or by semiempirical techniques (Victor and Dalgarno, 1970; Langhoff *et al.*, 1971). For $k = 6$ the isotropic value is 12.1 a.u. (from the semiempirical approach). For $k = 8$ a value of $C_8 = 116$ a.u. has been used in a number of model calculations; this value originates from an estimate by Margenau (1943) based on the C_8/C_6 ratio of the oscillator model and has become established in the literature. Recently, Meyer (1976) has reconsidered the long-range interactions in H_2 using an optimized basis set in Rayleigh–Schrödinger perturbation theory. He finds that the "established value" of C_8 was in error by almost a factor of 2 and that the C_{10} term is non-negligible. His values, which we recommend, are $C_6 = 12.14$ a.u., $C_8 = 215.2$ a.u., and $C_{10} = 4813.9$ a.u. Unfortunately, Meyer's anisotropic dispersion coefficients are imcomplete as he omitted some mixed-pole terms in his calculation (Thakkar, 1977; Mulder and van de Avoird, 1977).

3. All ranges

The only calculations of the H_2–H_2 potential over a broad range of intermolecular separation that predict reasonable values of the potential in the van der Waals well region are those of Gallup (1977a), Jaszúnski *et al.* (1977) and a recently published potential due to Schaefer and Meyer (1979). Gallup did a restricted CI calculation with configurations constructed from SCF orbitals for the individual H_2 molecules. He decomposed his potential into an isotropic and anisotropic part. The isotropic part shown in Fig. 8 has a well minimum of 34.3 K at $R_m = 3.57$ Å (6.75 a.u.) (Gallup

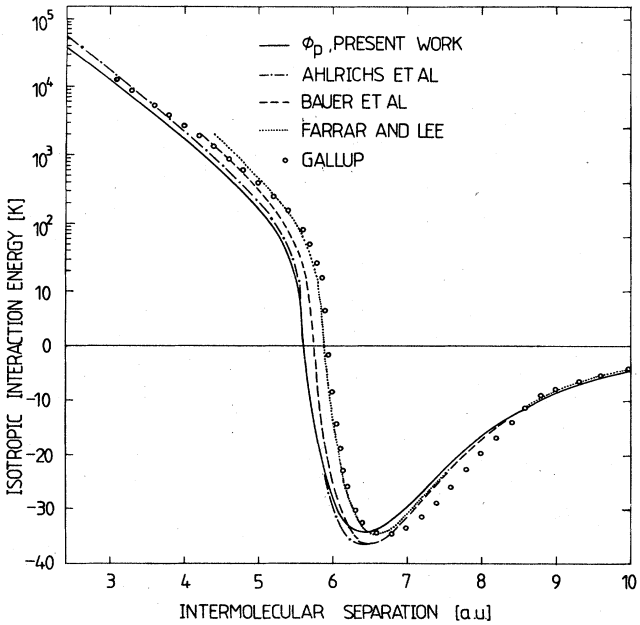

FIG. 8. Semiempirical isotropic pair potentials of H_2. The CI calculation of Gallup is shown for comparison. Present work refers to the potential of Silvera and Goldman. The remaining potentials have been proposed to explain molecular beam scattering crossections (after Silvera and Goldman, 1979).

states that $R_m = 3.49$ Å; however, evaluation of his spline function yields 3.57 Å). Although the depth is reasonable, the potential appears to be substantially shifted from the experimental curves (to be discussed in the next section).

Jaszúnski *et al.* calculate the potential in the well region using a SCF–CI and a perturbation approach. The latter yields a well energy and minimum comparable with that of Gallup. The well minimum in their SCF–CI calculation is too shallow with a value of ~21 K. Schaefer and Meyer find a well minimum of ~32.6 K at $R_m = 3.49$ Å.

Interaction energies arise from a number of sources: overlap energy including charge repulsion and charge transfer interactions, attractive dispersion forces due to molecular polarizability, induction energy due to the interaction of a permanent multipole moment on one molecule with the polarizability of the other, and the interaction of permanent multipole moments. Phenomenological or semiempirical potentials are often written as an appropriate (see following section) sum of the various contributions. Gallup (1977a) makes an interesting analysis of the contributions to his spherical potential. He shows that in the region of the van der Waals minimum, about $\frac{1}{3}$ of the attractive energy arises from charge transfer interaction (configurations with ±1 net electrical charge on the molecules), the rest coming from the dispersion contribution. He also shows that the spherically averaged SCF energy remains repulsive at long range as suggested by Margenau and Kestner. From his separation it appears that for a semiempirical potential made up of a dispersive term and an exponential repulsive term, the latter should be associated with an SCF repulsion.

In the following sections we discuss the decomposition of ϕ, given by Eq. (3.1), into an isotropic part ϕ_I and an anisotropic part ϕ_A; these are compared to experiment.

B. Semiempirical isotropic potentials

For a number of years, the most significant parameters characterizing the isotropic intermolecular potential were the well depth, ε, and the position of the well minimum $R = R_{\min}$, or almost equivalently, the position $R = \sigma$ where the potential crosses the energy axis and becomes positive; more recently, as more attention has been focused on solids under pressure, the details of the repulsive core have become important. The most popular form of the potential that has been used is the Lennard-Jones (6–12):

$$\phi_I(R) = 4\varepsilon[(\sigma/R)^{12} - (\sigma/R)^6]. \tag{3.7}$$

The most recent determination [see Hirschfelder *et al.* (1954) for earlier values] of the potential parameters was by Michels *et al.* (1960), who used measurements of gas phase isotherms to determine $\varepsilon/k_B = 36.7$ K, $\sigma = 2.96$ Å ($R_m = 3.32$ Å) for hydrogen, and $\varepsilon/k_B = 35.2$ K and $\sigma = 2.95$ Å ($R_m = 3.31$ Å) for deuterium.[3] However, the Lennard-Jones (LJ) was inadequate to give agreement to within experimental accuracy within the whole temperature range. Srivistava and Barua (1965) achieved a better fit to the data of Michels *et al.* for hydrogen using a modified Buckingham exp-6 potential:

$$\phi(R) = \frac{\varepsilon}{1-\sigma/\alpha}\left\{\frac{\sigma}{\alpha}\exp\left[\alpha\left(1-\frac{R}{R_m}\right)\right] - \left(\frac{R_m}{R}\right)^6\right\}, \quad R > R_{\max}$$
$$= \infty, \quad R < R_{\max} \tag{3.8}$$

with $\varepsilon/k_B = 38.2$ K, $R_m = 3.339$ Å, $\alpha = 14.0$, and $R_{\max} = 0.7864$ Å.

Determinations of the H_2–H_2 potential have also been made by fitting to the collision cross section obtained from crossed molecular beam scattering experiments. Dondi *et al.* (1972) first attempted to fit their data to an LJ 12–6 and a softer LJ 9–6 potential but obtained poor agreement using the LJ family. They found best agreement using a scaled helium–helium potential with $\varepsilon/k = 34$ K and $R_m = 3.45$ Å. Farrar and Lee (1972) fit their data to an MSV (Morse spline van der Waals) potential in which a short-range Morse exponential potential is connected by a spline function to an attractive multipole potential of the form of Eq. (3.6) with $C_6 = 12.08$ a.u. and $C_8 = 116$ a.u. Their best fit yielded $\varepsilon/k = 34.8$ K and $R_m = 3.49$ Å. Still another beam determination was made by Bauer *et al.* (1976). They fit their data to an exponential repulsion of the form of Eq. (3.5) added to an attractive potential of the form of Eq. (3.6), with $C_6 = 12.0$ a.u. and $C_8 = 240.0$ a.u. taken from Meyer (1976) so that C_8 effectively includes the attraction of the C_{10} term which they did not carry along. They found best agreement with experiment for $\varepsilon/k = 34.8$ K and $R_m = 3.43$ Å. A discussion of these various determinations will be made shortly. Some of these potentials are displayed in Fig. 8.

An approach which puts stringent demands on the potential is a fit to solid state properties. Given the structure of the solid at $T = 0$ K, the lattice energy E, the pressure P, and bulk modulus B_m can be calculated, all as a function of molar volume. The results for a given potential can be compared to the experimental P, V values at 4.2 K (Anderson and Swenson, 1974; Silvera *et al.*, 1978; and Driessen *et al.*, 1979) and the zero-pressure sublimation energy. Krumhansl and Wu (1972) calculated the energy and pressure of solid hydrogen as a function of molar volume using a variational technique for quantum crystals. They examined the LJ 6–12 and the exp-6 potential, among others. They found reasonable agreement with experiment at low density, but serious systematic disagreement at higher densities. Since some of the calculational approximations used could be questionable, Bruce (1972) repeated the calculations for these potentials using a Monte Carlo variational technique which enables reliable evaluation of integrals without appeal to a cluster approximation. He found good agreement with the zero-pressure volume $V_0 = 23.16$ cm^3/mol and energy/particle = −85.5 K; however, systematic deviations remained at higher densities. At 10 cm^3/mol, the calculated pressure was ~40 kbar, approximately twice the experimental value. This implied that the LJ 6–12 and

[3]Sources of the small isotropic differences as well as dependence on the rotational state have been discussed by Knaap and Beenakker (1961).

the exp-6 had serious problems in the repulsive core of the potential.

England *et al.* (1974) and later Etters *et al.* (1975), with some refinement, succeeded in obtaining good agreement with the experimental data in the range 10–23 cm^3/mol. The potential they used was a composite of the best available theoretical short-range and long-range potentials. For the short-range part, they employed the spherical average for the four basic orientations shown in Fig. 6 using results of a number of SCF, CIF calculations. An analytical fit was made. For the long-range part they used $-C_6/R^6 - C_8/R^8$; however, they used the older value of $C_8 = 116$ a.u. The repulsive and attractive terms cannot just be added together as the negative multipole term, which is infinite at the origin, will eventually dominate the finite repulsive term at short ranges and give unphysical results. To alleviate this problem, they damped out the attractive term with a function

$$F(R) = \{1 + \exp[-4(R - 3.5)]\}^{-1} \tag{3.9}$$

with R in a.u. The effect is to attenuate the multipole term to zero for $R \lesssim 2.5$ a.u. with essentially zero attenuation in the well region of the potential. [We note that Kim and Gordon (1974) have shown that the dispersion forces are already measurably attenuated in the vicinity of the well minimum due to overlap effects.] With this potential they used a quantum solid theory to calculate E and P (as well as the second virial coefficient). The calculated pressure agreed with experiment to within 10% in the high density range; they found a zero-pressure molar volume of 22.65 cc/mol (experiment 23.16 cm^3/mol), and energy of −89.8 K/molecule (exptl:−85.5 K). Their potential is shown in Fig. 9 and has $\varepsilon/k \simeq 34$ K and $R_m \simeq 3.4$ Å.

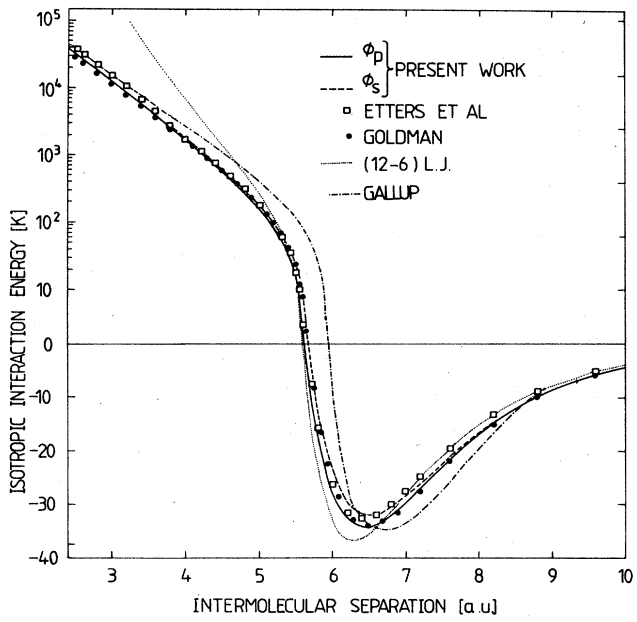

FIG. 9. A number of H_2 intermolecular potentials. Those of Etters *et al.* (1975), Goldman (1973), and "present work" (Silvera and Goldman 1978) have been fit to solid properties (ϕ_p is isolated pair potential, ϕ_s is effective solid potential). The remaining potentials have been proposed to represent isolated pairs. A complete discussion and comparison is given in the text.

Goldman (1975, 1976) used a Barker–Pompe type potential of the form

$$\phi(x) = \varepsilon[A_0 + A_1(x-1)]\exp[-\alpha(x-1)] - \frac{C_6'}{x^6+\delta} - \frac{C_8'}{x^8+\delta} \tag{3.10}$$

with $x = R/R_m$, $R_m = 3.44$ Å, $\varepsilon \simeq 34$ K, $\alpha = 9.3$, $A_0 = 0.80366$, $A_1 = -3.902354$. His C_6 and C_8, in atomic units, were 12.08 and 116, respectively. The $\delta = 0.01$ serves to keep the attractive terms finite at the origin. This was fit, using self-consistent phonon theory, to the zero-pressure lattice energy and the experimental 4.2 K $P-V$ solid isotherm of Anderson and Swenson (1974). The potential is plotted in Fig. 9 and compares closely to Etters *et al.*

The solid state properties are highly sensitive to the values of $\varepsilon, R_{\min}$, and the slope of the repulsive core, making the solid an important testing ground for potentials. The potential of Etters *et al.* (1975) can be criticized for the following. First, they do not examine corrections due to many-body forces. Second, although they added the theoretical repulsive and attractive potentials together, this must not be considered as a correct procedure for generating the theoretical potential, and depends in fact critically on how the potentials are patched together [see the damping function, Eq. (3.9)]. As an example, they used the old value of $C_8 = 116$ a.u., with $C_{10} = 0$. If one uses the latest values due to Meyer (1976), then their potential would be lowered by 21 K at the well minimum and R_m would be shifted inwards. This would then give very poor agreement with solid state experimental values. Their potential must be considered as semiphenomenological due to the attenuation function, with a somewhat incorrect long-range asymptotic form.

The potential of Goldman must to a certain extent contain the many-body forces, hidden in the parameters as it is a phenomenological potential fit to solid state properties. This means that to the extent that many-body forces are important, this potential cannot be used to represent a pure pair interaction. In addition Goldman used the old value of C_8 for the long-range behavior and use of Meyer's values for C_8 and C_{10} would require a new fit.

To overcome these deficiencies Silvera and Goldman (1978) have used solid state data to determine the following potential:

$$\phi(R) = \exp(\alpha - \beta r - \gamma r^2) + f(R)\left\{\sum_{\substack{i=6,\\8,\,10}} C_i/R^i + C_9/R^9\right\} \tag{3.11}$$

with

$$f(R) = \exp\left\{-\left[\left(1.28\frac{R_m}{R}\right) - 1\right]^2\right\} \quad R < 1.28R_m$$
$$= 1 \qquad\qquad\qquad\qquad R > 1.28R_m, \tag{3.12}$$

where $\alpha = 1.713$, $\beta = 1.5671$, $\gamma = 0.00993$, $C_6 = -12.14$, $C_8 = -215.2$, $C_{10} = -4813.9$, and $C_9 = 143.1$, all in a.u. $R_m = 3.41$ Å is the well minimum with $C_9 = 0$. Their potential is designed to represent pair interactions plus many-body effects, accounted for by the term with C_9.

For the pure pair potential [Eq. (3.11) with $C_9=0$] they constrained the fit to conform to theoretical asymptotic values. The long-range constants C_i of Meyer are used. These are attenuated by a useful function, given by Eq. (3.12) and suggested by Alhrichs *et al.* (1976), which we have used earlier in the fit for atomic hydrogen, Eq. (2.14). The function $f(r)$ should be considered as a phenomenological cutoff (Tang and Toennies, 1977). Note that the attenuation already begins in the vicinity of the well, unlike that of Etters *et al.* The short-range repulsive part was constrained to fit the spherically averaged theoretical SCF–CI potentials discussed earlier. It is believed that the dominant many-body forces in closed shell systems such as H_2 are the nonadditive three-body Axilrod–Teller–Muto (ATM) (see Bell and Zucker, 1976) forces which vary as the inverse third power of the density (or R^{-9}). The effect of these forces is incorporated in an average way by the C_9/R^9 term, where C_9 was determined so that the effective pair interaction of Eq. (3.11), when summed over the lattice, gives the same energy as the true ATM forces. This is about 10% of the energy arising from pure pair interactions at zero-pressure densities. These forces are nonbinding and thus C_9 is positive. It is known that this term is attenuated at short ranges and then becomes attractive (Kim and Gordon, 1975); thus it is also attenuated here by $f(R)$. The use of this effective pair potential should provide the most important many-body corrections for isotropic properties in the solid; this approach may be inadequate for anisotropic properties such as sound velocity, etc.

The potential was fit to the $P-V$ data in deuterium and the sublimation energy of Clusius and Bartholomé (1935) as corrected by Schnepp (1970). For the pure pair potential $\varepsilon/k_B=34.3$ K, $R_m=3.41$ Å; when the ATM term is included $\varepsilon/k_B=32.2$ K and $R_m=3.44$ Å. These two potentials are shown in Fig. 9 (ϕ_p is the potential with $C_9=0$; ϕ_s is the solid effective pair potential, $C_9\neq 0$).

This provides a useful analytic form for the isotropic potential that can be used in solids as well as for true pair interaction. Rulis and Scoles (1977) have checked a number of pair potentials on molecular beam scattering data, including those of Bauer *et al.*, Farrar and Lee, Dondi *et al.* and the solid potentials, among others. They find that the potentials of Goldman, and Silvera and Goldman, fit the beam data better than the potentials ariginally proposed by the beam workers. Alternately, Silvera and Goldman (1978) have used the beam potential of Bauer *et al.* in the solid and find a pressure of 37 kbar at 10 cm^3/mol in H_2 substantially higher than the experimental value (22.9 kbar). Three-body forces would make the discord greater.

At this time, until more accurate data is available at very high density, we recommend the use of Eq. (3.11) for the isotropic potential of H_2 and D_2.

Finally, we observe that the *ab initio* potential of Gallup is shifted out about 0.16 Å from the solid state potentials. Silvera and Goldman (1978) used Gallup's potential to calculate solid state $P-V$ values and found 580 bar at V_0 and 34 kbar at 10 cm^3/mol in substantial discord with experiment. A closer analysis of Gallup's potential shows that his long-range tail has an R^{-6} character with a reasonably accurate value of C_6, but no R^{-8} or R^{-10} character. This is a result of his basis set, which is made up of s and p functions. To obtain the higher multipole terms, the basis set would have to be expanded to include d and f functions.

In criticism of the determination of the potential from solid state data, recently Chandrasekharan and Etters (1978) have suggested that small changes in H_2 vibrational frequencies in the solid and gas phase contribute about 6% to the $T=0$ K sublimation energy. This effect could account for a small difference between the *ab initio* and solid state potentials.

C. The anisotropic potential

The anisotropic interactions give rise to an array of interesting phenomena in the solid state which will be discussed in detail in later sections. These phenomena enable a rather precise determination of ϕ_A of Eq. (3.1). Determination of ϕ_A in the solid is advantageous because the molecules are at a fixed separation (except for zero-point motion) and at low enough temperatures so that the molecules populate the lowest orientational states; under certain circumstances the spectrum of reorientational excitations can be used to determine potential parameters. By contrast, in gas phase or molecular beam measurements, interactions are averaged over large trajectories in space and consequently these are usually not very sensitive techniques for determination of the radial dependence of anisotropic potential parameters.

The orientational energy of an H_2 molecule depends sensitively on its rotational state and its environment. In the low density solid, J is a good quantum number, and we need only consider the $J=0$ and 1 states. The $J=0$ state is spherically symmetric and thus has no orientation dependent energy. For the $J=1$ state a number of circumstances can arise, illustrated in Fig. 10. An isolated $J=1$ molecule has a threefold orientational degeneracy (ignoring the intramolecular hyperfine interaction and nuclear spin). This degeneracy will be partially lifted by the crystal field of a $J=0$ neighbor. In the hcp or fcc lattice, substantial cancellation occurs in the interaction of the $J=1$ with 12 nearest neighbor; however, the degeneracy is still lifted. When nearest neighbor $J=1$ molecules are isolated in such a lattice by $J=0$ neighbors, the ninefold degeneracy of the pair is partially lifted by the dominant electric quadrupole interactions; the splitting is further modified by smaller anisotropic terms and many-body effects as shown in Fig. 10(d). When more than two $J=1$ molecules are interacting the picture rapidly becomes more complicated, finally simplifying for a lattice of $J=1$ molecules where translational symmetry is recovered (to be discussed later).

It is useful to express the anisotropic part of the potential in terms of an analytic function of the orientations of the molecules which can be fit to the interaction energies of the four (or five) geometries such as shown in Fig. 6. The most useful expansion is in terms of spherical harmonics since these are also, to a very good approximation, the rotational wave functions of the molecules at low density. Such a choice permits simplification and ease of evaluation of rotational ma-

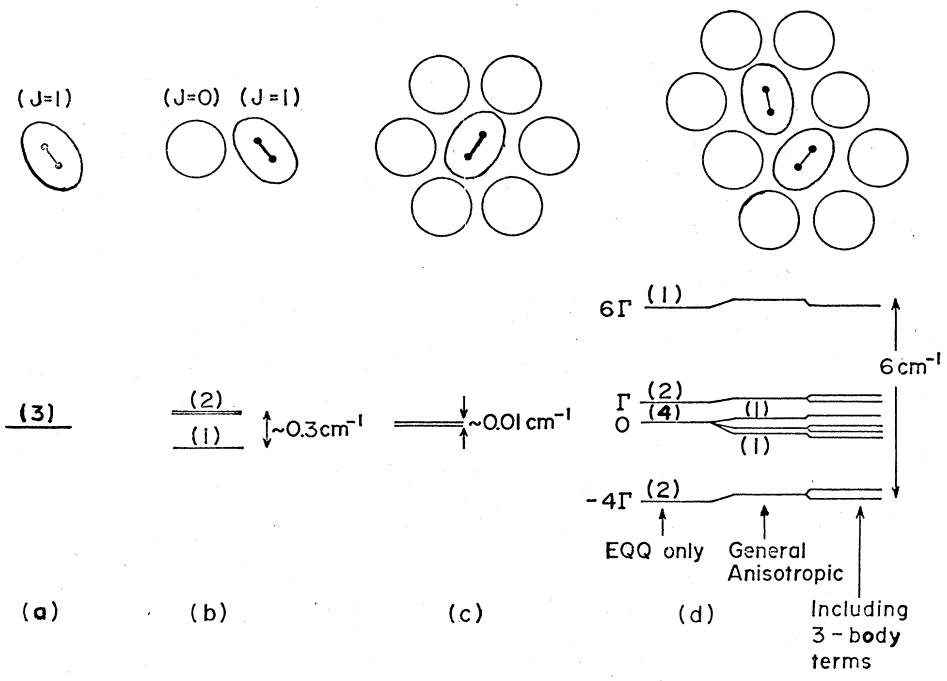

FIG. 10. Various environments and energy levels for $J=1$ molecules. (a) An isolated molecule. (b) Molecule with a single $J=0$ neighbor. (c) Molecule with a complete shell of nearest neighbor $J=0$ molecules (only 6 of the 12 neighbors of an hcp lattice are shown). (d) A pair of $J=1$ molecules surrounded by $J=0$ molecules in an hcp solid (only 8 of the neighbors are shown) (after Hardy, Berlinsky, and Harris, 1977).

trix elements of the potential.

The most general expression for the anisotropic potential, given by Van Kranendonk (1960), and later discussed by many authors [I refer also to Harris (1970), Ng *et al.* (1976), and Nakamura (1970)], can be written

$$\phi_A(R_{12},\Omega_1,\Omega_2)=\sum_{l_1,l_2}\sum_{n}\varepsilon_{l_1l_2}(R_{12})a_nY^n_{l_1}(\omega_1)^*Y^n_{l_2}(\omega_2)\,, \quad (3.13)$$

where[4] ω_1 and ω_2 specify the angles of the molecular axes with respect to the vector R_{12} connecting molecular centers (see Fig. 5), l_1 and l_2 are summed over all integer values. Because the molecules are homonuclear, having inversion symmetry, only even values of l_1 and l_2 occur and $a_n=a_{-n}$; the term with $l_1=l_2=0$ is the isotropic potential and has been removed from Eq. (3.13). Terms with $l_1+l_2>4$ are generally small[5]; in the ground state of low-pressure solid H_2, molecules are in the rotational state $J=0$ or 1 and matrix elements of ϕ_A within the ground manifold vanish for terms with l_1 or $l_2>2$. We can then write Eq. (3.13) in the form

$$\begin{aligned}\phi_A(1,2)=&(16\pi/5)^{1/2}B(R_{12})[\,Y^0_2(\omega_1)+Y^0_2(\omega_2)]\\&+4\pi\sum_{j=0,2,4}\varepsilon_j(R_{12})\alpha_j\\&\times\sum_{\mu}C(22j;\mu,-\mu)Y^{\mu}_2(\omega_1)Y^{-\mu}_2(\omega_2)\,, \quad (3.14)\end{aligned}$$

where $\alpha_0=\sqrt{5}$, $\alpha_2=\sqrt{7/2}$, $\alpha_4=\sqrt{70}$, and $\varepsilon_j\alpha_j$ vanish for odd j; $C(l_1l_2j;\mu,-\mu)$ is a Clebsch–Gordan coefficient. The R dependent terms $B(R)$ and $\varepsilon_j(R)$ measure the strength of the interaction. The term with $B(R)$ arises from an anisotropic charge distribution on one molecule interacting with the spherical part of another. The coefficients ε_0, ε_2, and ε_4 arise from charge overlap (and exchange), referred to as valence forces (v), anisotropic dispersion-induction forces (di), and the permanent electric quadrupole–quadrupole (EQQ) interactions.

For completeness we also present the decomposition of the potential into its irreducible tensorial sets, following van Kranendonk. The second part of Eq. (3.14) is composed of the product of two spherical harmonics which are irreducible tensors of rank two. The direct product space can be decomposed, in general, into five irreducible tensors of ranks 0, 1, 2, 3, and 4 by use of the Wigner $3j$ symbol, $\begin{pmatrix}2&2&j\\m&-m&0\end{pmatrix}$:

$$Y^m_2(\omega_1)Y^{-m}_2(\omega_2)=\sum_j\begin{bmatrix}2&2&j\\m&-m&0\end{bmatrix}Y_{j0}\,.$$

From this we can see that the second part of Eq. (3.14) can be written as

$$\frac{4\pi}{5}\sum_{j=0,2,4}A_jY_{j0}$$

since odd values of j vanish identically. Again, the coefficients A_j can be decomposed into valence, dispersion, and EQQ components:

$$A_4=A_4^{\mathrm{EQQ}}+A_4^{\mathrm{v}}+A_4^{\mathrm{di}},\ A_2=A_2^{\mathrm{v}}+A_2^{\mathrm{di}},\ \text{and}\ A_0=A_0^{\mathrm{v}}+A_0^{\mathrm{di}}\,.$$

In 1955, Nakamura treated ϕ_A theoretically and

[4]In later sections, we shall also use the notation V for the potential, i.e., $\phi\equiv V$.

[5]Terms with $l_1=4$, $l_2=0$, and $l_1=0$, $l_2=4$ also arise but are considered small (Gush and Van Kranendonk, 1966; Noolandi, 1970); the weak quadrupole–hexadecapole interaction corresponding to $l_1+l_2=6$ has been considered by Gush and Van Kranendonk (1966).

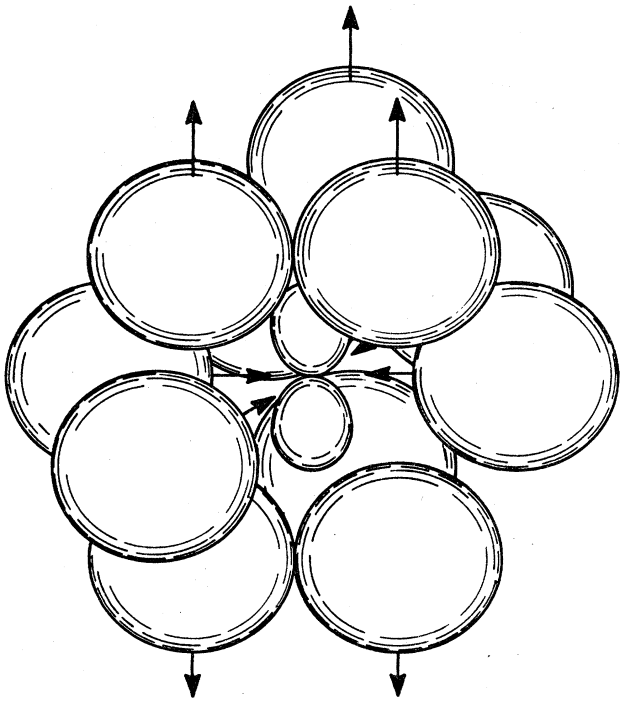

FIG. 11. Schematic representation of the local lattice distortion in the neighborhood of a $J=1$ molecule surrounded by $J=0$ molecules in an hcp lattice (after Raich and Kanney, 1977).

showed that the EQQ interaction corresponding to $j=4$ in Eq. (3.14) was the dominant term at nearest neighbor distances R_0 of the zero-pressure solid. This has been confirmed experimentally. It is also consistent with the work of Raich *et al.* (1976), who analyzed a number of *ab initio* calculations, the potentials of Gallup (1977) and Schaefer and Meyer (1979). The results of Raich *et al.* lack accuracy in the interesting region of intermolecular separation corresponding to zero-pressure solid H_2 ($R\sim 3.79$ Å) as they are based on calculations which are not accurate in this region; the more optimal results of Gallup and Schaefer and Meyer[6] are probably more accurate, yet still not sufficiently so to be taken as a standard in this region. Ng *et al.* (1976) suggest that the anisotropic interaction should be dominated by the pure EQQ interaction to ranges ~5 a.u. due to the very small anisotropy in the molecular charge distribution (see Fig. 1).

In a perfect, rigid, close packed lattice the interaction due to the $B(R)$ term, which is often referred to as the crystal field term, is zero when summed over the first and the second shell of neighbors, and alternates in sign for further shells, resulting in a negligible contribution to the lattice energy. Zero-point motion gives rise to small distortions from perfect packing which break the symmetry (Van Kranendonk and Sears, 1966; Raich and Kanney, 1977, Luryi and van Kranendonk, 1979); however, the effective crystal field term, $V_c(R)$, that a molecule feels due to its environment remains very small [$V_c(R)$ will be defined later in this section]. The distortion considered by Raich and Kanney is shown in Fig. 11.

In the low-pressure solid ϕ_A can, to a good approximation, be taken to be pure EQQ, which is often expressed as

$$\phi_{\mathrm{EQQ}}(R_{12}) = 4\pi \sum_{\mu} \frac{5}{6}\sqrt{70}\, C(224;\mu,-\mu)\Gamma(R_{12}) Y_{2\mu}(\omega_1) Y_{2-\mu}(\omega_2), \tag{3.15}$$

where $\Gamma = (\frac{6}{25})e^2Q^2/R_{12}^5$ is the EQQ coupling parameter and Q is the EQ moment given in Table VIII. At nearest neighbor distances of the zero-pressure solid (R_0 = 3.789 Å for H_2 and 3.605 Å for D_2) $\Gamma/k_B \equiv \Gamma_0/k_B$ = 0.949 K for H_2 and 1.175 K for D_2. The classical quadrupolar energies of the four configurations of Fig. 6 are given in Table IX; the interaction energy of a pair of molecules is lowest when in the "T" configuration and highest in the "L" configuration (see Fig. 6). If one of the molecules is in the $J=0$ rotational state, then it has spherical symmetry [$Y_{00}(\omega_i)$ = const] and the quantum mechanical average of ϕ_{EQQ} is zero. If both molecules are in the $J=1$ state, due to the angular distribution of the quadrupoles [see Eq. (2.19)], the classical energies are reduced by $(\frac{2}{5})^2$ when the quantum-mechanical averages are taken. In Table IX, a special configuration that is important in the orientationally ordered state of H_2 is also considered. Here the two molecules are oriented along two different body diagonals in a cubic lattice. In the last column, we give the eigenenergies of a pair of molecules, both in $J=1$ rotational state with a pure EQQ interaction. Each molecule has $2J+1=3$ possible orientational states resulting in a ninefold multiplicity. The energies are found by diagonalizing the Hamiltonian, Eq. (3.15), within the set of nine states. The eigenstates are shown in Fig. 12, both in the representation J_1M_1, J_2M_2 and in the total angular momentum representations $F=J_1+J_2, M_F$. In both cases the line connecting the molecular centers is the axis of quantization. Analogies to the classical configurations can be made by noting that the degenerate ground states 8 and 9 (Fig. 12) are linear combinations of T configurations, i.e., ϕ_8: [in a vector picture the angular momentum J is perpendicular to the intermolecular axis; in the $m_i=0$ state J lies in a plane perpendicular to the quantization direction, z, and thus the molecular axis is "along" z. For $m=\pm 1$, the molecular axis is "perpendicular" to z. Thus we make the association $(m_1m_2) = |10\rangle$ with].

In the solid it is often necessary to reference the orientation of the molecules to the crystal frame, rather than the vector connecting molecular centers, as in Eq. (3.13). Gray (1968) has shown in a very elegant way that

$$\phi_A = 4\pi \sum_{l_1 l_2} \sum_{\substack{m_1 \\ m_2, m}} \varepsilon_{l_1 l_2}(R_{12}) C(l_1 l_2 l; m_1 m_2 m) \times Y_{l_1 m_1}(\Omega_1) Y_{l_2 m_2}(\Omega_2) Y_{l m}(\Omega_{12})^*, \tag{3.16}$$

where Ω_1, Ω_2, and Ω_{12}, specify, respectively, the orientation of the molecular axes and the vector connecting

[6] The EQQ part of the Shaefer-Meyer potential evidently suffers from some inaccuracy. This has been corrected in an as yet unpublished improved potential.

TABLE VIII. The best available values for the interaction parameters in zero pressure solids in the limit that all molecules are in the $J=0$ state.

Quantity	Units	H_2	HD	D_2	Comment	Reference
V_0	cc/mole	23.16	20.57	19.95	Molar volume hcp structure	a, b, i
R_0	Å	3.789	3.642	3.605	hcp $J=0$ solid at zero pressure, 4.2 K	a, b
Q	au	0.485	0.481	0.477	$v=0\,J=1\rightarrow J=1$	c
		0.488	0.483	0.478	$v=0\,J=1\rightarrow J=3$	
		0.486	0.482	0.477	$v=0\,J=0\rightarrow J=2$	
Γ_0	K	0.949	···	1.175	In the $v=0\,J=1$ state	···
ξ_{54}	···	0.942	···	0.968		d
$\overline{\Gamma}=\frac{6}{5}\overline{\epsilon}_4$	K	0.827	···	1.026		e, g, f
$\langle\Delta\epsilon_4\rangle=\langle\epsilon_4-\epsilon_4^{EQQ}\rangle$	K	−0.057	···	−0.094		···
ϵ_0	K	−0.018	···	···		g
ϵ_2	K	0.016	···	···		g
$\lvert V_c\rvert$	K	0.0083 ± 0.002	···	···	Isolated $J=1$	j
				0.087		h
$V_{cp-\text{in}}$	K	−0.021	···	···	$p\equiv$ pair of $J=1$ molecules	g
		0.0068				e
$V_{cp-\text{out}}$	K	−0.0082	···	···		e
		0.0068	···	···		g
$V_{\Delta B-\text{in}}$	K	0.0075				g
$V_{\Delta B-\text{out}}$	K	−0.0158	···	···		g

[a] Silvera *et al.* (1978).
[b] Bostanjoglo and Kleinschmidt (1967).
[c] Birnbaum and Poll (1969).
[d] Goldman (1979).
[e] Hardy *et al.* (1977).
[f] Silvera *et al.* (1971).
[g] Luryi and van Kranendonk (1979).
[h] Roberts *et al.* (1976).
[i] Krause and Swenson (1979).
[j] Schweitzer *et al.* (1979).

molecular centers with respect to the crystalline frame as shown in Fig. 5, and $l_1+l_2=1$. The pure EQQ interaction, Eq. (3.15), becomes

$$\phi_{\text{EQQ}}(R_{12})=(20\pi/9)(70\pi)^{1/2}\Gamma_{12}\sum_{M,N}C(224;MN)\times Y_{2M}(\Omega_1)Y_{2N}(\Omega_2)Y_{4,M+N}(\Omega_{12})^*. \quad (3.17)$$

This form is also very useful in performing lattice sums.

From the theoretical side ϕ_A is expected to be dominated by ϕ_{EQQ}. Let us now consider the experimental picture. The coefficient $\varepsilon_4(R)$ in Eq. (3.14) has been determined in the solid at zero pressure. In interpreta-

TABLE IX. Electrical quadrupole–quadrupole interaction energy normalized to the coupling constant Γ. The classical case corresponds to quadrupoles with fixed orientations along the molecular symmetry axes; the semiclassical to the substitution of $\overline{Q}=2/5Q$ corresponding to the average of Q in the $J=1$ rotational state. This reduces the energy by 4/25. Quantum-mechanical refers to the energy of an isolated pair of molecules, each in the $J=1$ rotational state; the states are identified in Fig. 12. BD is a special configuration in which the two molecules are oriented along different body diagonals in a cubic lattice. This is of importance in discussions of the orientationally ordered state of H_2. This orientation is not an eigenstate for a pair. The QM value is determined within a molecular field approximation (James and Raich, 1967).

Configuration	Classical $\langle Q\rangle=Q$	EQQ Energy/Γ Semiclassical $\langle Q\rangle=\overline{Q}=\frac{2}{5}Q$	State	Quantum–mechanical
T	−12.5	−2	8, 9	−4
X	3.125	$\frac{1}{2}$	4, 5, 6, 7	0
H	9.375	$\frac{3}{2}$	2, 3	1
L	25.0	4	1	6
BD	−6.60	−19/18 = −1.056	BD Mol field	−1.056

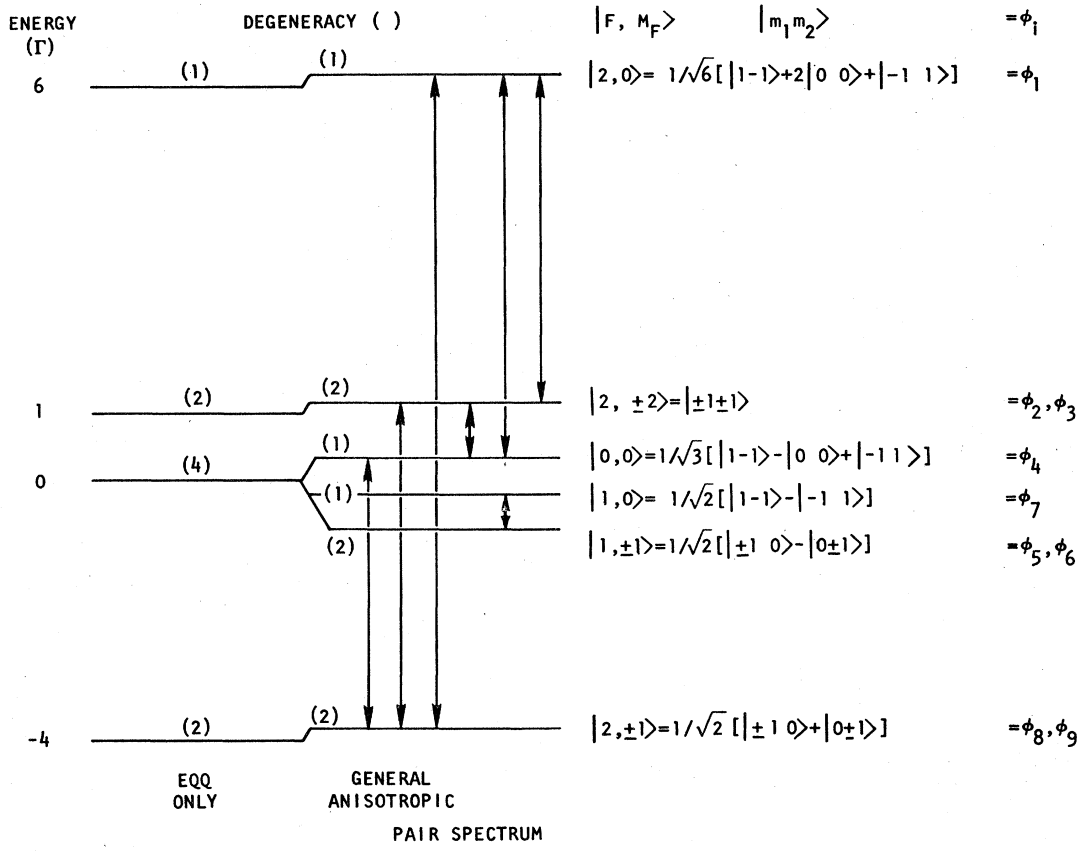

FIG. 12. The energy level diagram of a pair of neighboring $J=1$ molecules in the hcp solid showing the effects of an EQQ and a cylindrically symmetric (cs) (general anisotropic) interaction. Non-cs interactions can completely lift the degeneracy. Arrows indicate Raman active transitions. All transitions are ir active (depending on the orientation of the pair axis in the solid). The quantum number for the end-over-end rotation of the pair does not appear as this degree of freedom is constrained by the lattice.

tions, this has usually been attributed to the permanent EQ moment, so that $\varepsilon_4(R)=\frac{5}{6}\Gamma(R)$ with $\Gamma(R)=\frac{6}{25}e^2Q^2/R^5$. The experimental value of $\Gamma\equiv\overline{\Gamma}$ in the solid is 0.828 K in H_2 (Hardy *et al.*, 1977) and 1.026 K in D_2.[7] We see (Table VIII) that $\overline{\Gamma}$ is about 15% smaller than Γ_0, the value found by evaluating at $R=R_0$, and referred to as the rigid lattice value. We write

$$\overline{\Gamma}=\xi\Gamma_0\,, \tag{3.18}$$

where ξ is the solid reduction factor and $\overline{\Gamma}$ is referred to as the effective coupling constant in the solid and can also include non-EQQ contributions. Values are given in Table VIII. Harris (1970) (see also Noolandi and Van Kranendonk, 1970) proposed that the reduction arises from zero-point motional effects which weight $Y_{4m}R^{-5}$ in such a way that $R^{-5}\neq R_0^{-5}$. Zero-point averages are determined by evaluating the expectation value of the interaction in the ground translational state of the solid (see Sec. VIII). Such an average of Eq. (3.17) has the effect that Γ can be replaced by

$$\langle\Gamma\rangle=\xi_{54}\Gamma_0\,, \tag{3.19}$$

where the 5 refers to the power of R and the 4 to the order of the spherical harmonic that is involved in the average. Although these averages can be performed quite accurately from a computational point of view, knowledge of the many-body ground state wave function has limited the precision of ξ_{54}. Until recently it was believed that $\xi_{54}=0.905$ for H_2 and 0.94 for D_2 (at zero pressure). However, Goldman (1979) has reconsidered the pair distribution function of the solid and finds $\xi_{54}=0.94$ for H_2 and 0.968 for D_2 at zero pressure. This is a rather significant change when compared to the precision of present measurements ($\sim10^{-3}\text{cm}^{-1}$). Indeed, one sees that $\langle\Gamma\rangle\neq\overline{\Gamma}$ and the ε_4 term of the potential must have small valence and dispersion contributions, in addition to that due to the permanent EQ moment. More accurately, one has

$$\varepsilon_4(R)=\varepsilon_4^{\text{EQQ}}(R)+\varepsilon_4^{\text{v}}(R)+\varepsilon_4^{\text{di}}(R)\,. \tag{3.20}$$

In the zero-pressure solid, $\varepsilon_4^{\text{v}}+\varepsilon_4^{\text{di}}$ must reduce $\varepsilon_4^{\text{EQQ}}$ by 5%–10% to explain the discrepancy. The non-EQQ potential contributions have been considered in general by Nakamura (1970) who finds that ε_4^{v} and $\varepsilon_4^{\text{di}}$ have opposite signs and tend to cancel each other. More recently Ng *et al.* (1976) have considered the valence forces and

[7]For this value I have analyzed the results of Silvera *et al.* (1971), using the theory of Harris *et al.* (1977), estimating D_2 correction values from the H_2 results.

Mulder *et al.* (1978) have reexamined the long-range dispersion and induction forces. They find agreement with Meyer (1976) for the isotropic terms, but note that he omitted cross or mixed multipole terms which severely effect the anisotropic coefficients. At 6.5 a.u. they find the term ε_4^{di} to be 12% of ε_4^{EQQ} (and of opposite sign).

From the experimental side we can write

$$\bar{\Gamma}=\langle\Gamma\rangle+\tfrac{6}{5}\langle\Delta\varepsilon_4\rangle=\xi_{54}\Gamma_0+\tfrac{6}{5}\langle\Delta\varepsilon_4\rangle\equiv\xi\Gamma_0\,, \tag{3.21}$$

where $\langle\Delta\varepsilon_4\rangle$ is the contribution to ε_4 from sources other than the permanent EQ moment. Evaluating, we find $\langle\Delta\varepsilon_4\rangle/k_B=-0.057$ K for H_2 and -0.094 K for D_2. Probably the largest source of error here is in the determination of $\bar{\Gamma}$ for D_2. We note that these values are for the zero-pressure solids in the limit that C_1 goes to zero. A precise analysis of the $J=0\rightarrow 2$ roton spectrum would provide additional and useful information for pinning down the potential parameters. Noolandi (1970) has analyzed the roton frequencies; however, his analysis is incomplete, as a non-negligible contribution from the interaction with two and three roton states has not been treated.

The terms ε_0 and ε_2 of Eq. (3.14) have also been determined from the microwave absorption experiments in solid H_2 at zero pressure. The analysis of the spectrum is quite complex. It was first considered by Hardy and Berlinsky (1975), who found the existing theory to be incomplete. Harris *et al.* (1977) extended the theory by examining a number of subtle and complex contributions. More recently Luryi and van Kranendonk (1979) have also analyzed the spectrum and made some additions and corrections to the analysis of Harris *et al.* We use their values in Table VIII.

Let us consider in greater detail the crystal field which arises from the term $B(R_{12})$ in Eq. (3.14). For a $J=1$ molecule at site 1, the crystal field arises from the interaction with the spherical part of all surrounding molecules given by

$$\phi_c=\sum_i(16\pi/5)^{1/2}B(R_{1i})Y_2^0(\omega_1)\,, \tag{3.22a}$$

where ω_1 specifies the orientation of the molecule in the $\mathbf{R}_{1i}$ frame. To evaluate ϕ_c one transforms from the $\mathbf{R}_{1i}$ frame to a coordinate system where the z axis is along the c direction of the (hexagonal) crystal (see Fig. 5). This is easily done with the spherical harmonic addition theorem (Rose, 1957) to find

$$\phi_c=\sum_m Y_{2m}(\Omega_1)\sum_i\tfrac{8}{5}\pi B(R_{1i})Y^*_{2m}(\Omega_{1i}). \tag{3.22b}$$

Due to the hexagonal symmetry $Y_{2m}(\Omega_{1i})=Y_{2m}(\Omega_{1i})\delta_{m0}$ in (3.22b) and we have

$$\phi_c=(\tfrac{4}{5}\pi)^{1/2}Y_{20}(\Omega_1)\sum_i\tfrac{16}{5}\pi)^{1/2}B(R_{1i})Y_{20}(\Omega_{1i})\,. \tag{3.22c}$$

Finally, we note the c axis is the axis of quantization and use operator equivalents in the $J=1$ manifold of states (Nakamura, 1955) to write $Y_{20}(\Omega_1)\rightarrow 1/\sqrt{5\pi}\,(\tfrac{3}{2}J_z^2-1)$ yielding

$$\begin{aligned}\phi_c&=[-\sum_i\tfrac{6}{5}B(R_{1i})(\tfrac{4}{5}\pi)^{1/2}Y_{20}(\Omega_{1i})](J_z^2-\tfrac{2}{3})\\&\equiv V_c(J_z^2-\tfrac{2}{3})\,.\end{aligned} \tag{3.22d}$$

With this definition, V_c is the splitting between the $J_z=0$ and ± 1 states.

In a rigid close packed hexagonal structure the sum over $Y_{20}(\Omega_{ij})$ in Eq. (3.22d) is zero when restricted to the first two shells of neighbors. As a result the crystal field is essentially zero. In a hexagonal lattice, deviations of V_c from zero occur if $c/a\neq\sqrt{8/3}$. Furthermore, zero-point motion and rotation–lattice coupling can result in $V_c\neq 0$. In addition $B(R)$ for two $J=1$ molecules can differ from that of a $(J=1)$–$(J=0)$ pair. The lattice sum is then no longer zero and the resulting crystal field term is called $V_{\Delta B}$.

Raich and Kanney (1977) and Raich and Albert (1979) have calculated the crystal field for a single $J=1$ in a $J=0$ lattice and a nearest neighbor pair of $J=1$ molecules in a $J=0$ lattice, respectively. They determined the energy splittings of the rotational levels within the $J=1$ manifold due to the local lattice distortions (see Fig. 11). Luryi and van Kranendonk (1979) have subsequently considered the single $J=1$ impurity problem. They calculate V_c arising from differences in the zero-point motion for in-plane and out-of-plane pairs in the hcp lattice, as well as that arising from lattice distortions due to phonon–rotation coupling. They criticize the approach of Raich and Kanney (this is also applicable to the work of Raich and Albert), showing that the interaction Hamiltonian they used was incomplete, having omitted important terms. They also find that the rotation–lattice interaction mixes the $|J=1,M\rangle$ rotational states so that M is of course not a good quantum number, although the degeneracy imposed by the symmetry is not further lifted. Evidently, one must consider J, J_z given in Eq. (3.22d) to be an effective spin one Hamiltonian. Finally we point out that the crystal fields are not additive, i.e., the crystal field of a pair of $J=1$ molecules is not simply related to that of an isolated $J=1$ molecule. This can arise from distortion of the pair separation due to the EQQ interaction, cross terms in second-order perturbation theory, etc., as well as the $V_{\Delta B}$ effect already mentioned. The existence of two pair environments in the hcp lattice, in- plane and out- of- plane, also means that these pairs can have differing V_c's.

An experimental determination of $B(R)$ or V_c has turned out to be rather challenging. In the solid it is very small because of the lattice sum cancellation already discussed. This cancellation does not occur in molecular beam scattering experiments and Zandee *et al.* (1976) have used polarized H_2 beams to find B/k_B ~2 K. This value is characteristic of the region of the isotropic potential well minimum (~3.4Å); the beam measurements are not very sensitive to the radial dependence of $B(R)$.

For the case of an isolated $J=1$ molecule in a $J=0$ lattice V_c has been studied by an analysis of the free induction decay (FID) of NMR signal at low temperatures for samples with ortho-H_2 lightly doped in a para-H_2 host. Hardy and Gaines (1967) analyzed NMR FID data taken at 0.3 K in H_2 to find $|V_c|/k_B=0.0082\pm0.0021$, showing that $|V_c|$ was at least 5 times smaller than had been suspected; however, lower temperatures were required to ease the analysis. They were unable to determine the sign of V_c and thus determine if $J_z=\pm 1$ or 0

was the ground state. Constable and Gaines (1971) repeated these experiments at $T \simeq 0.045$ K and found $V_c/k_B = -0.023 \pm 0.015$ K, which would mean that the ground state was $J_z = \pm 1$. The most recent work by Gaines *et al.* (1978) was on a sample which they believed to be single crystal. They found that an accurate analysis of the data to determine V_c depends critically on the crystal orientation; in earlier experiments the state of the crystal (single—or powder) was unknown. They find $V_c = +0.040$ K, which "can be considered to be reliable to within a factor of two." These results would mean that $J_z = 0$ is the ground state.

The most recent, and probably the most reliable determination of V_c is by Schweitzer *et al.* (1978, 1979), who studied single crystals of hydrogen with $C_1 < 0.01$ at temperatures as low as 18 mK. In their first paper they reported a value $|V_c|/k_B = 0.025$ K which was corrected in an erratum to 0.014 K due to a calculational error. Their most recent and more refined measurements have settled down to $|V_c|/k_B = 0.0083 \pm 0.002$ K.

Pedroni *et al.* (1975) and Buzerak *et al.* (1977) interpret their study of NMR linewidth as a function of density in terms of the crystal field. At zero-pressure density, $\rho = \rho_0$, Buzerak *et al.* found $|V_c/k_B| \leq 0.023$ K. This value increases by about a factor of 30 at $\rho/\rho_0 = 1.7$. The theory of Raich and Kanney (1977) discussed earlier agrees well with the experiment, perhaps fortuitously.

We believe that the measurements by Schweitzer *et al.* are the most reliable. Nevertheless, determination of V_c by an alternate technique, sensitive also to the sign of the interaction, is in want. A critical experiment would be the direct determination of V_c by rf absorption or by Raman scattering, both of which are, in principle, feasible.

In the case of an isolated pair of $J = 1$ molecules, we write

$$\phi_{cp} = V_{cp}\left[3J_{z1}^2 + 3J_{z2}^2 - \tfrac{4}{3}\right]. \tag{3.23}$$

A similar expression exists for the $V_{\Delta B}$ term. The $V_{\Delta B}$ term is cylindrically symmetric about the pair axis, whereas the V_{cp} term can have a lower symmetry and a different quantization axis. As a further complication, as mentioned earlier, V_{cp} can differ for in- and out-plane pairs.

In the case of the ioslated pairs of $J = 1$ molecules, determination of V_{cp} has come from analyses of microwave absorption experiments (Hardy and Berlinsky, 1975). The spectrum is quite complex. Hardy *et al.* (1977) interpreted the microwave spectrum with a fit using a single crystal field term, $V_{cp}/k_B = 0.014$ K. Luryi *et al.* (1977) also interpreted the spectrum finding values of $V_{\Delta B}$ and V_{cp} for the two types of pairs. Harris and Berlinsky (1977) compared the two theories, criticizing the latter on a number of points, also showing that it gave poor agreement with a pair transition not measured in the microwave work, but observed in Raman scattering experiments by Silvera *et al.* (1971). Luryi and van Kranendonk (1977) have presented refinements in the theory, which differs from that of Harris *et al.* in that V_{cp} differs for the two types of pairs, and they consider effects of anisotropy in the pair correlation function. In the refined theory there is also agreement with the Raman transition. Their values are given in Table VIII.

In recapitulation, experiments show that in the zero-pressure solid the anisotropic interactions are dominated by the EQQ interaction. Nevertheless the determination of the smaller interaction constants is a useful and challenging pursuit. This should become easier as density increases. Berkhout and Silvera (1977) and Berkhout (1978) have shown that, up to densities $\rho/\rho_0 \simeq 1.8$, the anisotropic interactions are still dominated by EQQ forces which vary as $\rho^{5/3}$. As we have mentioned, Pedroni *et al.* (1975) showed that at these densities V_c increases by a factor of 30, making it a simpler quantity to measure. However, as the anisotropic interactions increase at still higher densities, other complications set in as J can no longer be treated as an approximately good quantum number. Finally we consider the values of ε_0, ε_2, and the crystal field terms, all given in Table VIII, to be tentative, as the values depend critically on renormalization factors which Goldman has recently shown to be different than those used in the analyses.

IV. THE ROTATIONAL STATE IN THE SOLID

In Sec. VIII we shall discuss the motion of quantum solids, i.e., solids in which the lattice particles have a large zero-point motion or a broad spatial distribution around the lattice sites. Such a motion can also be used to classify solids with orientational order (Silvera, 1978). Orientational quantum solids are molecular solids in which, even at $T = 0$, the angular distribution is broad, or nonlocalized. Molecular hydrogen and its isotopes are the most extreme (and only) examples. H_2 is an almost free rotor in the solid and in the ground rotational state has a fully spherical distribution; by contrast the symmetry axes of N_2 molecules are well localized at $T = 0$ K in the solid state.

Let us confine our attention to linear molecules with pairwise interactions. Then the Hamiltonian describing the solid is

$$\mathcal{H} = \sum_i \left(\frac{-\hbar^2\nabla_i^2}{2m} + BJ_i^2\right) + \tfrac{1}{2}\sum_{i\neq j}\phi_I(ij) + \tfrac{1}{2}\sum_{i\neq j}\phi_A(ij), \tag{4.1}$$

where ϕ_I and ϕ_A were defined in the previous section. To demonstrate why H_2 is a free rotor in the solid let us set $\phi_A = 0$ and study two neighboring molecules, 1 and 2, ignoring the rest of the lattice. We solve the pair wave equation

$$\left\{\frac{-\hbar^2}{2m}[\nabla_1^2 + \nabla_2^2] + B(J_1^2 + J_2^2) + \phi_I(r_{12})\right\}|\psi\rangle_0 = E|\psi\rangle_0. \tag{4.2}$$

The wave function is separable,

$$|\psi\rangle_0 = |\psi(\Omega_1)\rangle\,|\psi(\Omega_2)\rangle\,|\psi(r_1, r_2)\rangle, \tag{4.3}$$

and the solution of the angular part is that of the well known free rotor with $E = B\sum_{i=1,2} J_i(J_i+1)$ where $B = \hbar^2/2I$. J_i is the rotational quantum number and the rotational wave function is the spherical harmonic $Y_{J_iM_i}(\theta_i, \phi_i)$ which we specify as $|J_iM_i\rangle$. Thus returning to the many-body solid we have an assembly of free rotors localized at lattice sites to within the translational zero-point motion of the molecules. For the lowest rotational state, with all molecules in the $J = 0$ state, the rotational part of the solid wave function is a product

state of $Y_{00}(\Omega_i)$'s. Since Y_{00} is a constant the angular distribution is spherically symmetric, i.e., the molecules are not at all angularly localized. For each level Y_{JM}, all $(2J+1)$ of the M sublevels will be equally populated and again there is no localization.

To see how valid this picture is, we now remove the restriction $\phi_A = 0$. Then if ϕ_A is small we can use first-order perturbation theory to correct the zeroth order wave function, which we write as a product of free rotor states:

$$|J_1 M_1 \ldots J_N M_N\rangle_0 = |J_1 M_1\rangle \ldots |J_N M_N\rangle .$$

The many-body perturbed wave function is then

$$|J_1 M_1 \ldots J_N M_N\rangle = |J_1 M_1 \ldots J_N M_N\rangle_0 + \sum \frac{{}_0\langle J_1' M_1' \ldots J_N' M_N' | \frac{1}{2} \sum_{i,j} \phi_A(ij) | J_1 M_1 \ldots J_N M_N\rangle_0 |J_1' M_1' \ldots J_N' M_N'\rangle_0}{E_{J_1 \ldots J_N} - E_{J_1' \ldots J_N'}} . \tag{4.4}$$

Because the anisotropic interaction ϕ_A is a two-particle interaction we can focus our attention on a two-particle wave function and confine ourselves to the dominant EQQ anisotropic interaction

$$|J_i M_i J_j M_j\rangle = |J_i M_i J_j M_j\rangle_0 + \sum_{\substack{J_i' M_i' \\ J_j M_j}} \frac{{}_0\langle J_i' M_i' J_j' M_j' | \phi_{\mathrm{EQQ}}(ij) | J_i M_i J_j M_j\rangle_0 |J_i' M_i' J_j' M_j'\rangle_0}{E_{J_i J_j} - E_{J_i' J_j'}} , \tag{4.5}$$

where

$$E_{J_i J_j} - E_{J_i' J_j'} = B[J_i(J_1+1) + J_j(J_j+1) - J_i'(J_i'+1) - (J_j'(J_j'+1)] \tag{4.6}$$

and $J_i, J_j \neq J_i', J_j'$. Using Eq. (3.15) for the EQQ interaction we see that the coefficient of $|J_i' M_i' J_j' M_j'\rangle$, or the mixing parameter, is proportional to Γ_{ij}/B which has a value of 0.011 for H_2 and 0.028 for D_2 for nearest neighbors in the zero-pressure solid. When we take into account the 12 nearest neighbors in the solid and the numerical values of the matrix elements and energy denominators we still find about 1% mixing of rotational states in H_2.

Berkhout and Silvera (1977) tested the validity of these considerations by Raman scattering. The Raman scattering efficiency is proportional to the matrix elements.

$$|\langle J_i' M_i' \ldots J_N' M_N' | \sum_i \alpha_1^{2m}(i) | J_1 M_1 \ldots J_N M_N\rangle|^2$$

where α_1^{2m} is given by Eq. (2.25a). For unmixed states the selection rules are $\Delta J_i = 0, \pm 2$, $\Delta M_i = 0, \pm 1, \pm 2$. In the solid, one expects to see the transition $J=0 \rightarrow 2$, $J=1 \rightarrow 3$ and $J=1 \rightarrow 1$, $\Delta M \neq 0$ at frequency shifts corresponding to $6B$ and $10B$, and a band centered around zero frequency shift, respectively. In Fig. 13 we see the results of Raman scattering experiments on H_2 and D_2 under a moderate pressure and at nominal ortho–para concentrations. In addition to the allowed transitions, very weak transitions are seen at integral values of B. These correspond in part to double transitions of pairs of molecules due to mixing and are identified by the initial and final rotational states of a pair, $|J_i J_j\rangle \rightarrow |J_i' J_j'\rangle$. The intensity and selection rules for these double transitions follows directly by substituting the mixed wave functions, Eq. (4.5), into the Raman matrix element. In addition there is a small contribution to the Raman scattering from a perturbation to the polarizability so that

$$\alpha_{\mathrm{crystal}} = \sum_i \alpha(i) + \sum_{i,j} \alpha(i,j) , \tag{4.7}$$

where the two-particle term arises from intermolecular interactions. We shall not discuss this effect, referred to as BIPA (breakdown of the independent polarizability approximation). However, the second term in Eq. (4.7) also gives rise to double transitions.

The ratio of the intensities, I, of the forbidden to the allowed transition enables a determination of the admixture of the free rotor states. For double transitions due to mixing $I \sim (\Gamma/B)^2 \sim \rho^{10/3}$, where ρ is the density. The dependence of mixing on density, relative to that at zero pressure, ρ/ρ_0, was also studied and is shown in Fig. 14 for the $|01\rangle \rightarrow |23\rangle$ transition. One finds a reasonably good accord between theory and observation supporting the use of J as a good quantum number, even to pressures of order 5 kbar. The theoretical curves used are for a rigid lattice and do not include the zero-point motion renormalization which would lower the curves to give better agreement with experiment. We see that mixing is a larger effect in D_2, as expected, since $B_{D_2} \simeq \frac{1}{2} B_{H_2}$. Eventually, as pressure increases, the anisotropic interactions will become large enough to severely mix the free rotor states and para-H_2 and ortho-D_2 will no longer be spherically symmetric. One result of this will be discussed at the end of Sec. VI.

In the coming sections we shall discuss the orientational ordering in $J=1$ H_2 and D_2. At low temperatures the molecules align along certain crystalline directions due to the weak anisotropic interactions. However, J can still be treated as a good quantum number. In the ordered state the molecules are in a $J=1$, $M=0$ state where the direction of quantization for M is the ordering axis. It is the wave function orbital $\psi \sim Y_{10}(\omega) \sim \cos\theta$ that orders and not the molecular axis. By contrast, in solid nitrogen, $B \simeq 2$ cm^{-1} and $\langle \phi_A \rangle / B \simeq 8$. Here it is more accurate to consider the ordering of the molecular axes. In the extreme case of a "rigidly" oriented molecule, the wave function is $\psi \sim \delta(\omega - \omega_0)$. The angular delta function can be written as an infinite sum over all spherical harmonics, showing that in such a case all J's are admixed.

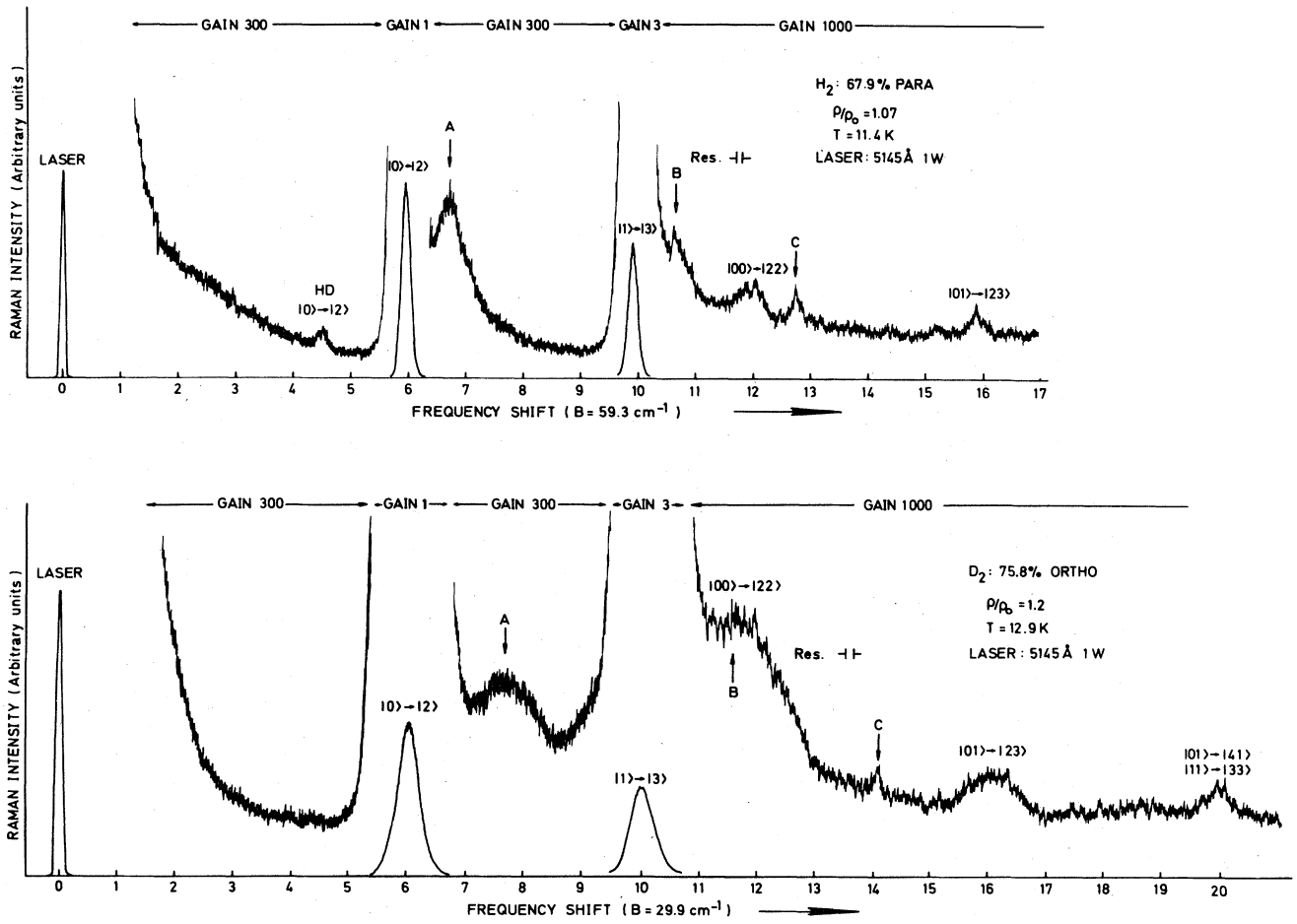

FIG. 13. Typical Raman spectra for solid H_2 and D_2 showing allowed ($|J\rangle \rightarrow |J'\rangle$) and forbidden ($|J_1J_2\rangle \rightarrow |J_1'J_2'\rangle$) transitions. Features A and B are phonon sidebands; c arises from sapphire cell windows. $B_{H_2} = 59.3\ \text{cm}^{-1}$; $B_{D_2} = 29.9\ \text{cm}^{-1}$ (figure after Berkhout and Silvera, 1977).

V. ORTHO AND PARA SPECIES: PREPARATION, CONVERSION, AND DIFFUSION

In this section we shall discuss in some detail the preparation, conversion, and diffusion of ortho–para species. Not only is this a fascinating subject, but control of the concentration can be a key to a successful experimental research program. In Sec. III, we discussed the symmetry classification of the molecules into the ortho and para species (see Table V). As we shall see, the ortho–para molar concentration of the hydrogens has a profound influence on the low-temperature behavior in the solid state. The thermodynamic equilibrium concentrations for even rotational states, ρ_e, and odd rotational states,[8] ρ_o, are given by (see, for example, Hill, 1960)

$$\rho_e = \frac{g_I^e}{Z} \sum_{J=0,2,\ldots} (2J+1)\exp(-E_J/kT)\,, \tag{5.1a}$$

$$\rho_o = \frac{g_I^o}{Z} \sum_{J=1,3,\ldots} (2J+1)\exp(-E_J/kT)\,, \tag{5.1b}$$

with

$$Z = g_I^e \sum_{J=0,2,\ldots} + g_I^o \sum_{J=1,3,\ldots}\,, \tag{5.1c}$$

where the g_I are the nuclear weights or degeneracies given in Table V and E_J is the rotational energy which can be approximated by the first term in Eq. (2.16) (see Table IV). The *equilibrium* concentrations for H_2 and D_2 are plotted in Fig. 15. In the high-temperature limit $\rho_o/\rho_e = 3$ for H_2 and $\frac{1}{2}$ for D_2, whereas these ratios go to zero as $T \rightarrow 0$. We see that room temperature equilibrium hydrogen, referred to as *normal-H_2*, is essentially in the high-temperature limit with $\rho_o = 0.749$ (for normal-D_2, $\rho_o = 0.333$). In the following we shall also refer to the nonequilibrium concentration of even molecules by c_e and odd molecules by c_o.[9]

[8] Note in Table V that para-H_2 and ortho-D_2 refer to even rotational states and ortho-H_2 and para-D_2 to odd rotational states. To achieve a uniform notation, we here refer to the odd and even nature of the rotational states.

[9] One also frequently encounters the notation $c \equiv x$ for molar concentration and, e.g., $x_1 \equiv c_1$ for the molar concentration of the $J=1$ species.

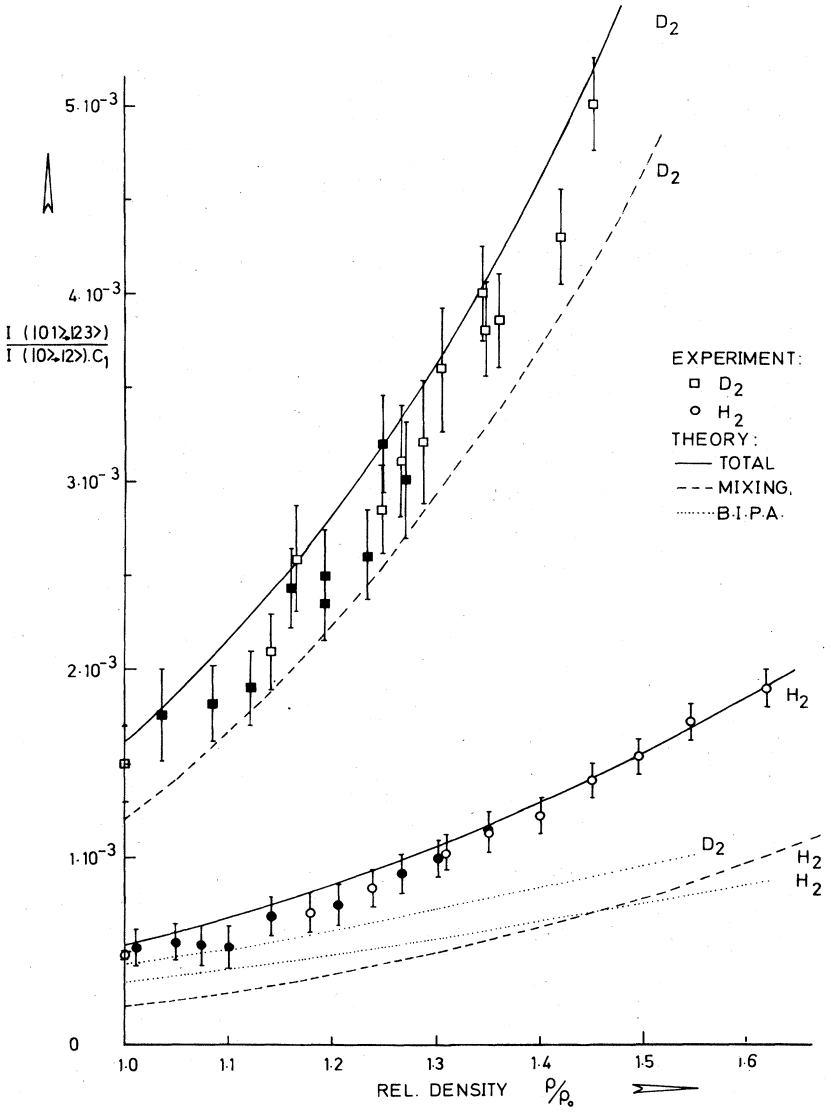

FIG. 14. Normalized integrated intensity of forbidden pair transition $|J_1J_2\rangle = |0,1\rangle \rightarrow |2,3\rangle$ as a function of density normalized to zero-pressure density. Various theoretical contributions are shown by the drawn lines. c_1 is the concentration of $J=1$ species.

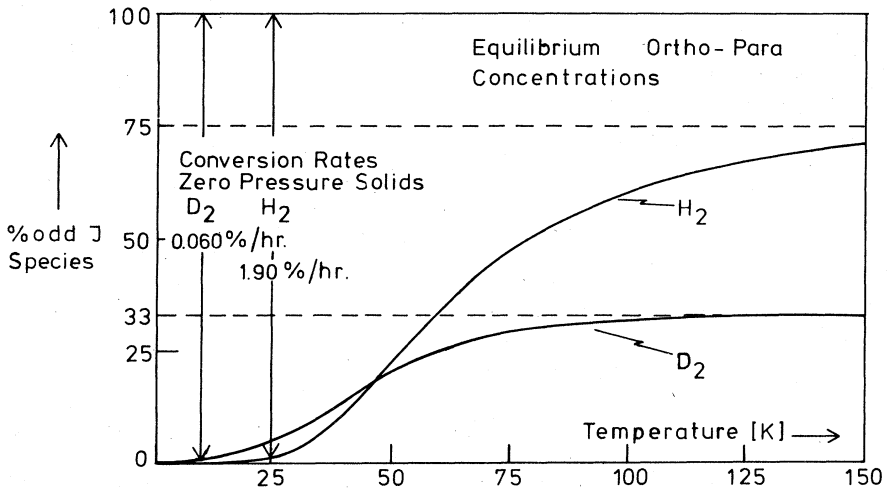

FIG. 15. Equilibrium ortho–para concentration of noninteracting hydrogen and deuterium as a function of temperature.

A transition from an ortho to a para state in the hydrogens is called *conversion*. For isolated or noninteracting molecules, conversion is forbidden. As the temperature is varied, the population of the respective even or odd states varies due to interactions between molecules which can cause conversion. For hydrogen, a magnetic field gradient (to be discussed later) can catalyze the transition, whereas for deuterium a magnetic or an electric field gradient will suffice. If a H_2 molecule is converted by the magnetic field gradient due to the magnetic dipole moment on another H_2 molecule, then the conversion is *intrinsic* or homogeneous. In the solid state at zero pressure intrinsic conversion towards equilibrium takes place with a rate constant of 1.90%/h for H_2 and .060%/h for D_2. In the low-density gas phase conversion is extremely slow and accurate values are not known as measurements are usually perturbed by walls or magnetic contaminants such as O_2. Out-of-equilibrium samples of H_2 at NTP will typically convert a percent or two in a week's time; properly stored samples of D_2 at ~NTP have been known to show little change in the period of one year.

As a result of the slow conversion rates, if out-of-equilibrium samples are prepared they will remain so metastably for long enough periods of time to allow detailed studies.

A. Preparation of nonequilibrium ortho-para samples

Techniques exist for preparing the hydrogens in concentrations >99% even-J to >99% odd-J species. We shall describe these techniques. Intermediate concentrations can be obtained by mixing measured amounts of gas of known concentrations.

1. High-purity even-J species

The even-J species can be prepared by cooling samples and allowing them to convert to equilibrium. At 20.4 K the temperature of liquid hydrogen at 1 atmosphere pressure) equilibrium concentration is 0.998 para-H_2 and 0.978 ortho-D_2. Normal-H_2, when liquified, will be strongly converted after several days, but to approach equilibrium would require weeks. This can be greatly accelerated by bringing the hydrogen in contact with a paramagnetic salt which acts as a catalyst. The H_2 comes in contact with the surface, and strong magnetic field gradients arising from electronic magnetic moments on ions at the surface of the salt catalyze conversion with time constants of order seconds to minutes. These processes are first order and the approach to equilibrium is exponential with the rate equation in

$$\frac{dc_e}{dt} = -K_1 \frac{(c_e - \rho_{eq})}{1 - \rho_{eq}}, \tag{5.2}$$

where c_e is the concentration of even rotational species, ρ_{eq} is its equilibrium value, and K_1 is the even → odd rate constant. Two commonly used salts are ferric oxide gel and Apachi nickel silica gel.[10] The latter is apparently the most efficient. The salts must be activated to work effectively. We activate the Apachi salt by heating to 150–175 °C for a few hours and flowing a slow stream of H_2 gas over the catalyst. The activation removes adsorbed water and air which evidently saturates the active magnetic surface sites, "poisoning" the catalyst. Apachi has an effective surface area of 500–600 m^2/g.

The most efficient conversion technique is to adsorb about a monolayer of gas on the catalyst and then desorb. A convenient geometry, in the form of a long stainless steel wand (tube) of order 1 cm in diameter and 70–100 cm in length, as shown in Fig. 16, is employed. The catalyst is confined between fine screens. The wand is immersed in a bath at ~20 K (liquid hydrogen is an ideal cryogen). H_2 or D_2 is flown in the gas inlet (several liters NTP are adsorbed) to a pressure of a few cm Hg. For H_2, the wand is then slowly withdrawn from the bath desorbing the gas which flows out the inner tube, always having its last contact with the catalyst at 20.4 K. If the bottom of the wand comes out of the cryogen and warms up during desorption the yield of high-purity even J will be reduced, as the last part of the gas will be at a higher equilibrium temperature. The converted gas can be produced up to pressures of order 1 atm when desorbing. This pressure cannot be achieved for D_2 at 20.4 K as it will liquify with a vapor pressure of 26.6 cm Hg. In the drawing of Fig. 16, the small reservoir at the bottom of the wand serves to collect the converted liquid D_2; in withdrawing the wand, it can be boiled off to a pressure of order 1 atm for storage.

Out-of-equilibrium samples must be stored in containers free of magnetic impurities. Pyrex bulbs can be used for this purpose if they are baked to ~400 °C and pumped to remove oxygen impurities. The ortho–para concentration can be determined by use of an ana-

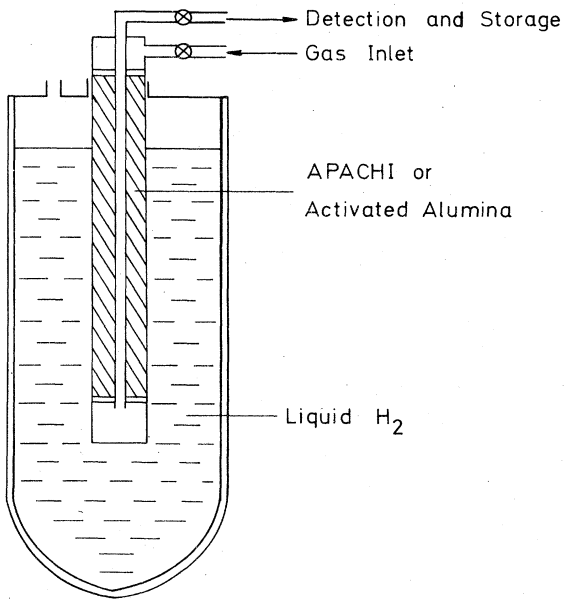

FIG. 16. Cryostat and wand for use in the preparation of high concentration ortho or para H_2 or D_2.

[10] Apachi Nickel-Silica catalyst No. 197-CP. Manufacturer: Houdry, Division of Air Products and Chem. Inc., Philadelphia, Pennsylvania.

lyzer based on the difference in thermal conductivity of the ortho–para species (Grilly, 1953). A pair of matched Pirani vacuum gauges are placed in a bridge circuit which is balanced with both gauges filled with normal-H_2. One arm is then evacuated and filled with the sample of unknown concentration. If the bridge is operated at liquid nitrogen temperatures, where the difference in thermal conductivity of the two species is large, a bridge imbalance that is almost linear in concentration and large enough to measure with an accuracy of order 1% will be achieved.

Thermal conductivity bridges can be calibrated with samples with a known concentration prepared by catalysis at a known temperature. This requires some consistency checks to be assured that the catalyzer is operating properly. A direct determination of the concentration can be made by means of Raman scattering. In this case, the Raman scattering efficiency, $S(i \to f)$ is proportional to

$$S(J \to J+2) \sim \omega\omega'^3 \sum_{if} P_i \left|\langle f \left|\alpha_{\text{anis}}\right| i\rangle\right|^2 \delta(\omega_s - \omega_{if}) , \quad (5.3)$$

where ω is the frequency of the incident light, ω' that of the scattered light, ω_{if} is the frequency shift, P_i is the probability that the initial state is occupied, and α_{anis} is the anisotropic polarizability of the gas. P_i is given by

$$P_i = e^{-E_i/kT} / \sum_{\substack{J \text{ even} \\ \text{or} \\ J \text{ odd}}} (2J+1)\exp(-E_J/kT) , \quad (5.4)$$

where the even sum is taken for even i and odd for odd i.

The matrix element of the gas is proportional to $c_e\rho$ for even molecules and $(1-c_e)\rho$ for odd molecules times the matrix element for a single molecule (ρ is the number density of the gas). Evaluation of the matrix element yields

$$\frac{S(0\to 2)}{S(1\to 3)} = \frac{5}{3}\frac{c_e}{1-c_e}\left(\frac{\omega-\omega_{02}}{\omega-\omega_{13}}\right)^3 \left\{\frac{1+\frac{7}{3}e^{-10B/kT}+\cdots}{1+5e^{-6B/kT}+\cdots}\right\} . \quad (5.5)$$

Calling the quantity in the curly brackets τ, we find

$$c_e = \frac{S(0\to 2)/S(1\to 3)}{S(0\to 2)/S(1\to 3) + \frac{5}{3}\tau[(\omega-\omega_{02})/(\omega-\omega_{13})]^3} . \quad (5.6)$$

For $kT \ll 6B$, $\tau = 1$. At $T = 293$ K $\tau = 0.597$ for H_2 and 0.447 for D_2.

Ortho–para concentration measurements can also be made by NMR, monitoring the signal strength arising from one of the nuclear species. However, this also requires calibration with a sample of known concentration.

As a final comment we note that although $c_e = 0.998$ for H_2 is usually sufficient for high-purity even-J samples, $c_e = 0.978$ for D_2, catalyzed at 20.4 K, can be inadequate. By catalyzing at ~18.7 K, the melting temperature of D_2, c_e can be increased substantially to 0.985. A technique of achieving even higher purities will be suggested at the end of the next section.

2. High-purity odd-J species

At first view of Fig. 15 of the equilibrium concentrations of H_2 or D_2 it would seem impossible to produce concentrations of o-H_2 higher than 75%, or of p-D_2 higher than $33\frac{1}{3}$%, without the aid of a Maxwell's demon. However, Sandler (1954) first noted that at low temperature the ortho–para concentration ratio of H_2 adsorbed on TiO_2 was greater than that of the gas reservoir from which it was adsorbed. Cunningham *et al.* (1958) used this preferential adsorption on γ-alumina at 20.4 K to produce enriched o-H_2 and p-D_2 in the gas phase. The technique was further developed by Depatie and Mills (1968), who used Alcoa activated alumina[11] (AAA).

In order to be effective for enrichment, the separation coefficient, defined as

$$S = (c_o^a/c_e^a)/(c_o^g/c_e^g) , \quad (5.7)$$

must be greater than 1, where c_o^a/c_e^a is the ratio of the adsorbed mole fraction of odd and even rotational states, and c_o^g/c_e^g is the corresponding ratio in the gas phase. Silvera and Nielsen (1976) measured $S = 39^{+2}_{-8}$ for H_2 and $S = 5.0 \pm 0.3$ for D_2 on AAA.

The enrichment process of Depatie and Mills can be described with the help of Fig. 16, with the wand filled with AAA. At 20.4 K, the AAA is saturated with normal H_2, and at a pressure of about 4 cm Hg, n-H_2 is slowly flown through the wand. The effluent, which is continually monitored for concentration, is initially rich in even J, as the odd J is "leached" by the AAA. Eventually the system will come into steady state with n-H_2 entering and leaving the wand, and the adsorbed H_2 enriched by the separation coefficient (in steady state equilibrium with n-H_2 at 20.4 K). It is important to flow the gas slowly enough so that molecules can exchange between the gas and surface and come into equilibrium. At this point the inlet valve is closed and the wand is slowly (a few cm/minute) withdrawn from the bath. Enriched H_2 desorbs from the top and passes down the column, further enriching the adsorbed H_2. Finally there remains only a highly enriched zone of adsorbed H_2 which is detected by the ortho–para analyzer at the outlet. When this is achieved a valve is opened to a storage bulb and the wand is rapidly withdrawn, desorbing the high-purity ortho-H_2. This process can yield ~5 l NTP (depending on the volume of AAA) of purity ~0.99 ortho-H_2 and 0.98–0.99 para-D_2. It is important to withdraw the wand slowly enough to allow gas–surface molecular exchange. However, too slow a withdrawal results in a reduced yield or purity due to slow back conversion on the surface, evidently due to magnetic impurities.

AAA must be activated by heating to ~125 °C and pumping or flowing H_2 to carry off the desorbed gas. An x-ray analysis has identified its main constituents as χ-Al_2O_3 and γ-AlOOH (Silvera and Nielsen, 1976).

B. Enrichment mechanisms

In order to have preferential adsorption, it is necessary that the adsorbed molecules have rotational energy levels different than those in the gas phase. This means that the H_2–surface interaction must be anisotropic, and to be effective the anisotropic potential barrier must be of the order or greater than the rota-

[11] Alcoa Chemicals, activated alumina grade F-1, mesh 8-14.

tional constant, B. To calculate the separation coefficient S, we assume that there is no conversion in the gaseous or adsorbed molecules. Then we have two independent systems. The odd species in the gas must be in equilibrium with those on the surface and likewise for the even species. If the surface energy states are known, the ratios ρ_o^a/ρ_o^g and ρ_e^a/ρ_e^g can be calculated using expressions of the form Eq. (4.1). Sandler (1954) suggested that the molecules might be confined to rotation in two dimensions (2-D). The rotational energies are easily shown (Eyring *et al.*, 1944) to be given by $E_m^{2D} = Bm^2$ where $m = 0, \pm1, \pm2, \ldots$ (even-m functions are symmetric and odd-m functions are antisymmetric). For ideal 2-D rotor surface states, one finds $S = 43.8$ for H_2 and 5.45 for D_2. White and Lassetre (1960) attempted to explain early measurements of S using an axial surface barrier potential ϕ that would either have lowest surface energies if the molecules lay in the plane of the surface (2-D model for $\phi \to \infty$) or lowest if the molecular axis was confined to the barrier axis (1-D oscillator for $\phi \to \infty$). However, they could not fit the available data to either model. More recently, Silvera and Nielsen (1976) have made a microscopic study of the surface energy states by inelastic neutron scattering of H_2 on AAA. Due to its nuclear moment, the neutron can cause a conversion (ortho–para) transition. Measurements in solid para-H_2 show a peak in the $J = 0 \to 1$ inelastic group at an energy transfer $\Delta E = 2B$, corresponding to the 3-D energy levels $E = BJ(J+1)$. Scattering from H_2 adsorbed on AAA shows a broad peak at about $\Delta E = B$ shown in Fig. 17, and no peak at $2B$. Although $\Delta E = B$ is consistent with a 2-D model, the large wing going to values of $\Delta E < B$ is not. Silvera and Nielsen interpreted this to be arising from a distribution of adsorption sites with an axially confining potential. The energy level diagram as a function of the barrier is shown in Fig. 18(a). In Fig. 18(b) the energy levels are shown both for the gas phase and for the adsorbed states with a barrier height $\phi = 5B$, lowered by an isotropic adsorption potential ε. This barrier splits the lowest ortho state into a singlet and a doublet, separated from the ground para state by Δ_0 and Δ_1, respectively. The inelastic neutron peak was interpreted as a $\Delta E = \Delta_0$ transition. The main difficulty in this interpretation is the absence in the scattering group of the $\Delta E = \Delta_1$ transition. This possibly could be broadened by strong mixing with translational states. Using this model and considering only the lowest rotational states for low temperature, one calcu-

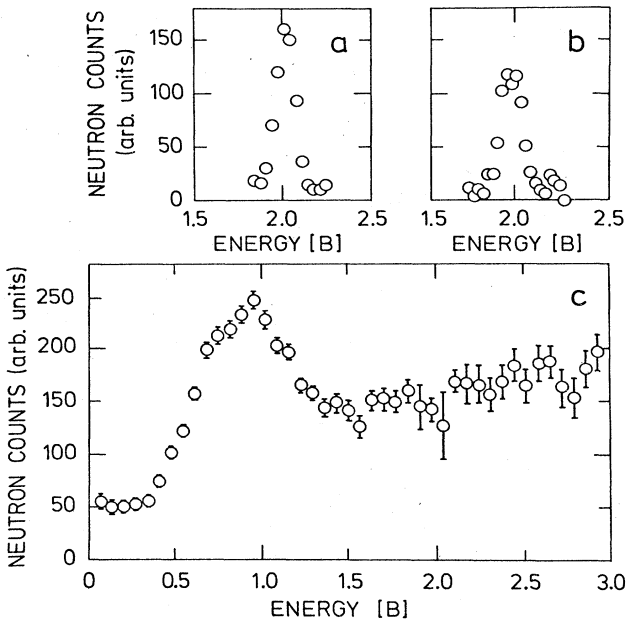

FIG. 17. Inelastic neutron scattering groups for (a) solid H_2, (b) H_2 adsorbed on graphoil and (c) H_2 adsorbed on activated alumina. Scattering counts from the base *AAA* are subtracted off. Sample temperature was 5 K. Energy transfers are given in units of the rotational constant ($B_{H_2} = 7.35$ meV) (after Silvera and Nielsen, 1976).

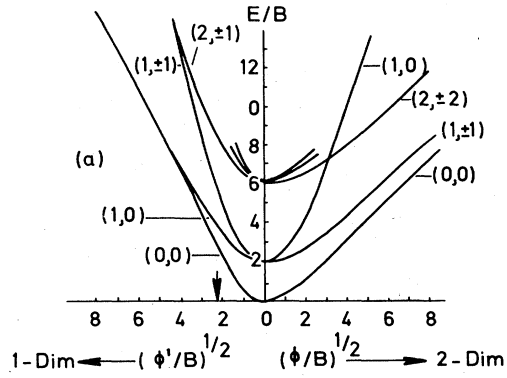

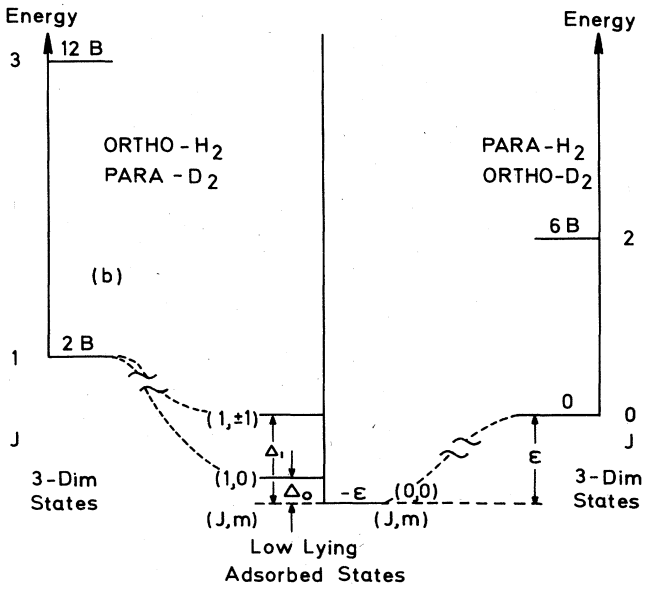

FIG. 18. (a) Energy of the low-lying rotational states of a hindered diatomic molecule as a function of ratio of the barrier height ϕ to the rotational constant (the barrier potential is $\phi \cos^2\theta$, where θ is the angle between the molecular axis and the normal to the surface). (b) Energy levels in the gas state and for adsorbed molecules with $\phi = 5B$ indicated by the arrow in (a). ε represents an isotropic adsorption energy (after Silvera and Nielsen, 1976).

lates

$$c_o^a/c_o^s = \frac{\{3\ \exp[(\varepsilon-\Delta_0)/kT]+6\ \exp[(\varepsilon-\Delta_1)/kT]\}}{9\ \exp(-2B/kT)}, \quad (5.8a)$$

$$c_e^a/c_e^s = \exp(\varepsilon/kT), \quad (5.8b)$$

and from Eq. (5.7),

$$S = \tfrac{1}{3}\exp[(2B-\Delta_0)/kT]+\tfrac{2}{3}\exp[(2B-\Delta_1)/kT].$$

A mean barrier potential of $\phi = 5.5B$ gives a value of $\Delta_0 = 52\ \text{cm}^{-1}$, $\Delta_1 = 184\ \text{cm}^{-1}$, and $S = 39$.

The value of S can be determined independently. Note that if conversion takes place on the surface, which is the case for AAA, then at equilibrium

$$\rho_o^a/\rho_e^a \simeq 3(e^{-\Delta_0/kT}+2e^{-\Delta_1/kT})/1, \quad (5.9)$$

where the first excited para state can be ignored. A measurement of the equilibrium value of ρ_o^a/ρ_e^a on the surface, combined with Eqs. (5.1), gives S from Eq. (5.7). Because catalytic conversion rates on AAA are rather slow, H_2 can be adsorbed, allowed to convert, desorbed, and analyzed to determine (5.9). This can be done repeatedly at time intervals less than $1/K_1$, the conversion rate constant, to determine K_1. The back conversion rate constants on H_2 and D_2 are $K_1 = 0.05 \pm 0.02\ \text{h}^{-1}$ for H_2 and $0.2 \pm 0.08\ \text{h}^{-1}$ for D_2 as determined from Fig. 19 by Silvera (unpublished). The equilibrium value yields $S = 39^{+2}_{-8}$ for H_2 and 5.0 ± 0.3 for D_2, in agreement with the neutron scattering measurements.

Finally we suggest here a technique for producing high-purity ortho-D_2. D_2 could be adsorbed on AAA and allowed to convert to equilibrium at low temperatures. At 4.2 K, $c_e = 0.9996$. The D_2 could then be rapidly desorbed with little back conversion due to the small first-order rate constant for catalytic conversion.

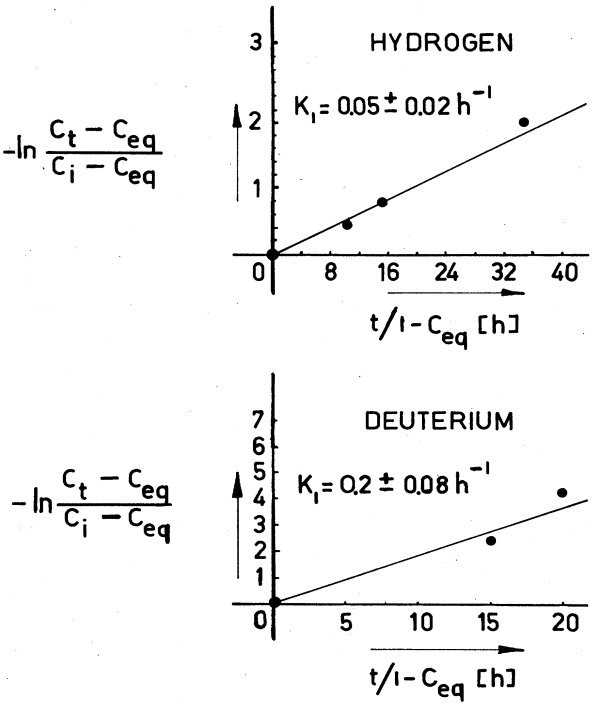

FIG. 19. Data for the determination of the conversion rate of H_2 and D_2 adsorbed on *AAA* at $T = 20.4$ K. The slope of the straight line fit provides K_1, as can be seen from the solution of Eq. (5.2) (in the figure $c_t \equiv c_e$, $c_{eq} \equiv \rho_{eq}$) (after Silvera, unpublished).

C. Conversion

Soon after the discovery of the ortho–para species of hydrogen, experimental investigations (Cramer and Polanyi, 1933; Farkas, 1933) showed that the rate equation governing conversion in the solid or liquid was second order:

$$\frac{dc_o}{dt} = -Kc_o^2 \quad (5.10)$$

with the solution

$$1/c_o(t) - 1/c_o(0) = Kt, \quad (5.11)$$

where K is the rate constant. Conversion requires a simultaneous change of rotational angular momentum by $\Delta J = 1$ and the nuclear spin state must change between the triplet and the singlet states. An isolated molecule is stable and will not convert; the perturbation that causes the transition arises from interactions with neighboring molecules. In particular, the nuclear spin transition requires a magnetic field gradient. Classically speaking the field must vary over the dimension of the molecule to create a torque on the proton magnetic moments to reorient them from parallel to antiparallel. Quantum-mechanically, a uniform field has no matrix elements between the singlet and triplet spin states, but a field gradient can mix these states and allow transitions. Thus an $I = 1$ ortho-H_2 molecule will be perturbed by the dipolar magnetic field of another ortho-H_2 molecule. This field can arise both from the nuclear spin magnetic moment and the rotational magnetic moment. A $J = 0, I = 0$ para molecule has no magnetic moment and cannot cause conversion. As a consequence the rate is quadratic as in Eq. (5.10).

In D_2 the rate equation is given by

$$\frac{dc_o}{dt} = -Kc_o^2 - K'c_o(1-c_o). \quad (5.12)$$

There are two important differences with H_2: (1) para-D_2 ($J = 1, I = 1$) can interact with not only the dipolar magnetic field of another para, but also with the $I = 2$ state of an ortho-D_2 ($J = 0, I = 0, 2$) molecule giving rise to the term in K', and (2) the spin 1 deuterons also bear a nuclear quadrupole moment which couples to the electric field gradient arising from the molecular electric quadrupoles of neighboring molecules; this only contributes to the term in K since the electric field gradients are zero for a $J = 0$ molecule. In the event that $K \simeq K'$, then D_2 obeys the differential equation $dc_o/dt = K'c_o$, which has an exponential solution.

Calculations of the intrinsic rate constants for zero-pressure H_2 have been carried out by Motizuki and Nagamiya (1956a) and Berlinsky and Hardy (1973), who studied conversion in the orientationally ordered phase of H_2, and in D_2 by Motizuki (1957, 1962). The calculations are quite detailed and we shall only present the important points here. The conversion rate is calcu-

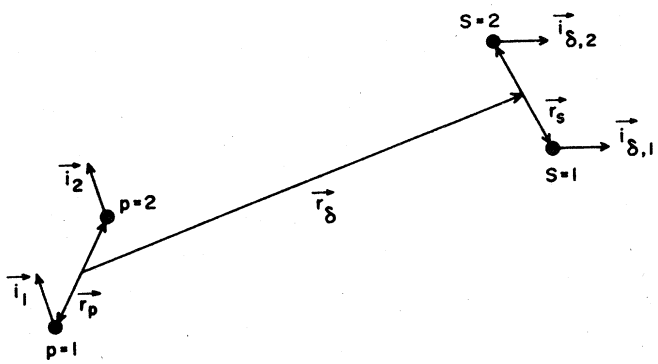

FIG. 20. Vectors that define the positions of the protons for two H_2 molecules (after Berlinsky and Hardy, 1973).

lated from the golden rule,

$$W=\frac{2\pi}{\hbar}\sum_{i,f}P_i|\langle f|\mathcal{H}_{\rm int}|i\rangle|^2\delta(E_i-E_f), \tag{5.13}$$

where P_i is the probability that the system is initially in one of the g_i states i, and f is the final state. The interaction is $\mathcal{H}_{\rm int}=\mathcal{H}_{ss}+\mathcal{H}_{rs}+\mathcal{H}_{EQ}$, where $\mathcal{H}_{ss}$ is the spin–spin interaction, $\mathcal{H}_{rs}$ is the rotation spin interaction, and $\mathcal{H}_{EQ}$ the electric quadrupole interaction. For purposes of discussion, we shall only write down $\mathcal{H}_{ss}$. The magnetic dipole–dipole interaction in spherical components, after Berlinsky and Hardy, is

$$\mathcal{H}_{ss}=\left(\frac{24\pi}{5}\right)^{1/2}\sum_{p,\delta,s}\frac{4\mu_p^2}{|\mathbf{r}_s+\mathbf{r}_\delta-\mathbf{r}_p|^3}\times\sum_{m,n}C(112;mn)i^m_{\delta,s}i^n_pY_2^{m+n*}(\Omega_{\delta,s,p}). \tag{5.14}$$

The vectors defining the positions of the nucleons are shown in Fig. 20; μ_P is the magnetic moment of the nucleon with nuclear spin i and $\Omega_{\delta,s,p}$ specifies the orientation of vector $\mathbf{r}_s+\mathbf{r}_\delta-\mathbf{r}_p$. A similar term can be written down for $\mathcal{H}_{rs}$ as well as a term for $\mathcal{H}_{EQ}$, analogous to Eq. (3.15) with an R^{-5} dependence [this term differs from (3.15) in that the interaction is with the EQ moment of each nucleon, not the total molecular EQ moment]. Conversion involves the change of nuclear spin coordinates in the central molecule, p, explicitly given in (5.14), change of the rotational coordinate of p, which can be explicitly seen by expanding about $\mathbf{r}_p$, and creation of one or more phonons in the final state, required to conserve the energy $2B$ which becomes available from conversion. For H_2 $2B/k_B=171$ K and for D_2, 86 K. The largest phonon energy is characterized by the Debye temperature $\theta_D\simeq 120$ K for H_2 and $\simeq 109$ K for D_2. As a consequence final states of H_2 will involve two phonons, whereas for D_2 one phonon will suffice. The phonon coordinates of the interaction are made explicit by expanding around small displacement $\mathbf{u}_s$ of the molecule at δ:

$$\mathcal{H}_{\rm int}=(\mathbf{u}_s\cdot\nabla)(\mathbf{r}_p\cdot\nabla)\mathcal{H}_{\rm int}+\tfrac{1}{2}(\mathbf{u}_s\cdot\nabla)^2(\mathbf{r}_p\cdot\nabla)\mathcal{H}_{\rm int}. \tag{5.15}$$

We can now make a number of general statements. From (5.14) and (5.13) we see that for the (dominant) $\mathcal{H}_{ss}$ interaction the rate depends on μ_P^4. Since the magnetic moment of the deuteron is about $\frac{1}{3}$ that of the proton (see Table X), the rate for D_2 will be ~10^2 slower, all other things equal. However, D_2 has more conversion states, the EQ mechanism, and most important, converts with one-phonon creation, winning back part of this reduction due to the smaller magnetic moment. The explicit density dependence for H_2 is $\rho^{12/3}$ [the gradient operator in Eq. (5.15) increases the R dependence of $\mathcal{H}_{ss}$ to R^{-6} so that $W\sim R^{-12}$] with a more complicated factor due to the density dependence of the phonon density of states. For one-phonon conversion $W\sim\rho^{10/3}$ × (phonon density of states factor).

Motizuki and Nagamiya (MN) calculated $K=1.94\%/\text{h}$ for H_2 and Berlinsky and Hardy (BH) found 1.67%/h. For D_2 Motizuki (1962) found $K=0.1269\%/\text{h}$ and $K'=0.1779\%/\text{h}$ so that $K\simeq K'$ and $dc_o/dt\simeq -K'c_o$. We shall make a few remarks on the approximation and contributions of various sources. MN took $\theta_D=91$ K for H_2, whereas the current accepted value is $\theta_D\simeq 120$ K. The effect of this is discussed by BH. MN also used a lattice constant of 3.75 Å; the current value is 3.77–3.789 Å depending on the ortho–para concentration. With an R^{-12} dependence this can give up to a 12% reduction in their calculated rate constant. MN also considered three-phonon final states in H_2 which increased K by 10%. MN also showed that the rotation–spin interaction contributes only about 2.5% to the rate for H_2 since $\mu_r\simeq 0.3\mu_P$; for D_2 $\mu_r\simeq 0.5\mu_D$. For H_2 the nucleon has no quadrupole moment; the contribution of $\mathcal{H}_{EQ}$ to conversion in D_2 is about equal to the dipole–dipole contribution.

A number of experimental measurements exist for H_2 which are tabulated by Schmidt (1974); in addition there has been a recent measurement by Berkhout *et al.* (1978). All of these are in relatively good agreement. We find the weighted average of several independent measurements to give $1.90\pm0.05\%/\text{h}$. Schmidt performed long-term (~1200 h) NMR measurements on the conversion rate of H_2. At low temperatures and low concentration of $J=1$, he observed deviations from Eq. (5.11) such that the conversion rate apparently increases with decreasing c_o. This is attributed to a

TABLE X. Molecular and nuclear moments. The nuclear Bohr magneton is $\mu_N=5.050\,38(36)\times10^{-24}$ erg gauss^{-1}.

Molecule or atom	Molecular rotational magnetic moment, $\nu=0, J=1$	Nuclear magnetic moment	Nuclear quadrupole moment [cm^2]
Hydrogen	$0.882\,91\mu_N$ [a]	$2.792\,743\mu_N$ [c]	...
Deuterium	$0.442\,884\mu_N$ [b]	$0.857\,407\,3\mu_N$ [c]	$0.002\,738$ [c]

[a] Harric and Ramsey (1952).
[b] Barnes *et al.* (1954).
[c] See N. F. Ramsey (1956).

clustering of $J=1$ molecules due to attractive EQQ interactions (see following section).

The first measurements of conversion in solid deuterium were by Grenier and White (1964); however, their large experimental error, possibly due to oxygen impurities, prevented extraction of a rate constant. Milinko and Sibileva (1974, 1975) have studied conversion in deuterium (as well as in hydrogen) over a wide range of concentration and find $K \simeq K'$ with $K' = 0.053 \pm 0.003\%/\text{h}$. Berkhout *et al.* have also made a careful study of conversion in D_2 for $c_o > 0.9$ and found a rate constant $K' = 0.063 \pm 0.001\%/\text{h}$. Taking a weighted average we find $K' = 0.060 \pm 0.003\%/\text{h}$ for D_2 at zero pressure and 4.2 K. This is more than a factor 2 smaller than the theoretical value of Motizuki.

The density dependence of conversion in H_2 was first studied experimentally by Ahlers (1964). Although he saw an increase in conversion, due to the paucity of data points, he failed to observe an interesting dip in the conversion rate, found later by Pedroni *et al.* (1974). These data are shown in Fig. 21. Berlinsky (1975) provided a detailed calculation of the density dependence of K in H_2, in reasonable agreement with experiment. As density increases, the width of the phonon frequency spectrum increases. When the maximum is equal to $2B$, conversion with one-phonon final states is allowed, increasing the rate constant. As the density is increased, the one-phonon density of states is scanned through the conversion energy. The dip in K arises from a dip in the phonon density of states. The density dependence of conversion due to the phonon density of states evidently dominates the $\rho^{10/3}$ dependence due to the gradient of the dipolar fields. This suggests an interesting (but tedious) technique of studying the phonon density of states by final state relaxation spectroscopy, which is scanned by varying the sample pressure.

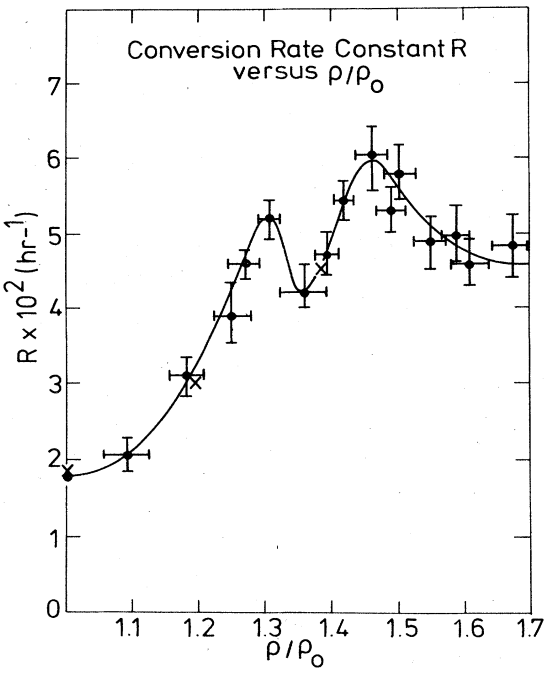

FIG. 21. The conversion rate (R) as a function of relative density in hydrogen. The circles are the data of Pedroni *et al.*, 1974; the crosses those of Ahlers (1964) (after Pedroni *et al.*, 1974).

As we have seen from Eqs. (5.13) and (5.14) the conversion rate depends on the square of the magnetic moment of the perturber and the square of the moment of the converted molecules. If a paramagnetic impurity such as O_2 is present in H_2, then since $\mu_{O_2}/\mu_P \simeq 1320$, this can have a dramatic effect on the conversion rate. MN (1956a) have calculated the effect of O_2 impurities on conversion in H_2. The formalism is the same as for homogeneous conversion and they considered only two-phonon final states, with a resulting $K_{O_2} = 25 \times 10^3 (R_0/R)^{12}\%/\text{h}$. The radius of the sphere for which $K_{O_2} = K_{H_2}$ is $R = 2.7R_0$. We see that an O_2 impurity rapidly develops a sphere of para molecules around it. Since H_2 can diffuse, the effective conversion rate can be strongly enhanced as ortho molecules move into the sphere of influence of an O_2 molecule, as has been shown by MN (1956b).

Although this calculation demonstrates how effective paramagnetic impurities can be, in a certain sense O_2 in H_2 is a poor example. Omar and Dokoupil (1962) have shown that the solubility of O_2 in liquid hydrogen (for T between 27 and 33 K, at pressures close to the equilibrium vapor pressure) is less than 0.2 ppm. Schmidt (1974) has also condensed gaseous mixtures of O_2 and H_2 and found no effect on K due to the separation of the two types of molecules. It is possible, however, that rapid cooling can quench O_2 in H_2 or that the solubility is higher under pressure. A slow cooling of liquid H_2 will result in an almost O_2 (as well as N_2)-free sample. If, however, O_2 condenses on the walls of the sample container, then this can effectively catalyze liquid H_2 which rapidly "samples" the walls.

O_2 impurities in gaseous H_2 are extremely effective catalyzers. This is discussed in Farkas (1935). Nielsen and Dahler (1967) have calculated the rate constants for this case.

Recently Krause and Swenson (1979) have studied conversion rates in solid H_2 for a series of isochores with molar volumes to about 16 cm^3/mol. In warming their samples they observed enhanced conversion rates for $T \gtrsim 0.08\theta_D$. No plausible explanation has yet been proposed, and it is not clear if this is an intrinsic or impurity mechanism. One can consider the possibility that under pressure the solubility of oxygen impurities is increased. As the temperature is raised o-H_2 molecules diffuse (see next section) into the range of the magnetic impurities and are converted. In any case further systematic studies are probably required to sort this problem out.

Conversion on magnetic surfaces is a rather complex phenomena which requires knowledge of the H_2 spin and translational time correlation functions, surface potentials, rotational states on the surface, and the distribution of surface spins (random or a dense magnetic lattice). We refer to the article by Petzinger and Scalapino (1973) for a general treatment.

D. Diffusion

Self-diffusion in the hydrogens can be separated into two types: classical translational diffusion which is

effective at high temperatures and quantum-mechanical rotational diffusion which is important for low $J=1$ concentrations and low temperatures.

1. Thermally activated diffusion

Classical diffusion was first studied in H_2 by Rollin and Watson (1955) by measurement of NMR nuclear relaxation times and subsequently by Bloom (1957), Haas *et al.* (1961), and Weinhaus and Meyer (1972). In H_2 at zero pressure, classical diffusion begins to become important (certainly for NMR relaxation) at $T \simeq 10$ K. Diffusion can be characterized by the time between jumps

$$\tau = \tau_0 e^{+E/k_B T}, \tag{5.16}$$

where E is the jump activation energy, and the diffusion constant

$$D = D_0 e^{-E/k_B T}, \tag{5.17}$$

where $D_0 = R^2/6\tau_0$ for a random walk with (lattice) step R. Weinhaus and Meyer summarize measurements on H_2 and find for the activation energy $E/k_B = 200 \pm 10$ K. The value of τ_0 depends on o–p concentration, but an average value is $\tau_0 = 7.9 \times 10^{-14}$ s and $D_0 = 3 \times 10^{-3}$ cm^2/s. At 10 K, this yields a time $\tau = 3.8 \times 10^{-5}$ s which a molecule spends on a site before it jumps to another. At 10 K one has $D = 6.3 \times 10^{-12}$ cm^2/s. Weinhaus *et al.* (1971) have also studied diffusion in D_2. Self-diffusion begins to become important for $T \gtrsim 13$ K. They find $E/k_B = 288$ K, $D_0 \simeq 2.3 \times 10^{-3}$ cm^2/s and $\tau_0 = 9.4 \times 10^{-14}$ s.

The theory of self-diffusion in H_2 and D_2 has been treated by Ebner and Sung (1972). They considered two mechanisms: quantum-mechanical tunneling and thermal activation over a potential barrier or vacancy motion. The first process could be important in hydrogen because the wave functions on neighboring sites can overlap appreciably (as in helium), allowing the particles to exchange positions. In their model they consider the vacancies to be localized. They use a single-particle quantum crystal calculation to calculate the energy levels and barrier for a molecule adjacent to a vacancy in hcp hydrogen, which gives a double well potential. The resulting diffusion coefficient has a high-temperature form $D = 6 \times 10^{-4} e^{-197/T}$ cm^2/s, due to classical thermal excitation over a barrier. They also find a low-temperature term due to quantum-mechanical tunneling with an activation energy of 112 K. The latter has not been observed experimentally. However, the high-temperature activation energy of 197 K is in remarkably good agreement with experiment. Oyarzun and Van Kranendonk (1971) have shown (see following subsection) that for most experimental situations, the $J=1$ concentration is sufficient to reduce the quantum-mechanical tunneling by a factor of order 10^{11} due to rotational "tumbling" which reduces the mass tunneling rate to a negligible quantity.

In D_2, Ebner and Sung find a high-temperature activation energy of 290 K, also in a good agreement with experiment. They considered the pressure dependence of D and found D_0 to be quite insensitive to density whereas the activation energy E increases sharply, as the molecules are localized with increasing density. Their calculations of E again are in accord with NMR measurements of E up to 230 bar by Smith and Squire (1958).

2. Quantum rotational diffusion

At 1 K in H_2 the thermally activated diffusion time is 10^{74} seconds! Nevertheless, at low temperatures Amstutz *et al.* (1968) detected diffusion of ortho–para species by means of NMR. Isolated $J=0$ species have no NMR spectra, whereas an isolated $J=1$ molecule or isolated pair of $J=1$ molecules, which exist at low concentration c_1, have distinct spectra. In lowering the temperature of solid H_2 from 4.2 K to 0.4 K, they observed a growth of the intensity of the pair spectrum at the expense of that of isolated $J=1$ molecules, implying ortho–para diffusion and clustering of ortho–H_2 molecules at low temperature. Equilibrium was approached exponentially with a time constant of order hours, depending on temperature and concentration. Subsequently such diffusion has also been observed by pressure changes at constant volume (Jarvis *et al.*, 1969), by its effect on conversion (Schmidt, 1974), specific heat (Roberts and Daunt, 1970), microwave absorption (Hardy *et al.*, 1977), infrared absorption (Roffey *et al.*, 1974), etc.

The effect was explained by Oyarzun and Van Kranendonk (1971, 1972). They studied two mechanisms for quantum diffusion. The first is the exchange mechanism discussed in the preceeding section. Although the intermolecular exchange rate is reasonably rapid for an isolated ortho molecule in a para lattice, it is severly reduced, already for $c_1 \simeq 0.01$, due to the EQQ interaction between ortho molecules. In exchanging, the orientational energy, which is large compared to the exchange energy, has to be conserved. If the ortho molecules are reoriented or would have a different number of ortho neighbors with a different energy after a hop, then the hop is energetically blocked. The reduction factor of the hopping rate is of order 10^7, giving a negligible rate constant of order 10^8–10^{12} h.

A second mechanism consists of the conversion of an ortho into a para molecule with the simultaneous conversion of a neighboring para into an ortho molecule. This resonant conversion is also reduced by the factor $\sim 10^7$ due to energy conservation requirements, but was found to be a much more probable process. The basic interaction responsible for the resonant conversion is the same as that due to conversion [see Eq. (5.15)]. In a detailed calculation Oyarzun and Van Kranendonk give a lucid description of the process and find a rate constant of order 2 h, in agreement with experiments. For D_2 the calculated rate is reduced by about 100, mainly due to the smaller nuclear magnetic moment; quantum diffusion has not been observed in D_2.

At low temperature, equilibrium favors configurations with ortho molecules clustered as nearest neighbors (nn) rather than next nearest neighbors (nnn), as pair energies arising from the EQQ interaction are lower in the nn configuration. Since nnn pairs have energy states which overlap those of nn pairs, resonant conversion is not blocked by the energy conservation requirement and the ortho-H_2 molecules cluster.

In the hcp lattice, two types of nn pairs exist. In the

microwave experiment of Hardy *et al.* (1977) they were able to observe different rate constants for the two distinct types of pairs. More recently Schweizer *et al.* (1978) have observed a strong unexpected increase in the clustering rates in samples at $\simeq 25$ mK. They find a disappearance of the signal due to one of the pair types, probably due to rotational hopping to the other pair type in the hcp lattice. However, Cochran and Gaines (1979) have proposed an explanation which does not require assuming enhanced diffusion rates at low temperatures.

VI. CRYSTAL STRUCTURES, ORDER, AND PHASE TRANSITIONS

The path to the understanding of the crystal structures or the phase diagram of the solid hydrogens has been long, difficult, and full of pitfalls. In this section we shall first give a historical description of the structural determinations. This perhaps sometimes contradictory array of information will then be analyzed to present a more detailed account of our current knowledge.

The first crystal structure determination was an x-ray diffraction study by Keesom *et al.* (1930) on pure para-H_2 at helium temperatures. Their seven x-ray reflections could be fit to the hexagonal closest packed (hcp) lattice. This remained unchallenged for 26 years, until Kogan *et al.* (1957) reexamined the crystal structure. These workers studied n-D_2 and n-H_2 at helium temperatures and determined the structure of n-D_2 to be body-centered tetragonal (bct), based on one reflection; they found the same for n-H_2, from two reflections. They also found the same structure for n-T_2 (Kogan *et al.*, 1960). Neutron studies by Kogan *et al.* (1961) on n-H_2 and n-D_2 at 12 K also indicated a tetragonal structure with a unit cell twice the dimension of the previous cell, interpreted as ordering of odd-J molecules. This Soviet work was reviewed by Kogan (1963).

In 1962, Van Kranendonk and Gush (1962) argued that the bct structure was not compatible with optical data, whereas hcp was. A few years later Kogan *et al.* (1964) and Bulatova and Kogan (1964) realized that they had been plagued by problems of oriented polycrystalline growth and the screening of important x-ray lines by the sample substrate: their x-ray patterns could only be indexed as hcp, consistent with the early Leiden work of Keesom *et al.* The structure of hydrogen was thought to be understood; however, the story was only beginning.

Curzon and Pawlowicz (1964a,b) studied H_2 and D_2 solidified from gas on a cold substrate by electron diffraction. Although their first report was in error (measurements were made on an N_2 contaminant instead of D_2), they corrected this to find a face-centered (fcc) structure for n-D_2 as grown from vapor at $T \simeq 7$ K. Similar results were obtained for n-H_2 (Curzon and Mascall, 1965) with some traces of hcp for thicker samples. Bostanjoglo (1965) and Bostanjoglo and Kleinschmidt (1967) obtained the same result for $T = 2.8$ to 7 K, also by electron diffraction on n-H_2 and n-D_2. Thus H_2 and D_2 could be prepared in hcp and fcc structures, depending on the growth technique.

Early measurements by Giauque and Johnston (1928) and by Simon *et al.* (1930) signaled a phase transition in H_2 by the anomalous increase in specific heat, down to temperatures of order 3 K. This implied transition was discussed by Pauling as a lifting of the rotational degeneracy of the molecules in the $J=1$ state. Much later, Hill and Ricketson (1954) observed the λ specific heat anomaly and Reif and Purcell (1953), an NMR anomaly in n-H_2 at $T \simeq 1.5$ K. This was also discussed as an orientational ordering of the $J=1$ molecules. In a classic paper, Nakamura (1955) discussed the anisotropic interactions in H_2 and analyzed the specific heat anomaly in terms of the lifting of the degeneracy of the $J=1$ states due to EQQ dominated interactions.

However, the hcp and fcc phases discussed above had nothing to do with this phase transition! In 1965 Clouter and Gush (1965) observed an abrupt change in the infrared spectrum of n-H_2 upon cooling, which could be interpreted as a change from hcp (high-temperature phase) to a structure with inversion symmetry at the molecular sites, possibly fcc. Shortly thereafter Mills and Schuch (1965) studied n-H_2 at low temperatures by x-ray diffraction and established that the phase transition involved a change of *molecular centers* from an hcp lattice at high temperature to an fcc lattice below 1.5 K; however, they could not locate the proton positions to establish that an orientational ordering of the $J=1$ molecule occurred. Schuch and Mills (1966) and Mucker *et al.* (1966) then studied enriched ortho-D_2 by x-ray and neutron scattering, respectively, and found the hcp→fcc transition. They also found the curious result that some of the cubic phase remained when the temperature was raised above the λ temperature, implying that the λ anomaly associated with the disordering of $J=1$ molecules was not a consequence of the hcp–fcc lattice transformation. In a classic experiment, Schuch, Mills, and Depatie (1967) studied the concentration and temperature dependence of the structural phase transition by means of x-ray diffraction on odd-J enriched H_2 and D_2, establishing the dependence of critical temperature, T_c, on concentration, as well as the approximate critical concentration and the large hysteresis in T_c. They further showed that cycling a sample several times through T_c would stabilize the fcc structure above T_c. One could then associate T_c with the orientational ordering of the $J=1$ molecules.

The structure of the orientationally ordered state also attracted theoretical interest and was first correctly predicted by Felsteiner (1965), classically [and Raich and James (1968), quantum-mechanically]; experimental proof of this state required several years, however. Felsteiner showed that an array of ordered EQ moments would have a lower lattice energy on an fcc lattice than on an hcp lattice and that the lowest energy, or ground state, was the Pa3 (T_h^6) structure with four molecules per unit cell shown in Fig. 22. Here the molecular centers sit on the sites of an fcc lattice; the molecular axes are oriented along the body diagonals. Correctly speaking, it is the molecular orbitals or the axes of quantization of the molecular angular momenta that orient along the body diagonals. The Pa3 structure can be decomposed into four interpenetrating simple cubic structures such that on any given sublattice the axes of

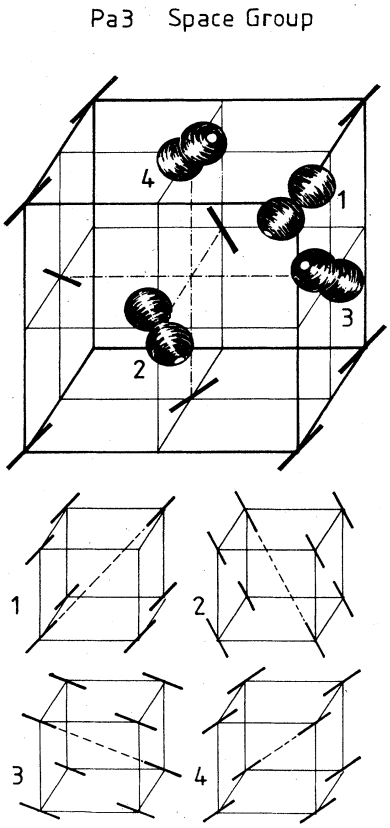

FIG. 22. The Pa3 space group of ordered hydrogen and deuterium. In the upper drawing the spatial distributions (Y_{10}) of the molecular axes of the four inequivalent molecules is shown. One must bear in mind that the charge distribution around the molecular axis is that given in Fig. 1. At the remaining sites we show the direction of quantization for the molecules. The division into sublattices is shown in the lower part of the figure.

the individual molecular orbitals are all parallel. The phase transition from disordered hcp to Pa3 is evidently driven by the EQQ interaction since the difference in energy of the hcp and fcc lattice for isotropic interactions (~10^{-3} K/molecule) is much smaller than the EQQ energy (~5 K/molecule).

Mucker *et al.* (1966, 1968) reported that their neutron diffraction peaks corresponded to the Pa3 structure. However, this identification did not receive strong acceptance, as the two weak diffraction peaks responsible for the identification were strongly masked by two strong coherent scattering peaks from the Al cell. Their intensity fit was based on a classical model of the form factor rather than the smaller quantum-mechanical form factor for the $J=1$, $M_J=0$ state of D_2. The first clear evidence of the sublattice structure was from far-infrared measurements by Hardy *et al.* (1968a) on 99% odd-J H_2 and D_2. They observed optical phonons which can only exist if the structure has more than one molecule per unit cell; this occurs if the molecules order on the fcc lattice of molecular centers. However, their spectrum had three peaks where only two phonon peaks had been expected from group-theoretical considerations for Pa3. They suggested that anharmonicity could allow for multiphonon peaks; a definitive assignment to Pa3 could not be made. Next, Hardy *et al.* (1968b) measured the librons (collective reorientational excitations) in high-purity odd-J H_2 and D_2 by Raman scattering. Theoretical considerations led to a prediction of three distinct peaks; four were observed, none of which could be easily fit to theory. They proposed that either the structure was Pa3 and the fourth peak was a two-libron band, or the structure was distorted from Pa3, possibly to $\bar{R}3$ (C_{3i}^2). The spectrum could be fit remarkably well to this latter structure under certain assumptions. This turned out to be a "red herring." Silvera *et al.* (1969) cast doubt on the $\bar{R}3$ structure by observing that the $J=0\rightarrow 2$ Raman spectra of even-J impurities was not consistent with the point symmetry of $\bar{R}3$, although calculations of the excitation spectrum could be provided to support the distorted Pa3 (Coll and Harris, 1970a). Nakamura and Miyagi (1970) supported one of the original suggestions of Hardy *et al.* (1968b) that three of the Raman lines were single-libron transitions and the remaining intensity was due to a two-libron band. Coll *et al.* (1970b), Coll and Harris (1971a), and Berlinsky and Harris (1971b) were able to rather accurately account for the experimental libron frequencies and two-libron intensity using the Pa3 structure. At this time Hardy *et al.* (1971, 1975) succeeded in growing large single crystals of H_2 and D_2. From the polarization ratios of the Raman spectra, they could unambiguously identify the one-libron transitions, removing all reservations concerning the Pa3 structure. Finally Mills *et al.* (1973) and Yarnell *et al.* (1974) determined the Pa3 structure from neutron diffraction studies on para-D_2, using a technique which had no problems due to background coherent scattering from the cell as in the case of Mucker *et al.*

However, as the problem of the ground state of ordered H_2 and D_2 was resolved, new phases emerged. Jarvis *et al.* (1969), Amstutz *et al.* (1969), and Ramm *et al.* (1970) carried out careful measurements of $(\partial P/\partial T)_v$ and NMR to about $T=0.5$ K to establish the critical concentration of odd-J H_2 and D_2 for ordering in the Pa3 structure to be $c_o \simeq 0.56$. Sullivan and Pound (1972) studied H_2 by NMR to $T \simeq 85$ mK and found that for $T \lesssim 0.3$ K and $c_o < 0.56$, a new phase appeared. This phase is believed to be a quadrupolar "spin glass," i.e., randomly distributed orientationally ordered quadrupoles. This is currently an area of intense research.

Still other phase transitions have been reported. Durana and McTague (1973) detected an hcp–fcc transition in para-H_2 at pressures of order 1 kbar, applied by a piston. This transition cannot be reproduced (Nielsen *et al.* 1975; Berkhout and Silvera, unpublished) in low strain crystals. Evidently the transition was induced by the large internal strains inherent to the piston technique.

Roder (1973) suggested that a new phase is present near the melting line and at moderate pressures up to a few hundred bars. Manzhelli *et al.* (1973), in a series of papers, have found such a high-temperature phase and identified it as fcc. This has recently been discussed by Mills (1978), who presents a possible new

phase diagram for $P-V-T$ and concentration. However, Silvera *et al.* (1978) have suggested that the premelting phase discussed in the Russian literature is again a strain induced nonequilibrium state, as several experimenters have been unable to reproduce this phase in low strain samples. Nevertheless, the possible existence of an fcc phase, presenting a phase diagram similar to that of helium as shown in Fig. 29, is an intriguing possibility. Holian (1978) has predicted such a behavior for parahydrogen on the basis of a quantum cell model.

Note added in proof: Wijrgaarden and Silvera (in press) have recently pressurized orthodeuterium to 150 kbar and find Raman spectra which are consistent only with the hcp structure.

For completeness, we mention here new phases that undoubtedly will appear at higher pressures. As the density is increased the anharmonic interactions increase and the rotational states are mixed so that they can no longer be characterized by a single rotational quantum number. This means that para-H_2 and ortho-D_2 will no longer be spherically symmetric in the ground state. They have been predicted to have orientational disorder–order phase transitions at pressures in the range $(0.5-4)\times 10^5$ bar (Raich and Etters, 1972). Finally, at pressures of order 3×10^6 bar, molecular H_2 is expected to have an insulator–metal transition and become an atomic solid.

A. The ordered phase of $J=1$ hydrogen and deuterium

The phase diagram of pure $J=1$ H_2 and D_2 is shown in Fig. 23. The most thoroughly studied region is at zero pressure. As temperature is lowered, the bulk liquid solidifies into the hcp orientationally disordered phase. At zero pressure and $T=T_c\simeq 2.8$ K for H_2 and 3.8 K for D_2, the solid transforms into the orientationally ordered fcc phase with the Pa3 space group already shown in Fig. 22. In Fig. 23 the thick line separating the ordered and disordered phases indicates that hysteresis exists in the transition temperature. The transition has not been studied in great detail for $P>0$; however, recent far-infrared spectroscopic studies of Jochemsen *et al.* (1979) indicate that the ordered state remains Pa3 up to pressures of order 6 kbar, and T_c scales as the density ρ to the $\frac{5}{3}$ power. This is consistent with the idea that the transition is driven by the EQQ interaction since the coupling parameter $\Gamma\sim R^{-5}\sim\rho^{5/3}$. They also observe the persistence of hysteresis at high pressures.

The structural phase transition at zero pressure was first studied in great detail by Schuch *et al.* (1968) by elastic x-ray diffraction, which is sensitive to the location of the molecular centers, but not the orientations. They studied the phase transition by monitoring diffraction lines characteristic of the hcp or fcc phases. From the disappearance and reappearance of hcp lines in lowering and raising the temperature, they could determine the transition temperature T_c and its hysteresis as a function of $J=1$ concentration. The simplified phase diagram is shown in Fig. 24, where T_{hc} refers to the hcp→fcc transition temperature and T_{ch} to that for fcc→hcp. The behavior of H_2 and D_2 was found to be similar. The higher transition temperature for D_2 is a result of its smaller molar volume at zero pressure, resulting in a larger interaction constant Γ. This is an indirect result of the mass differences. H_2 has a smaller mass and therefore a larger zero-point motion which expands the $T=0$ lattice. A remarkable observation which Schuch *et al.* also made was that the fcc phase could be stabilized above, as well as below, the ordering phase line by thermally cycling the sample around T_c. After the initial lowering of the temperature below T_c, when the temperature was raised above T_c, the fcc x-ray line did not completely disappear and the hcp line only partially recovered its initial intensity. However, the sum of the two intensities normalized to the virgin intensities did not add up to one, indicating that part of the lattice was neither fcc nor hcp, but

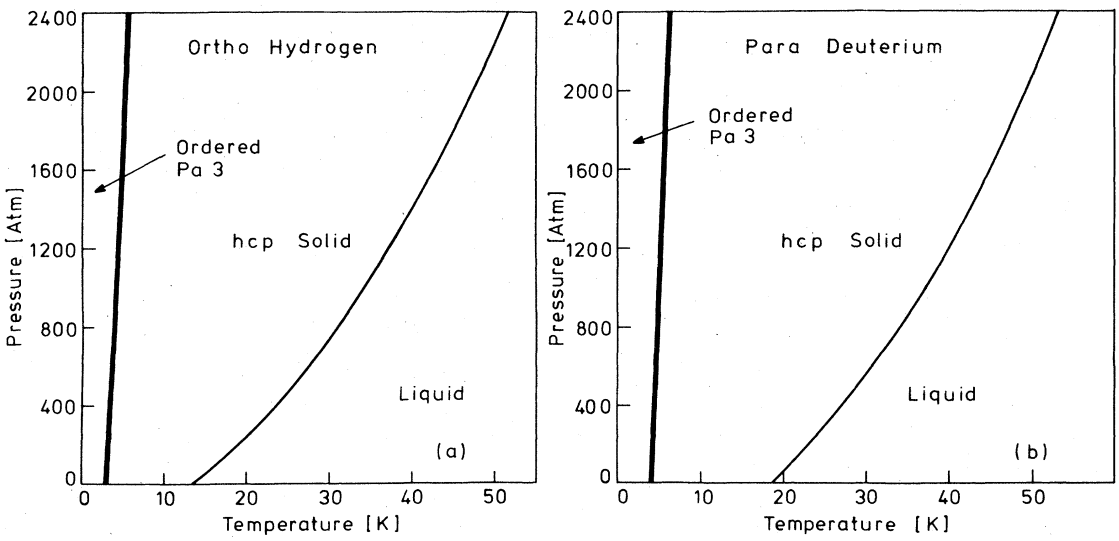

FIG. 23. The phase diagrams for pure ortho H_2 and para D_2 at $T=0$ as a function of pressure. Hysteresis between the Pa3 and hcp phase is indicated by the heavy line. The general pressure dependences shown have been established to $P\simeq 6000$ bars.

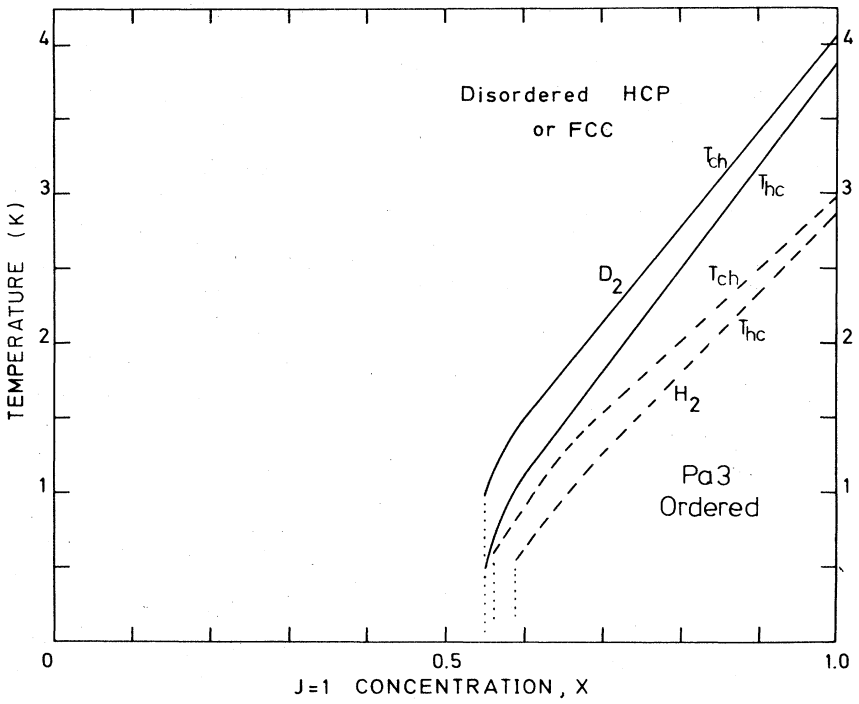

FIG. 24. Simplified phase diagram of solid H_2 and D_2 at zero pressure. Below the critical concentration $x_c \simeq 0.56$, no cooperative ordering in the Pa structure is observed.

probably translationally disordered regions which will be called the intermediate phase. As the temperature was cycled, more and more of the high-temperature phase was stabilized in the disordered fcc structure.

The behavior can be described with the help of a composition diagram for a three-component mixture.[12] This is shown and defined in Fig. 25. In Fig. 26 we show the behavior of 82% p-D_2 with the help of such a diagram, based on the x-ray work of Schuch *et al.* In this figure the odd-numbered trajectories represent lowering of temperature and the even-numbered, raising of temperature. In trajectory 1, we see that the crystal grows from the melt in the hcp phase and transforms to fcc ordered at T_{hc}. By cycling the sample several times up and down around $T_{hc}-T_{ch}$, we see that the fcc phase can be stabilized above and below the critical temperature. Thus one can have disordered fcc and ordered fcc. If the sample is heated up to the diffusion region (see Sec. IV), then it "anneals" back to disordered hcp. From the x-ray measurements, apparently, the higher the $J=1$ concentration the more easily is the disordered fcc stabilized. The ordering transition appears to go to completion at T_{hc}. Later, more sensitive neutron scattering measurements by Mills *et al.* (1973) and Yarnell *et al.* (1975) showed that below T_{hc} there was always a small residual amount of hcp phase that remained. In the original x-ray experiments of Schuch *et al.*, this small hcp component had been interpreted as background and had been normalized out (R. L. Mills, private communication). This is also indicated in Fig. 26. X-ray measurements of H_2 show the same behavior as for D_2, although the fcc phase evidently requires substantially more thermal cycling to be stabilized.

Measurements of $(\partial P/\partial T)_v$ in H_2 by Jarvis *et al.* (1969) and in D_2 by Ramm *et al.* (1970) also support the thermal cycling behavior. The orientational ordering is responsible for a sharp decrease in molar volume at constant pressure or change in pressure at constant volume, as was studied by the above authors. In Fig. 27 we show the cycling behavior for 77% p-D_2. This work supported the x-ray observation and showed that the orientational ordering took place in the cycled samples. Thus we arrive at the following picture. H_2 in the $J=1$ state condenses in the disordered hcp structure; at $T=2.8$ K a phase transition takes place to ordered fcc (Pa3). After some cycling the fcc phase can be stabilized above the ordering temperature so that orientational ordering takes place on an fcc lattice. The virgin hcp→fcc structural transition is driven by the EQQ interaction which can achieve the lowest crystal energy when ordered on an fcc lattice.

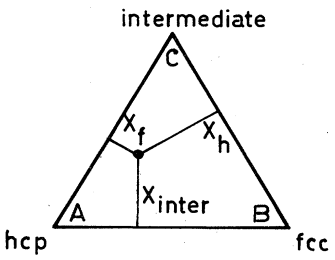

FIG. 25. Composition triangle for a three-component mixture. The circular point represents a mixture with the fraction x_c of fcc, x_h of hcp, and x_{inter} of the intermediate phase. Special points are A, pure hcp; B, pure fcc; and C, pure intermediate.

[12] I would like to thank M. Marrenga for suggesting this presentation.

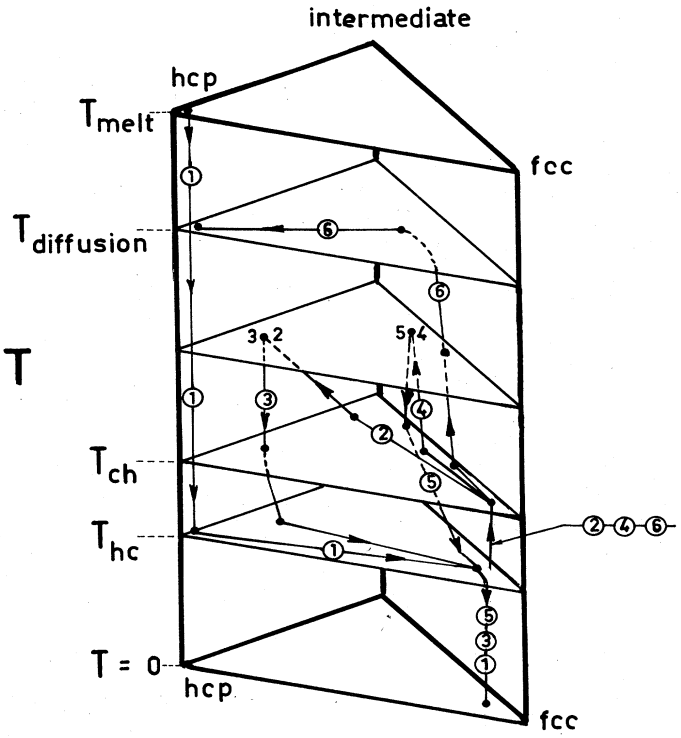

FIG. 26. The complicated structural behavior of 0.82 p-D_2 as a function of temperature. Use is made of the composition diagram described in Fig. 25. Thermal trajectories are numbered in sequential order; odd-numbered trajectories are for decreasing temperature; even for increasing temperature. The thermal trajectories are discussed further in the text.

The neutron studies of Yarnell *et al.* showed that the transition is martensitic in nature and a substantial density of stacking faults of the hexagonal planes was suggested by shifts and widths of the elastic neutron lines in both the hcp and fcc phases. Thus the perfect fcc crystal has a sequence ABCABC ...of hexagonal planes along a ⟨111⟩ direction. Faults of the type ABCABABC or ABCABCBACBAC can arise. In the hcp structure, the planes are stacked ABABAB along the c axis. Faults of the type ABABCACA or ABABCBCB can arise. Hardy *et al.* (1975) point out that, in the ordered state, there are two ways that the molecules can order with respect to each other to form domains in the Pa3 structure of perfectly stacked hexagonal planes.

Very little is actually known about the dynamics of the restructuring. Schuch *et al.* (1968) observed from intensity measurements that the hexagonal c axis probably transforms to the cubic ⟨111⟩ direction. Hardy *et al.* (1971, 1975) found this to be consistent with Raman scattering in the hcp Pa3 structures in a large quasi-single crystal (a crystal probably containing domains). Schuch *et al.* suggest that the structural transformation takes place by a simple sliding of hexagonal planes relative to one another. However, in a perfect crystal there is a rather large potential barrier for such a motion and at the low temperature of the phase transition the thermodynamic probability for such a motion is exceedingly small. The energy gained per molecule by orientational ordering is of the order of $T_c \sim 3$–4 K, whereas the barrier is at least of the order of the melting temperature, ~15–20 K per molecule. Hence the ordering will not be able to drive the planes over the barrier. The transition probably takes place by the motion of some type of fault so that the barrier does not have to be crossed. In this case, the presence of faults are fundamental for the transition.

B. Growth of crystals

Single crystals are vital in sorting out the experimental properties of the hydrogen. As discussed earlier, H_2 and D_2 samples tend to grow with a texture of small crystallites. This evidently plagued the Russian structural determination work of the 50's. Schuch *et al.* (1967), however, were able to pick out small crystallites and study their single crystal diffraction patterns. Hardy *et al.* (1971, 1975) succeeded in growing large single crystals of o-H_2, p-H_2, p-D_2, and o-D_2 with volumes of order 1 cm^3 for Raman scattering experiments. We shall describe their procedure.

Gaseous samples were condensed in a cylindrical Pyrex tube (~10 mm i.d.) with a thin (~1 mm) flat Pyrex bottom as shown in Fig. 28. A pointed copper rod insulated with styrofoam was attached to the bottom of the tube so that a point on the bottom was cooled while the side walls remained warmer. The tube was slowly lowered in the thermal gradient of the cold gas above a liquid helium surface. Crystal growth would initiate at a point at the bottom and would propagate upwards. Crystals ~10 mm long were grown in 20–40 min; growth of single crystals could be monitored by viewing the sample between crossed polarizers. Grain boundaries of the hcp crystals are easily seen by the light intensity variations. The hcp c axis tends to grow along the thermal gradient. Once a single crystal is grown, the most critical procedure is cooling from the vicinity of the melting temperature to 4 K. H_2 has a tremendous shrinkage, as much at 3% upon cooling to 1 K, and tends to stick to the walls. The induced strain results in cracked samples. Hardy *et al.* describe an anneal procedure by which the samples were freed from the Pyrex walls and were essentially strain free.

C. The question of hcp and fcc structures

At this point we discuss the sometimes unexpected appearance of the hcp and fcc structures. Bulk H_2 and D_2, when grown from the melt in equilibrium with their vapor pressure, are always found to be hcp for both ortho and para species. As mentioned in the introduction of this section, diffraction studies showed that films of H_2 or D_2 grow from the vapor phase at low temperature in the fcc phase. The structure could possibly be influenced by the epitaxy. However, Mills *et al.* (1973) grew D_2 at 4.2 K by injecting D_2 gas into boiling liquid helium to achieve a bulk powder of solid D_2. They found that the D_2 grew in the fcc structure for both ortho and para species. When heated to the diffusion region, it transformed to hcp and remained so when again lowered to 4.2 K. Finally, we have the behavior that $J=1$ H_2 and D_2 can be driven to the fcc structure by the orientational ordering and this fcc

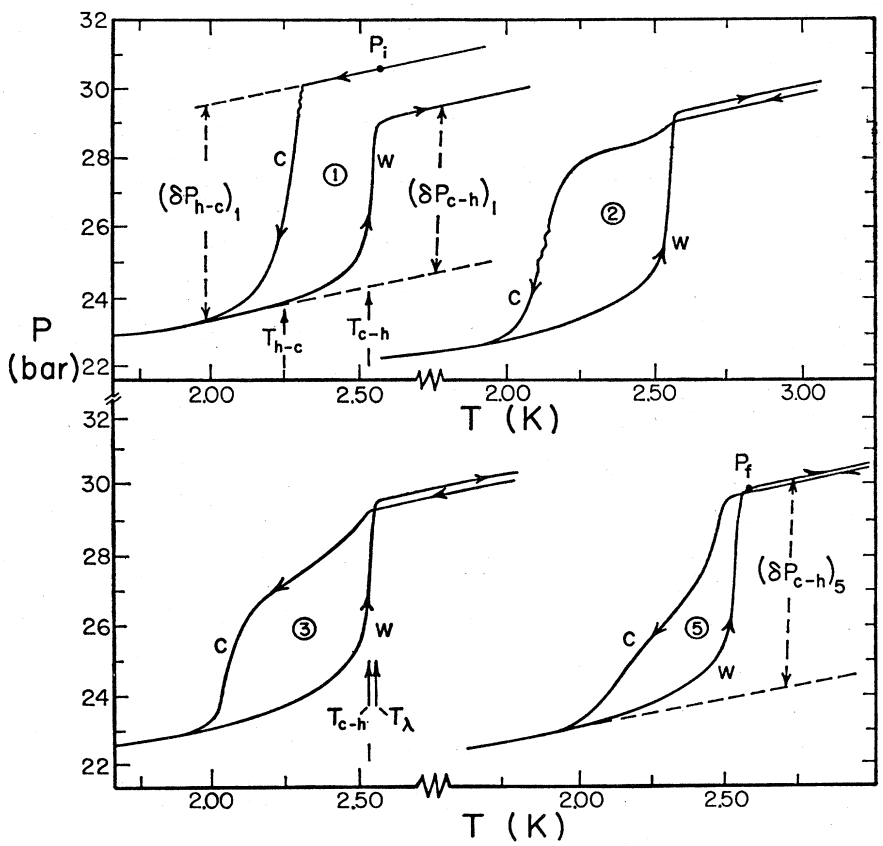

FIG. 27. Isochoric pressure for 0.77 p-D_2 during several thermal cycles through the phase transition. Labels on the curves number the thermal cycle and indicate cooling (c) or warming (w) (after Ramm *et al.*, 1970).

structure can be stabilized above T_c by thermally cycling the sample.

The stable structure of the lattice is that which has the lowest free energy. At $T=0$ this depends only on the lattice energy which has a static and a dynamic part (zero-point energy). The environment of a molecule in hcp and fcc is identical for the first three shells of nearest neighbors (here we are ignoring anisotropic interactions or orientational ordering), so the lattice energy will be strongly influenced by the long-range interactions. The static energies for hcp and fcc are quite similar: $(1-E_{\rm fcc}/E_{\rm hcp})\simeq 3\times 10^{-5}$ (Bell and Zucker, 1976) for a Lennard-Jones potential. Although the static energy is lower for hcp, the rare gases solidify in the fcc phase except for helium. The difference in lattice energy is quite small and the balance could be changed by anharmonic contributions in the dynamic energy, or non-additive interactions (Niebel and Venables, 1974), etc. Needless to say, a change in temperature could affect the balance.

We suggest that the behavior of the orientationally disordered hydrogens can best be understood by assuming that at high temperatures hcp is the stable lattice and at low temperatures (of order 4 K) fcc is more stable. Ordinarily the potential barrier between these macroscopic states prevents the appearance of fcc at low temperature. However, when grown at 4 K, the stablest state, fcc is favored. At higher temperatures vacancies and thermal motion enable the crystal to transform to the more stable hcp phase. Only the $J=1$ solids have a low-temperature mechanism—the orientational ordering—which can drive the crystal into the fcc structure. Upon warming slightly above T_c, the solid has a tendency to remain with the most favorable disordered lattice—fcc.

It would not be surprising if at higher densities the stability changed in favor of fcc (for the disordered phase). In the cases of ^{3}He and ^{4}He at high densities the fcc structure is favored, as shown in Fig. 29. The hypothesis discussed above can also provide an understanding of the hcp→fcc transition observed by Durana and McTague (1973) in p-H_2 under pressure. Evidently the inhomogeneous strains due to the piston displacement technique of applying pressure enable a partial transition to the fcc phase, presumably by displacement of crystal faults. The hcp→fcc phase transition near the melting line reported by Manzhelli *et al.* (1973) bears some resemblance to the behavior of helium. However, Silvera *et al.* (1978), H. Meyer (private communication), and C. Swenson (private communication) have been unable to reproduce this. Silvera *et al.* suggest that this transition may also be strain induced, possibly due to the presence of helium impurities which were present in some of the Russian experiments and

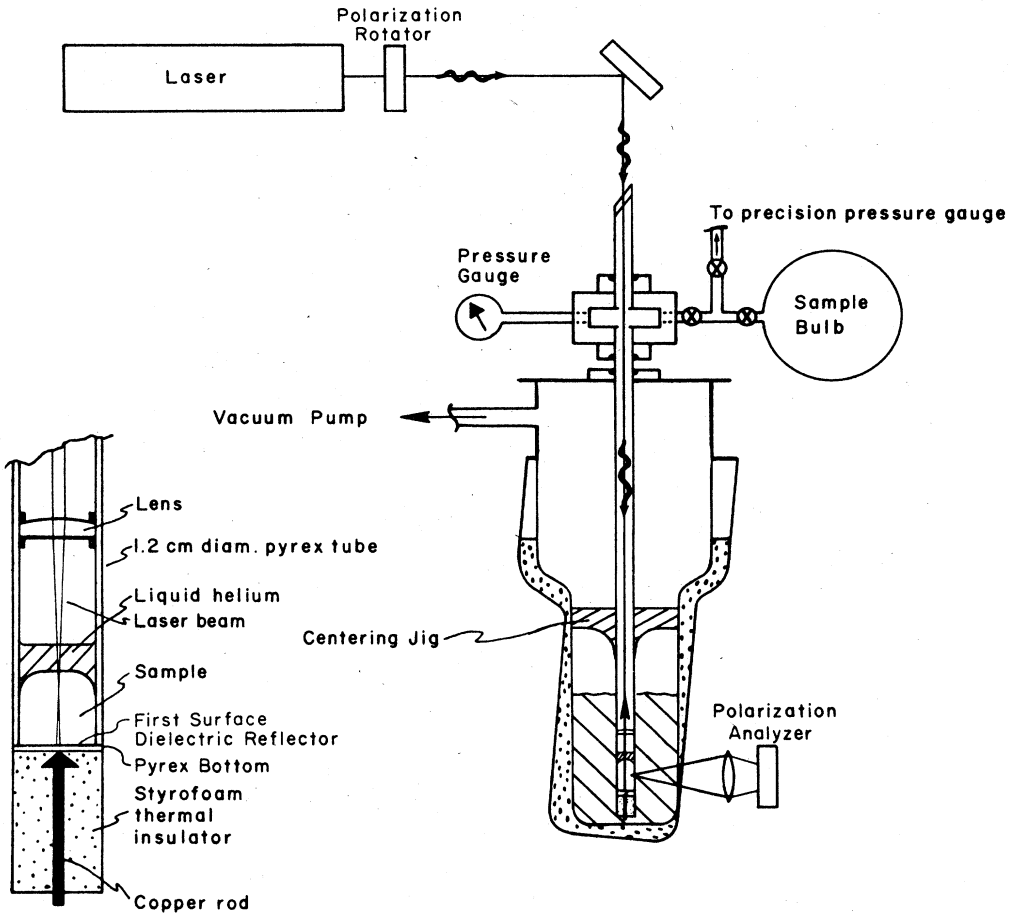

FIG. 28. Apparatus used for growth of single crystals of H_2 and D_2. See text for description (after Hardy *et al.*, 1975).

can dissolve in H_2 under pressure.[13] The experiments in which the transition was not observed were all characterized by conditions of rather uniform density samples.

D. Theory of the phase transition in $J = 1$ hydrogens

A large body of theoretical work on the orientational order–disorder phase transition exists, and we shall not attempt to provide a full coverage of this work. Most treatments are classical or molecular field approaches. Ordering of quadrupoles on lattices has been treated by Nagai and Nakamura (1960, general), Felsteiner (1965, fcc), Raich and James (1966, fcc), James and Raich (1967, fcc), Miyagi and Nakamura (1967, hcp, fcc), James (1968, hcp), James (1968, fcc, general), Felsteiner *et al.* (1971, 1972, general) and Sivardière (1972, general). There has been no successful treatment of the complete double phase transition, i.e., hcp → fcc and orientational ordering. Most treatments study the ordering on an assumed lattice.

We shall outline the quantum-mechanical molecular field treatment of James and Raich (1967). The Hamiltonian for the model is

$$\mathcal{H} = \sum_i \mathcal{H}_i(\Omega_i) + \frac{1}{2}\sum_{ij} V_{ij}(\Omega_i, \Omega_j), \tag{6.1}$$

where $\mathcal{H}_i$ is the rigid rotor energy, Eq. (2.16b), and $V_{ij}(\equiv \phi_{\mathrm{EQQ}})$ is taken to be the EQQ interaction, Eq. (3.17). A nearest neighbor approximation is used, and the molecules are assumed to be on a rigid lattice—i.e., no zero-point motion exists. J is taken to be a good quantum number and all molecules are in the states $|J=1,M\rangle$ with no excitation of higher rotational states. Thus within the manifold of $J=1$ states $\mathcal{H}_i$ is a constant and can be ignored. The EQ moment of a central molecule i interacts with the electric field gradients due to the EQ moments of the surrounding molecules—this is the internal field, U_i. In general the state ψ_μ^i of the central molecule will be a linear combination of the three $|1,M\rangle$ functions which is determined by U_i. Since U_i depends on the states of the molecules, the states must be determined self-consistently. The main objective is to determine the ground state of the crystal which is given by the wave function

$$\Psi = \prod \psi_\mu^i, \tag{6.2a}$$

[13] R. Jochemsen and I. F. Silvera have nonquantitative evidence of He dissolved in D_2 under pressure, unpublished.

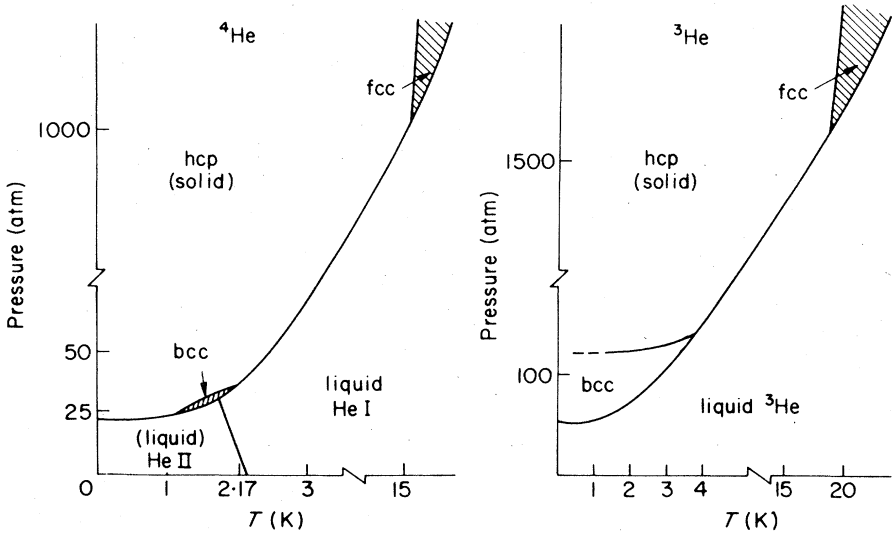

FIG. 29. Phase diagram of ^{3}He and ^{4}He.

where μ are the quantum numbers of the ith molecule. Three real basis functions, $\phi_1 = 2^{-1/2}(-Y_{11} + Y_{1-1})$, $\phi_2 = i2^{-1/2}(Y_{11} + Y_{1-1})$, and $\phi_3 = Y_{10}$ can be used to represent the function ψ_μ^i:

$$\psi_\mu^i = \sum \gamma_{\mu\alpha}^i \phi_\alpha , \tag{6.2b}$$

where the $\gamma_{\mu\alpha}^i$ are real coefficients. The molecular field at the ith molecule is

$$U_i = \sum_{j,\nu} \langle \psi_\nu^j \mid V_{ij} \mid \psi_\nu^j \rangle P_\nu^j , \tag{6.3}$$

where P_ν^j is the probability of state ψ_ν^j:

$$P_\nu^j = \exp(-\beta\varepsilon_\mu^j) \Big/ \sum_{i,\nu} \exp(-\beta\varepsilon_\nu^i) . \tag{6.4}$$

Here ε_μ^j is the energy of molecule j and $\beta = (kT)^{-1}$. The state of the system is determined by the solution of the equation

$$U_i \psi_\mu^i = \varepsilon_\mu^i \psi_\mu^i . \tag{6.5}$$

We note that the matrix element of U_i at $T = 0$ is given by

$$\langle \psi_\mu^i \psi_\nu^j \mid V_{ij}(\Omega_i, \Omega_j) \mid \psi_\mu^i \psi_\nu^j \rangle = \tfrac{4}{25} V_{ij}(\bar{\Omega}_i, \bar{\Omega}_j) ,$$

where $V_{ij}(\bar{\Omega}_i, \bar{\Omega}_j)$ is the classical EQQ energy for quadrupoles with fixed orientations, $\bar{\Omega}_i$, and $\bar{\Omega}_j$. In the quantum-mechanical states Y_{1m}, the interaction energy is reduced by $(\frac{2}{5})^2$. James and Raich show that this factor $\frac{4}{25}$ is the principal difference between the classical and quantum-mechanical calculations. They find self-consistent solutions to (6.5) on an fcc lattice. One solution is $P_\mu^i = \frac{1}{3}$ for all i, μ. This represents the state of complete orientational disorder and it is easily seen that $U_i = 0$, for all i. Below a critical temperature T_c, they found a lower free energy state, namely Pa3, with self-consistent solutions. For the ground state, eigenenergies are $\varepsilon_1(T=0) = -38\Gamma/3$, corresponding to the state Y_{10}; the states ε_2 and ε_3 are degenerate with $\varepsilon_{2,3} = -19\Gamma/3$, corresponding to states Y_{21}, Y_{2-1} or normalized linear combinations thereof. The effect of lifting the restriction of nearest neighbor interactions is to slightly increase $|\varepsilon_i|$ by a factor 1.116.

The axes of quantization of the self-consistent wave function are the symmetry axes of the molecular field, or the crystalline body diagonals of the fcc lattice. We can describe the ground state with the wave function (6.2)

$$\Psi = \prod_{\alpha,i} Y_{10}(\Omega_{\alpha i}) , \tag{6.6}$$

where $\alpha = 1$ to 4 indexes the four sublattices and i runs over the molecules on a sublattice. There are four axes of quantization, corresponding to the body diagonals with threefold symmetry for each sublattice.

The temperature dependence of the molecular field energies is shown in Fig. 30. A first-order phase transition takes place at a critical temperature

$$kT_c = 21.2\Gamma/4 \ln 2 , \tag{6.7}$$

where we include all neighbors in the interaction. Using the rigid lattice value $\Gamma = \Gamma_0$ (Table VIII), we obtain $T_c = 7.26$ K for H_2 and 8.98 for D_2; using the effective value in the solid, $\Gamma = \bar{\Gamma}$, which accounts for the effects of zero-point motion, etc., we obtain $T_c = 6.33$ K for H_2 and 7.85 K for D_2, about a factor 2 higher than found experimentally.

More thorough analyses and consideration of lattices other than fcc have shown that the Pa3 structure has the lowest energy (Miyagi and Nakamura, 1967). Summarizing, the molecular field approximation (mfa) does a good job in predicting the ground-state structure, but provides a poor approximation for the critical temperature. The problem undoubtedly lies in the absence of correlations in the mfa. The lowest energy for a pair of interacting molecules is the T configuration with $E_T = -4\Gamma$ (see Table IX). However, on the three-dimensional lattice all pairs cannot be mutually perpendicular. The total lattice energy is minimized in the Pa3

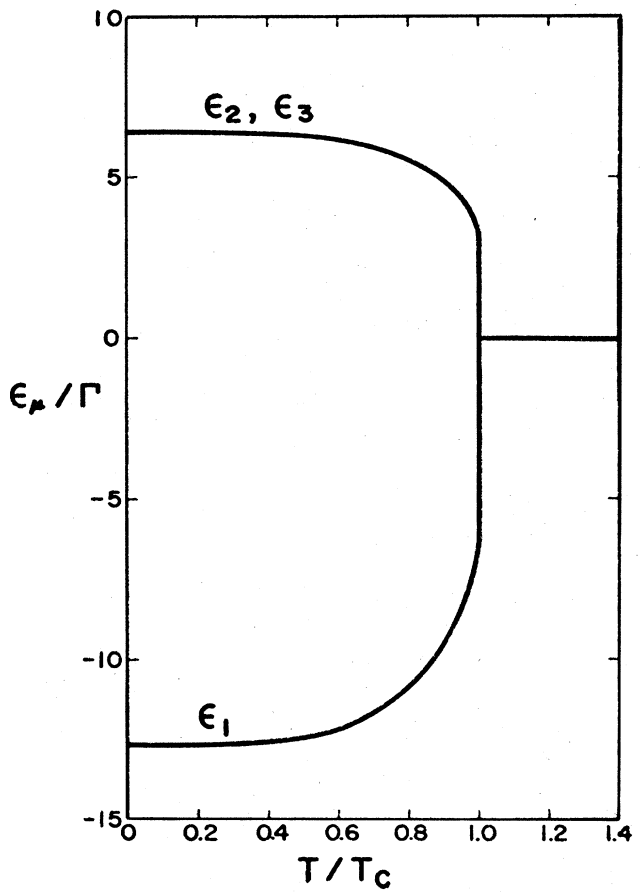

FIG. 30. Molecular field energy levels in Pa3 hydrogen. The upper level is doubtly degenerate (after James and Raich, 1967).

structure in which the energy per pair for nearest neighbor interactions is $-\frac{19}{18}\Gamma$. At high temperatures short-range order exists. As the temperature is lowered, there is a competition between short-range ordering which favors the T configuration and long-range order favoring the Pa3 structure with the lowest total energy. The correlations evidently lower the ordering temperature predicted by the mfa.

Raich and Etters (1968) attempted to account for correlations by applying the Bethe–Peierls approximation to hydrogen. They found no abrupt phase transition, in contrast to the molecular field approximation which predicted a first-order phase transition. However, order starts to set in at about the same (high) temperature as in the mfa. They also treated the ortho–para dilution problem, but found nothing comparable to experiment. An improvement was made by Lee and Raich (1972), who used a cluster variation method. They obtained $T_c \simeq 3.68$ K for H_2 and $T_c \simeq 5.03$ K for D_2. They predicted a first-order phase transition at T_c from ordered fcc (Pa3) to ordered hcp which existed in a narrow temperature region. The latter has never been observed.

Homma and Nakano (1975) and Sullivan (1976) also extended the mfa and found first-order phase transitions that compare favorably with experiment and yield approximately the same value for T_c as that of Lee and Raich. Sullivan treated the dilution problem and found a critical concentration of $c_{1c} = 0.50$ which compares well with experiment. The approximation used begins to break down for $c_{1c} \lesssim 0.60$, so that this theory is probably inadequate to accurately describe the curvature in the phase line near $c_1 = c_{1c}$.

E. The order of the phase transition

The molecular field approximation of James and Raich (1967) predicted a first-order phase transition for the orientational ordering of the molecules on the Pa3 structure. However, in this approximation, the EQQ Hamiltonian is effectively an Ising treatment and Harris (1968) rigorously showed that in the Ising limit, there is no transition. As was just discussed, theories which go beyond the mfa give varying predictions. Cullen *et al.* (1972) argued quite generally, using the Landau theory of phase transitions, to theoretically establish a first-order phase transition. They showed that for quadrupoles on an fcc lattice, a third-order invariant exists in the expansion of the free energy in the order parameter and the transition to the Pa3 structure takes place discontinuously. Thus, independent of the hcp–fcc structural transition, one expects the transition from disordered fcc to ordered fcc to be first order.

For a quadrupolar system ($J = 1$), two normalized local order parameters can be defined, $\sigma \equiv \frac{1}{2}\langle 3J_{zi}^2 - 2\rangle_T$ and $\eta \equiv \langle J_{xi}^2 - J_{yi}^2\rangle_T$. In the configuration of axial symmetry that occur for the Pa3 structure, η is zero. A number of equivalent definitions of the long-range order parameter have been used in the literature:

$$\sigma(T) = -\frac{1}{2NC_1}\sum_i \langle 3J_{zi}^2 - 2\rangle_T \tag{6.8a}$$

$$= \frac{(4\pi/5)^{1/2}}{NC_1}\sum_i \langle Y_{20}(\omega_i)\rangle_T \tag{6.8b}$$

$$= \frac{1}{2NC_1}\sum_i \langle 3\cos^2\theta_i - 1\rangle_T . \tag{6.8c}$$

Here we have included the possibility of dilution for generality. N is the number of molecules, $\langle\,\rangle_T$ is a thermal average, and $\omega_i \equiv (\theta_i, \phi_i)$, where θ_i is the deviation of the molecular axis from the ordering direction. With this definition σ is normalized to be 1 with full order ($J_z^2 = \cos^2\theta = 1$) and 0 when completely disordered ($J_z^2 = \frac{2}{3}, \cos^2\theta = \frac{1}{3}$).

The temperature dependence of the order parameter was first measured by Meyer *et al.* (1972) in D_2. They used NMR to study the splitting of the Pake doublet which is a direct measure of the local order parameter.

Later, Jochemsen *et al.* (1978) showed that the integrated intensity of the far infrared absorption due to IR active phonons is directly proportional to the square of the long-range order parameter. The results of both measurements for D_2 are shown in Fig. 31. One sees that σ is weakly temperature dependent and falls abruptly to zero at T_c, characteristic of a first-order transition. Few measurements are available for H_2, basically because of technical problems due to more rapid conversion. Silvera and Jochemsen (1979) have recently

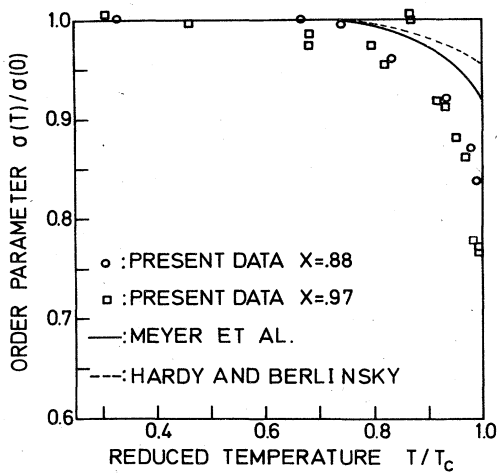

FIG. 31. Temperature dependence of the order parameter in D_2 at zero pressure. Data are due to Meyer *et al.* (1972), and Jochemsen *et al.* (present data) (1978). Theory is after Berlinsky and Hardy (1973) (after Jochemsen *et al.*, 1978).

determined σ by the infrared technique by "aging" of the sample. The crystal is held at a constant temperature and allowed to convert which lowers T_c and transcends from the ordered to the disordered phase. Results shown in Fig. 32 indicate a gentler transition. It is not clear if this arises from the smearing out of the transition due to the finite conversion rate or a characteristic of H_2 that differs from D_2.

F. The very-low-temperature phase

In 1972 Sullivan and Pound (1972a, b) studied the phase line of H_2 by means of NMR for $0.40 < c_1 < 0.70$ at temperatures below 100 mK, achieved with a ^{3}He–^{4}He dilution refrigerator. They observed the order parameter by studying the splitting of the Pake doublet, ν_{DD}. Samples were held at constant temperature and aged to lower the value of c_1. For $0.55 < c_1 < 0.60$ the splitting rapidly decreased. Ishimoto *et al.* (1973, 1976) studied the free induction decay of the nuclear magnetization for $c_1 \gtrsim 0.08$ and defined the transition line T_c^* by the disappearance of beat structure on their NMR signal. In this work it was suggested that below $c_1 \simeq 0.56$ an axial single molecule crystal field of the form of Eq. (3.22d), $\phi_A = V_c(3J_z^2 - \frac{2}{3})$, was responsible for the lifting of the degeneracy of the $J=1$ molecules and local orientational ordering. However, the implied value of A was much larger than found from other measurements.

T_c^* was also determined by Sullivan *et al.* (1975), Sullivan (1976), Vinegar *et al.* (1977), Husa and Daunt (1978), and Sullivan *et al.* (1978) from changes in the NMR line shape. The resulting phase line is shown in Fig. 33 (see also Fig. 36). The low-temperature phase occurs for $T \leq 0.37$ K and obeys the empirical relation

$$T_c^*(c_1) = 550(c_1 - 0.10)^{1/2} \pm 10 \text{ (mK)}. \tag{6.9}$$

Sullivan (1976) reported on the temperature dependence of the (local) order parameter as shown in Fig. 34. The rapid change with temperature in ν_{DD} was more characteristic of a collective type ordering than the behavior expected for depopulation of crystal field levels, indicated by the dotted lines. Although Vinegar *et al.* (1977) did not observe the abrupt temperature dependence, their samples probably suffered from thermal inhomogeneity which would smear out the transition. In cooling from 14 K, H_2 samples contract and tend to pull free from walls, giving reduced thermal contact. Sullivan's samples were frozen on fine wires, providing a better contact to carry away the substantial amount of heat generated by conversion.

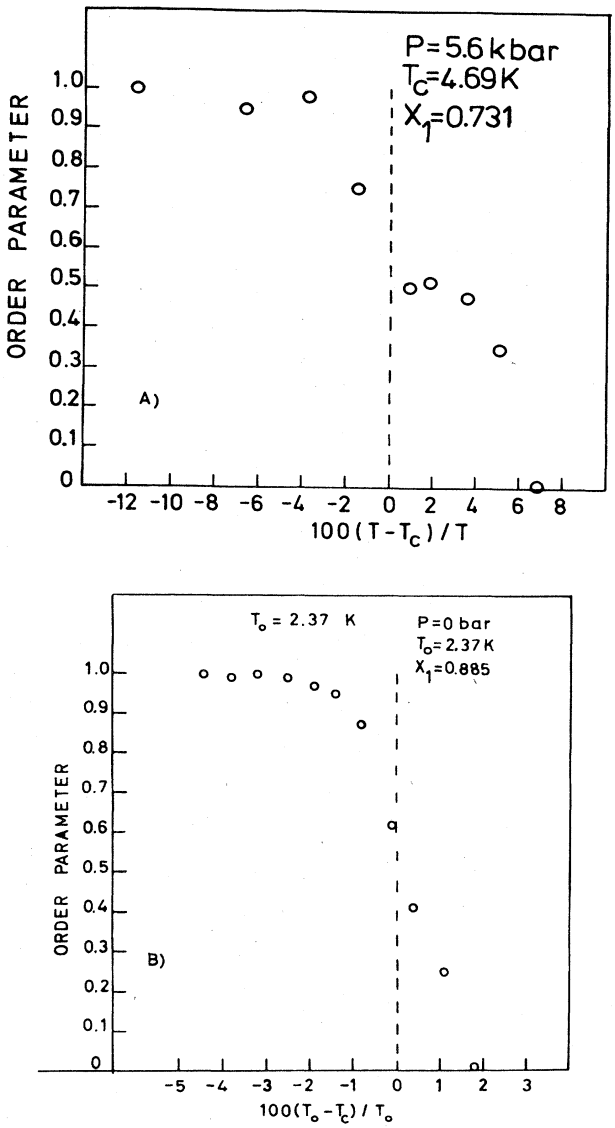

FIG. 32. Temperature dependence of the order parameter in H_2 for $P = 5.6$ kbars and $P = 0$. (A) Determination by variation of temperature at almost constant x_1. (B) Shows a determination of σ by variation of concentration $x_1 \equiv c_1$ at constant temperature (aging), T_0 (after Silvera and Jochemsen, 1979).

Based upon the abruptness of the transition and the NMR line shape Sullivan *et al.* (1978) have suggested that the very-low-temperature phase is a quadrupolar glass, in analogy with spin glasses. In this case the $J=1$ molecules are randomly distributed on a close packed lattice. For $c_1 \lesssim 0.55$ the long-range order is no longer sustained. For low enough temperatures,

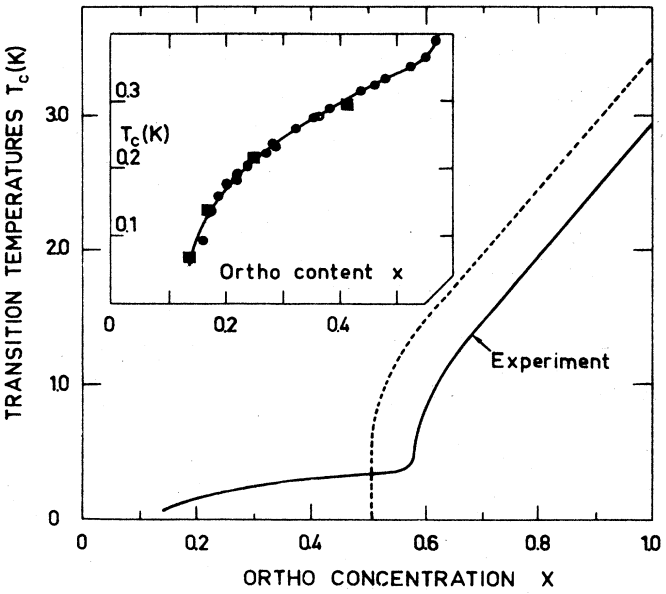

FIG. 33. Phase line of solid hydrogen as a function of ortho concentration, $x \equiv c_1$. The solid line is the experimental result (hysteresis is not shown); the broken line is a theoretical prediction for the Pa3 phase line (Sullivan, 1976) (after Sullivan *et al.*, 1978).

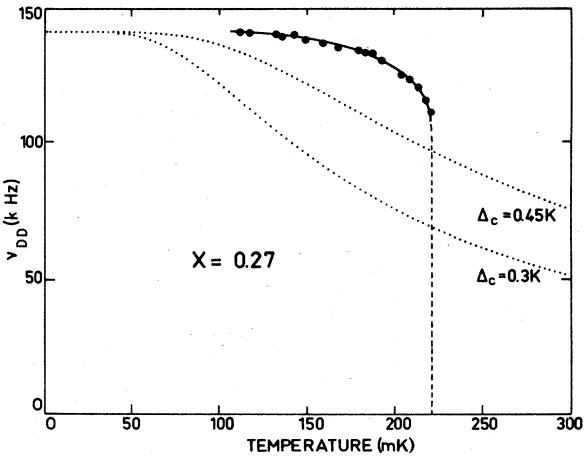

FIG. 34. Temperature dependence of the order parameter in the very-low-temperature phase as determined by NMR techniques. The dotted lines show the behavior to be expected if the temperature dependence were due to the depopulation of energy levels of $J=1$ molecules in a cylindrically symmetric crystalline field of strength Δ_c. Here $x \equiv c_1$ (after Sullivan, 1976).

interactions break the local symmetry so that quadrupole moments $\sigma_i = \langle 3J_{zi}^2 - 2 \rangle$ and $\eta_i = \langle J_{x_i}^2 - J_{y_i}^2 \rangle$ are frozen at random from site to site. An example, in two dimensions, is shown in Fig. 35. For a spin glass, under certain conditions, one expects a transition at a critical temperature $T_c^* \simeq (Z\gamma)^{1/2}/k_B$ where Z is the number of effective neighbors and γ the variance of the random interactions. For a close packed structure, taking $Z = 12c_1$ gives $T_c^* \sim c_1^{1/2}$ in reasonable agreement with experiment. However, Sullivan *et al.* (1978) estimate T_c^* to be 3 times higher than experiment. Recently Gates *et al.* (1978, 1979) have studied the hcp to fcc (≡ cfc) phase transition in single crystals of H_2 by x-ray diffraction at very low temperatures. Their results are shown in Fig. 36 (circles) on a logarithmic temperature scale along with other determinations of T_c^*. We note two striking features: (1) the very-low-temperature phase has an hcp and not an fcc structure as had been assumed. (2) The critical concentration, as determined by the fcc–hcp structural transition in an aging experiment, is $c_{1c} \simeq 0.49$ (circles). Yet, when we compare to the data of Sullivan *et al.* (1978) (open squares), the low-temperature phase line passes through the line for T_{od} to the phase line T_{do}. This apparently is a new complication in the phase diagram

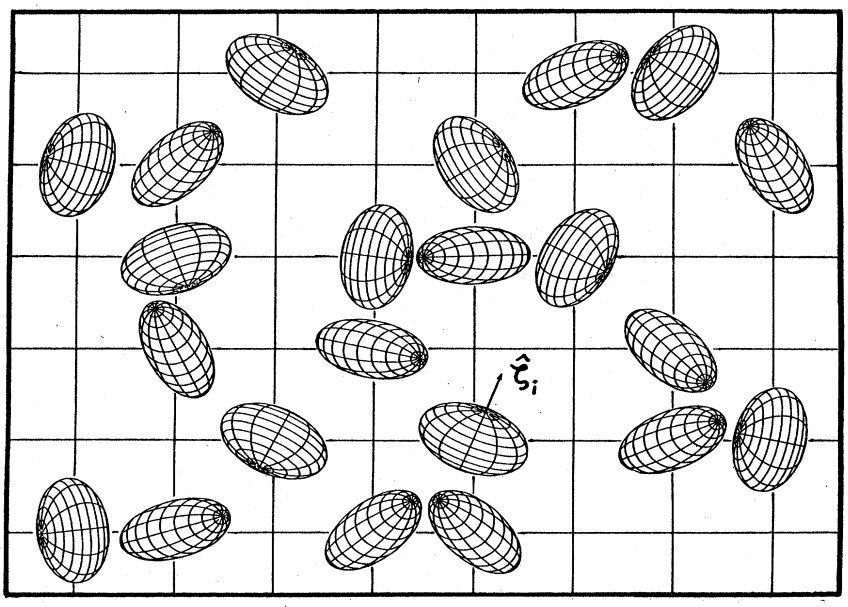

FIG. 35. A two-dimensional glass represented by a square grid. Only the randomly distributed "$J=1$ molecules" represented by ellipsoids which vary in shape and orientation are shown (after Sullivan *et al.*, 1978).

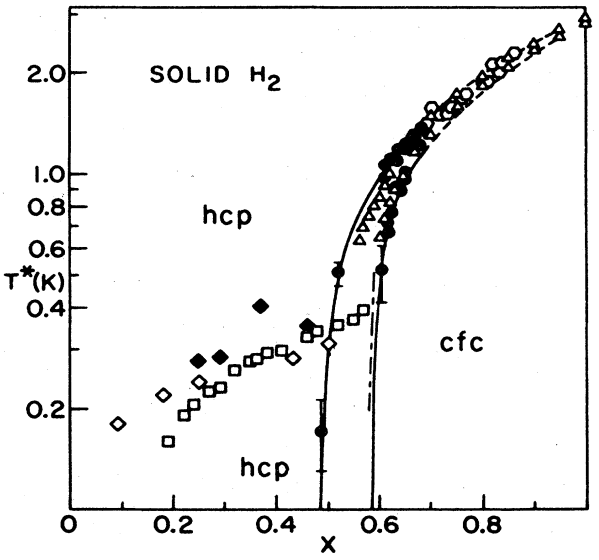

FIG. 36. The phase line of hydrogen as determined by x-ray diffraction (circles). Here, $x \equiv c_1$. Except for some points that we have removed, this figure is from Gates *et al.* (1978).

(excluding a problem of experimental error in the determination of c_1 and T in different laboratories). One possible implication is that in the low concentration regions the structural (hcp–fcc) and orientational ordering have different phase lines, since x-ray measures the former and NMR the latter of these phase lines.

All told, the quadrupolar glass state appears to be the most plausible explanation for the low-temperature phase. A similar behavior has recently been observed for D_2 by Sullivan and Devoret (1978), again by NMR techniques, for $c_1 = 0.33$. However, more experimental and theoretical work is still required. An early suggestion that aging experiments could result in a nonrandom distribution of $J=1$ molecules, giving rise to a new ordering due to next nearest neighbor interactions, seems to be eliminated by a measurement of Sullivan *et al.* (1978), who melted and refroze a sample with $c_1 \simeq 0.32$ and found line shape results identical to that for an aged sample. Another possibility is that clustering of $J=1$ molecules due to quantum diffusion is playing an important role, and destroys the random $J=1$ distribution in the lattice. Husa and Daunt (1978) studied samples under varying conditions of cooling and warming and conclude that clustering does not play an important role. However, for very low concentrations and temperatures Schweizer *et al.* (1978) observe the rapid disappearance of isolated ortho-H_2 molecules due to clustering. Muckerjee *et al.* (1978) and Gaines *et al.* (1978) have studied single crystals of H_2 at very low temperatures with extremely low concentrations, $0.0001 < c_1 < 0.003$, by means of nuclear free induction decay (FID). From the rapid temperature dependence of the structure on the FID, they suggest that a cooperative phase transition occurs for $T^* \simeq 0.18$ K. Extrapolation of the results of Ishimoto *et al.* (1973, 1976) to low c_1 agree with this; however, Sullivan *et al.*'s work does not. It would be of great use in sorting out the very-low-temperature behavior of H_2 and D_2 if techniques other than NMR were utilized. The recent x-ray work has been illuminating. We suggest that a FIR study would be useful as it is sensitive to the long-range order parameter by virtue of one-phonon absorption. Even if long-range order does not set in, the low-temperature properties can be examined by studying the temperature dependence of the dipole–dipole correlation function, as absorption occurs even in the disordered phase due to paralibron–phonon processes.

G. The effect of pressure on structure and ordering

Hydrogen is highly compressible and as a consequence pressure causes substantial changes in the molar volume or density (see following section). This affects the solid in two important ways: (1) the intermolecular forces change and (2) the single molecule rotational states change. The former is the most important effect to pressures ~20 kbar corresponding to a variation in ρ/ρ_0 of ~2, where ρ_0 is the zero-pressure density. For $P \gtrsim 10^5$ bar, the latter, (2), is also important.

1. Intermediate pressures

Studies of the phase diagram to $\rho/\rho_0 \simeq 1.7$ have recently been made by Silvera and Jochemsen (1979) by FIR spectroscopy. They find the spectra to be consistent with a Pa3 structure for the ordered state. For $c_1 = 1$, the phase line scales approximately as $(\rho/\rho_0)^{5/3}$. This implies that the EQQ interaction remains the dominant interaction responsible for the ordering since the critical temperature is expected to scale as [see Eq. (3.17)]

$$T_c \sim \langle\langle 0 | \phi_{\mathrm{EQQ}} | 0 \rangle\rangle_T = \frac{20\pi}{18}(70\pi)^{1/2}\langle\Gamma\rangle\left\langle \sum_{\substack{i,j \\ M,N}} C(224;MN) Y_{2M}(\Omega_i) Y_{2N}(\Omega_j) \times [Y^*_{4,M+N}(\Omega_{ij})\Gamma_{ij}/\Gamma_0]\right\rangle_T . \tag{6.10}$$

Here $\langle 0|0\rangle$ implies an average over the phonon ground state and $\langle\ \rangle_T$, a thermal average. $\langle 0|0\rangle$ renormalizes the radial dependence of the interaction, represented by $\langle\Gamma\rangle = \xi_{54}\Gamma_0$ (see Sec. VIII). From Eq. (6.10) we see

$$T_c \sim \xi_{54}(\rho)\Gamma_0 \sim [\xi_{54}(\rho)/\xi_{54}(\rho_0)](\rho/\rho_0)^{5/3} T_c(\rho_0) . \tag{6.11}$$

The experimental results for H_2 are shown in Fig. 37; for D_2 the scaling as ϕ_{EQQ} agrees even better (Jochemsen, 1978). A striking result is the density dependence of the critical concentration shown in Fig. 38. The measurements show that as ρ increases, c_{1c} decreases. From the form of Eq. (6.10) we might expect c_{1c} to be independent of density as long as the form of the interaction did not change, as appears to be the case. Evidently c_{1c} is not just determined by geometric factors. Percolation certainly does not appear to be an important factor as the percolation concentration for an fcc lattice is 0.195 (for nearest neighbor interactions). This decrease of c_{1c} may arise from a subtle interplay of the competition between long-range order, which is optimized on the Pa3 structure for $c_1 = 1$, and short-range order which gives a lowest pair energy for the T

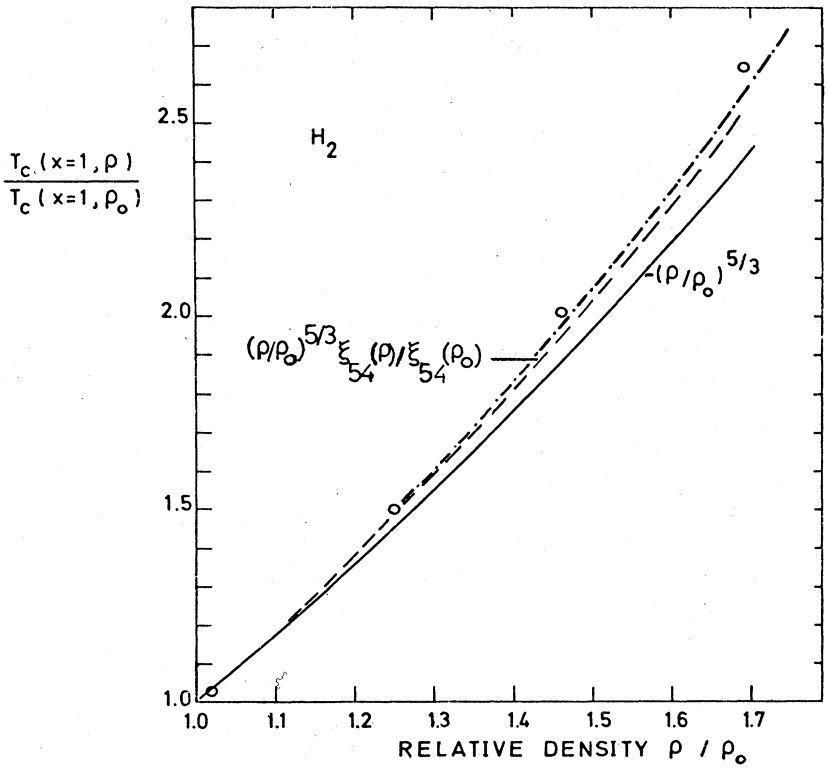

FIG. 37. Density dependence of the (Pa3) order-disorder transition temperature in ortho hydrogen, normalized to that at zero pressure. The dashed–dot line includes the effect on T_c of the mixing of the $J=3$ rotational state into the $J=1$ state (after Silvera and Jochemsen, 1979).

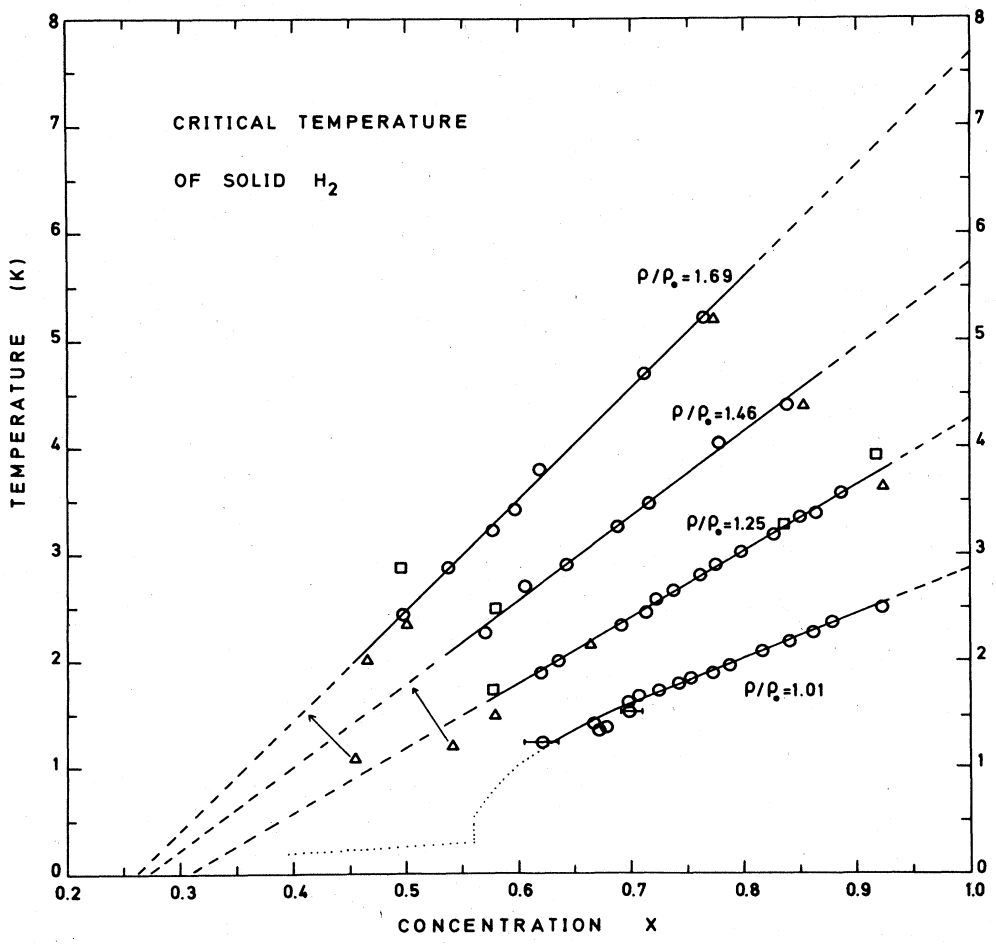

FIG. 38. The phase diagram of solid H_2 as a function of ortho concentration ($x\equiv c_1$) and density. The dashed lines are linear extrapolations. The dotted line shows the known behavior at $P=0$ (after Silvera and Jochemsen, 1979).

configuration and is the ground state for isolated pairs which arise for low c_1. These studies were limited to $T>1$ K so that the density dependence of the low-temperature phase line remains unknown.

2. High pressures

At higher pressures, only theoretical predictions of the phase diagram exist. Raich and Etters (1972), Felsteiner and Friedman (1973), and England *et al.* (1976) have investigated molecular ordering in hydrogen and its isotopes at high densities. At zero pressure, to a good approximation, J is a good quantum number. As a consequence the p-H_2 and o-D_2 molecules are spherically symmetric, and these species do not display orientational ordering. As shown earlier, the anisotropic interactions mix the rotational states, so that even rotational species (p-H_2, o-D_2) will have a nonspherical spatial distribution; if the admixture is sufficient, an orientational ordering transition will take place.

In the molecular field treatment the transitions considered (or found) are to the $Pa3$ structure. For axial symmetry the molecular field is taken as in Eq. (6.3), $U_i = U_0 Y_{20}(\omega_i)$. In this case, in contrast to the zero-pressure treatment, $\mathcal{H}_i = BJ_i^2$ is important in determining the wave function of the system. The single molecule ground state is of the form

$$\psi_{00} = a_0^{00} Y_{10} + a_2^{00} Y_{20} + a_4^{00} Y_{40} + \cdots \tag{6.12a}$$

for even states, and

$$\psi_{01} = a_0^{01} Y_{10} + a_3^{01} Y_{30} + a_5^{01} Y_{50} + \cdots \tag{6.12b}$$

for odd states. The coefficients a_r^{ml} are density dependent and are found from the self-consistent solutions of Eqs. (6.3) (including $\mathcal{H}_i$) and (6.5). The $T=0$ K values for the order parameter versus intermolecular separation normalized to the zero-pressure lattice parameter are shown in Fig. 39, after England *et al.* We see that the heavier the isotope the larger R/R_0 (or lower the pressure) for a transition of the even species. This follows since the mixing of rotational states depends on $\bar{V}_{\text{anis}}/B$, and the rotational constant B scales inversely as the mass. England *et al.* estimate transitions at 375 kbar, 175 kbar, and 24 kbar for H_2, D_2, and T_2, respectively. We have recalculated the transition pressures using the equation of state resulting from the recent potential of Silvera and Goldman (1978), Eq. (3.10), and find 270 kbar for H_2 and 73 kbar for D_2, for the critical densities of England *et al.*

Recently Sharma *et al.* (1979) have been able to pressurize normal-H_2 to 630 kbar at room temperature in a diamond anvil cell. They determined the solidification point to be 55 kbar at 22 °C. Rotational and vibrational transitions were observed by Raman scattering. Although vibrational lines were seen to first increase in frequency and then decrease as the pressure was raised, no clear evidence of ordering emerged from these first studies probably due to the high (room) temperature and mixed ortho–para nature of the samples.

VII. THERMODYNAMIC PROPERTIES

In this section we present and discuss the substantial body of work having to do with thermodynamic properties of the solid hydrogens. We shall attempt to give a guide to the literature and present a number of useful representative results in figures and tables. As the theory is often quite standard, we shall not handle this in great detail. We begin by presenting the P–(or B_m)–V–T–C, relations and the sublimation energy; this is followed by treatment of $(\partial P/\partial T)_V$, specific heat, Debye temperature and elastic constants, and thermal conductivity.

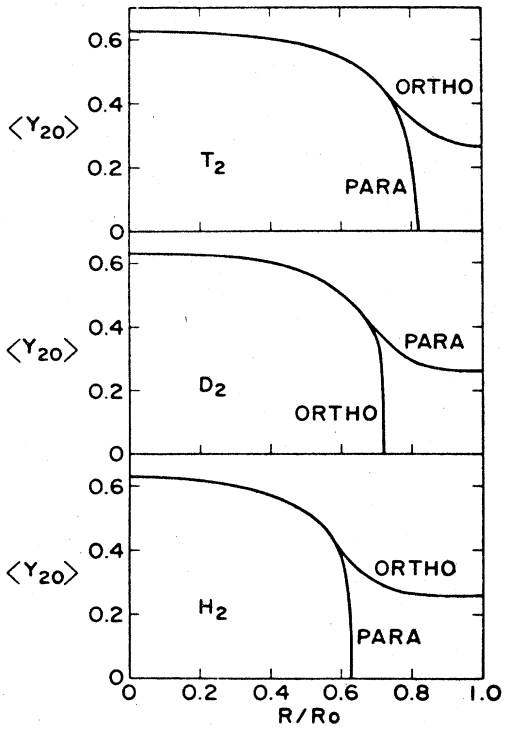

FIG. 39. The ordering parameter curves for ortho- and para-H_2, D_2, and T_2 at $T=0$ K, as a function of nearest neighbor distance R, normalized to that at zero pressure, R_0 (after England *et al.*, 1976). These are obtained within a molecular field approximation.

A. The equation of state

The equation of state (EOS) implies knowledge of the relationship between P–V–T–C where C is the ortho (para) concentration. This is known with reasonable accuracy for H_2 and D_2 to ~25 kbar in the solid state. An accurate knowledge of the molar volume as a function of P–T–C is vital in the interpretation of properties of the solid as some properties vary as very high powers of the intermolecular separation.

Available measurements of the EOS tend to localize on the melting lines, the 4.2 K isotherms, and the molar volume at zero pressure. Simon *et al.* (1929) measured the melting line to 5 kbar; Mills and Grilly (1956) repeated these measurements with greater accuracy to a pressure of 3.5 kbar. The accuracy was further refined by Goodwin and Roder (1963) at lower pressures. Kechin *et al.* (1977) have recently measured to 10 kbar in H_2. Molar volumes on the melting line have been determined by Dwyer *et al.* (1965) to pressures of 412

bars and recently by Krause (1978) to 2 kbar. The 4.2 K isotherms of H_2 and D_2 were first measured by Stewart (1956) from 2–20 kbar and were repeated and extended by Anderson and Swenson (1974) from 0.5 to 25 kbar. Durana and McTague (1975) also determined the 4.2 K isotherm, to 5 kbar, but for para-H_2 rather than normal H_2. There is a large group of measurements dealing with the determination of the molar volume at zero pressure. These have been made by thermodynamic techniques, x-ray, electron and neutron diffraction. Silvera *et al.* (1978) and Driessen *et al.* (1979) have recently measured isochores of H_2 and D_2 to 2 kbar and have used these, along with earlier measurements, to provide tables of $P-V-T-C_1$ to ~25 kbar.

Thermal expansion in H_2 up to pressures of 200 bar has been studied by Manzhelii *et al.* (1975).

Ultrahigh pressure measurements on H_2 are discussed by Ross (1974). The EOS of the fluid hydrogens to 20 kbar have been studied by Mills *et al.* (1977, n-H_2) (1978, n-D_2) and (1978, T_2).

Hydrogen is a quantum solid and is therefore highly compressible. In heavier solids in equilibrium at low temperature, the atoms (or molecules) sit at the minimum of the potential well presented by the neighboring atoms (see Figs. 8, 9). When pressure is applied the atoms are "pushed into" the hard cores of the potential; as a result of this core, the compressibility is usually quite small. Typically a pressure of 10 kbar results in a few percent change in molar volume. For H_2 10 kbar result in a ~100% change in volume. The physical reason for this is that at $T=0$ the lattice is highly expanded due to the zero-point kinetic energy. Although the minimum of the potential well is at ~3.44 Å separation, the molecules have an average separation of ~3.79 Å at zero pressure. The initial compression is against the weaker "kinetic pressure" rather than the harder "core pressure." At pressures of a few kbar the compressibility of hydrogen is decreased about sixfold and it begins to behave more like a "nonquantum solid."

Due to the large compressibility, the weak anisotropic forces have a non-negligible effect on the molar volume. For example at $T=0$ K the molar volume of ortho-H_2 is ~2% smaller than that of para-H_2, for which the anisotropic interactions are zero.

1. Theoretical considerations: Quadrupolar pressure

We shall be interested in the pressure and the bulk modulus, B_m (instead of the compressibility), defined in terms of the free energy F:

$$P=-\left(\frac{\partial F}{\partial V}\right)_T \tag{7.1}$$

$$B_m=-V\left(\frac{\partial P}{\partial V}\right)_T \tag{7.2}$$

The free energy can be separated into a zero temperature part F_0 and an incremental thermal part F^*:

$$F(V,T,C_1)=F_0(V,C_1)+F^*(V,T,C_1) \tag{7.3a}$$

and analogously

$$P(V,T,C_1)=P_0(V,C_1)+P^*(V,T,C_1) \tag{7.3b}$$

with $F^*=P^*=0$ at $T=0$. The free energy has translational (lattice) contributions (L) and orientational contributions (Q) arising from the isotropic and anisotropic interactions, respectively. Because the rotation–translation coupling is weak, these can be taken to be additive:

$$F=\sum_\alpha F_\alpha=F_L+F_Q. \tag{7.4a}$$

We shall restrict attention to F_Q arising from EQQ interactions. As a result of (7.4) and (7.1) we see that we can speak of a normal lattice pressure and a quadrupolar pressure:

$$P=P_L+P_Q. \tag{7.4b}$$

It was shown by Spain and Segall (1971) that the Mie–Grüneisen equation of state could be accurately applied to solid helium; Driessen *et al.* (1979) have generalized this to include quadrupolar forces and applied it to H_2 and D_2. In this picture one assumes that the $P-V$ relations are known at $T=0$ and $C_1=0$ and calculates the incremental thermal part F^* of Eq. (7.3) or the analogous thermal incremental pressure, P^*. One has the basic relations

$$P^*(V,T,C_1)=\frac{\gamma_\alpha(V)}{V}U^*_\alpha(V,T,C_1) \tag{7.5}$$

with

$$\gamma_\alpha(V)=\frac{-d\ln\theta_\alpha(V)}{d\ln V} \tag{7.6}$$

and

$$U^*_\alpha(V,T,C_1)=\int_{x=0}^{T}C_{V\alpha}(V,x,C_1)\,dx. \tag{7.7a}$$

Here γ_α is the Grüneisen constant, θ_α is a characteristic temperature, and $C_{V\alpha}$ is the αth component of the specific heat at constant volume. The lattice contribution can be well represented by the Debye model with

$$C_{VL}(V,T)=9N_0k_B\left(\frac{T}{\theta_D}\right)^3\int_0^{T/\theta_D}\frac{x^4e^x}{(e^x-1)^2}, \tag{7.7b}$$

where N_0 is Avogadros number and $\theta_D\equiv\theta_L$ is the (temperature dependent) Debye temperature. For the quadrupolar pressure Jarvis *et al.* (1969) have shown that $\gamma_Q=d\ln\Gamma/d\ln V=-V/\Gamma(\partial\Gamma/\partial V)\simeq\frac{5}{3}$.

The reason why the Mie–Grüneisen model has been found to work so well for quantum solids is that all of the complications due to zero-point motion and anharmonicity are included in F_0 or P_0, which are taken as measured quantities. The thermal increments are apparently well behaved and can be used to fill in the EOS from selected measurements of the isochoric specific heat or isochoric pressure. Intermediate values can be easily and accurately calculated.

The quadrupolar specific heat C_{VQ} can be obtained from a semiempirical expression derived by Berlinsky and Harris (1970) which gives a reasonably good fit to experimental data in the disordered state for $kT/\Gamma\gtrsim 8$. Driessen *et al.* integrated this expression to determine P^*_Q, which is parametrized in terms of Γ. Since data only exist for C_{VQ} at $P=0$ they made the reasonable scaling assumption that

$$\Gamma_{H_2}(V)=\Gamma_{D_2}(V)=154V^{-5/3}, \tag{7.8}$$

where V is in units of cm^3/mol and Γ in degrees Kelvin. They present a table which enables a straightforward evaluation of P_Q at a given temperature and volume in the disordered state.

In the orientationally ordered state, for $T \ll T_c$, P_Q can be calculated from consideration of the ground-state orientational energy, E_{QG}, which is identical to the free energy at $T=0$. Harris *et al.* (1973) calculated

$$E_{QG} = N(-7.37\Gamma - 32.02\Gamma^2/B), \quad (7.9)$$

where B is the rotational constant and N the number of molecules. From Eq. (7.1) it follows that

$$P_Q = -2.13\times 10^4\, C_1^2 V^{-8/3}(7.37 + 115.5 V^{-5/3}\delta)\ \text{(bar)}, \quad (7.10)$$

where $\delta = 1$ for H_2 and 2 for D_2, V is in cm^3/mol. An expected quadratic dependence on C_1 is taken into account. The quadrupolar pressure difference between $J=1$ and $J=0$ H_2 and D_2 in the ordered state is shown in Fig. 40.

2. Zero-pressure molar volume

The molar volume at zero pressure is of special importance because so much research has been done at this pressure. In spite of the large number of determinations of V_0, there is substantial scatter in the values and some uncertainty in the best value, in particular for H_2. All told there are some 20–30 published and unpublished determinations of V_0. Part of the responsibility for the large scatter lies in the improper control or knowledge of the concentration C_1. We shall take the molar volume of $J=0$ H_2 and D_2 as a reference volume, following Driessen *et al.* (1979). At $P=0$ and 4.2 K the preferred values are $V_0 = 23.16 \pm 0.06$ cm^3/mol for p-H_2 and $V_0 = 19.95 \pm 0.04$ cm^3/mol for ortho-D_2. The zero-pressure molar volume as a function of $J=1$ concentration is shown in Fig. 41. In the disordered phase at 4.2 K, one has $V_0(C_1) = 23.16 - 0.091C_1 - 0.217C_1^2$ cm^3/mol for H_2 and $V_0(C_1) = 19.95 - 0.16C_1 - 0.04C_1^2$ cm^3/mol for D_2.

The earliest measurements of V_0 were indirect thermodynamic measurements by Clusius and Bartholomé (1935) at the triple point and Megaw (1939) at 4.2 K. Neither of the values have been used in the determination. Megaw's values of 22.65 and 19.56 cm^3/mol for H_2 and D_2 are substantially lower than most later determinations. Some problems that can arise in thermodynamic measurements is the undetected flow of solid H_2 or D_2 in capillaries which are deliberately frozen in performing isochoric measurements (see discussion of solid flow by Cook *et al.*, 1965). The technique capable of highest accuracy is neutron, x-ray, or electron diffraction. Even in these cases we have been informed (by private communication) by the authors of some published values that the quoted results and accuracy should be disregarded. For the determination of V_0 we have used the average of the values given in Table XI as corrected to $J=0$ using values of the bulk modulus and the quadrupolar pressure. The new measurement by Krause (1978) on p-H_2 is the largest value ever reported and comes from direct measurements of the molar volumes for $P \neq 0$, extrapolated to $P=0$. Considering the long history of changing values, we have used an

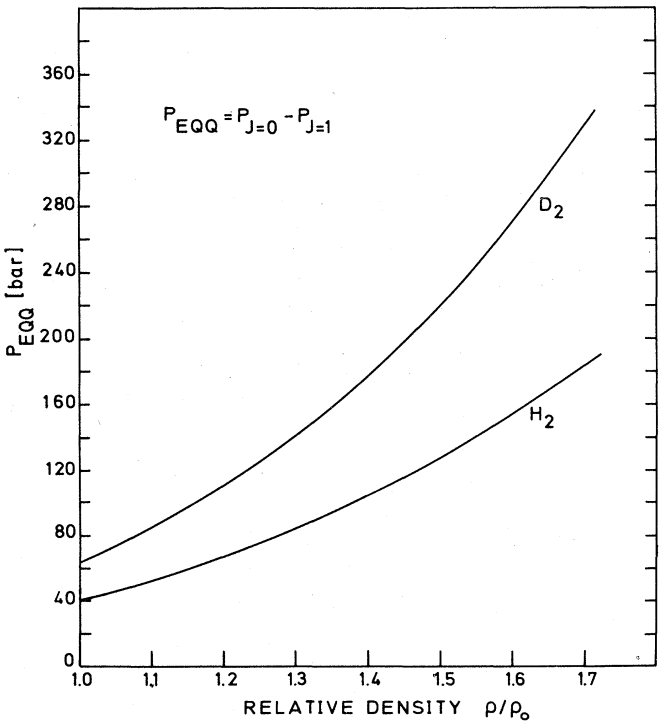

FIG. 40. The calculated quadrupolar pressure in H_2 and D_2 in the Pa3 ordered state at $T=0$ K (after Jochemsen, 1978).

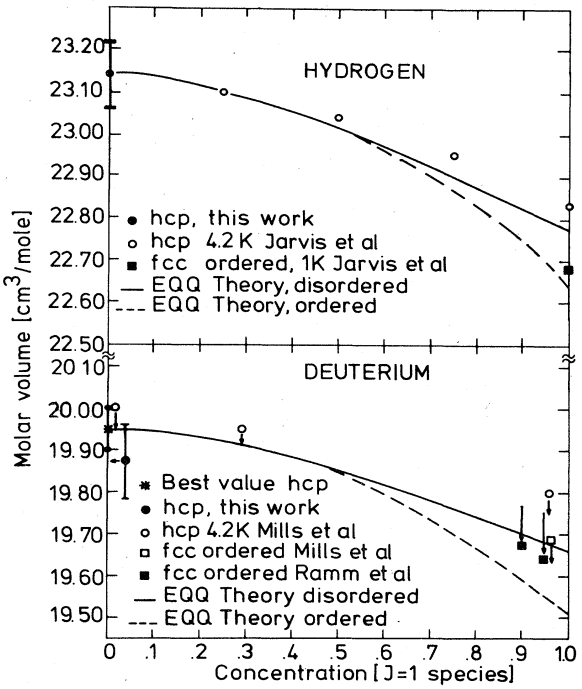

FIG. 41. The molar volume of zero pressure H_2 and D_2 as a function of ortho (para) concentration. The lines are calculated values. For D_2 the arrow tips on the data points indicated by circles point to the most probable values (after Driessen *et al.*, 1979). When the recent determination by Krause for H_2 is included, the mean value of V_0 for p-H_2 becomes 23.16 cc/mole.

TABLE XI. Zero-pressure molar volumes in the hcp hydrogens at 4.2 K. The recommended average values in cc/mole are H_2: 23.16 ± 0.06, HD: 20.57 ± 0.12, and D_2: 19.95 ± 0.04.

	Molar volume (cc/mole)				
	$C_1 = 0$	0.75		Comment	Reference
	(23.10 ± 0.13) [a]	22.91 ± 0.13		Elect. diff.	Bostanjoglo and Kleinschmidt (1967)
H_2	23.14 ± 0.08			Thermodyn.	Silvera *et al.* (1978)
	23.23 ± 0.04			Thermodyn.	Krause (1978)
	$C_1 = 0.025$	0.33	1		
D_2	20.00 ± 0.01	19.94 ± 0.01	19.80 ± 0.01	Neutr. diff.	Yarnell *et al.* (1975)
	(19.95 ± 0.11) [a]	19.90 ± 0.11		Elect. diff.	Bostanjoglo and Kleinschmidt (1967)
	19.94			Neutr. diff.	Nielsen (1973)
	19.91			Neutr. diff.	Mucker *et al.* (1968) corrected to 4.2 K
	(19.93 ± 0.09) [a]	19.87 ± 0.09		Thermodyn.	Driessen *et at.* (1978)
HD	20.57 ± 0.12			Elect. diff.	Bostanjoglo and Kleinschmidt (1978)

[a] As corrected from n-H_2 or n-D_2 value.

unweighted average for the value of V_0. In Fig. 41 the values of $V_0(C_1)$ for disordered H_2 are determined using the measured quadrupolar pressure and the bulk modulus. The solid line is calculated by Silvera *et al.* (1978) using the Mie–Grüneisen theory for the quadrupolar pressure; the broken line representing the molar volume in the ordered state is calculated using Eq. (7.10) and the bulk modulus.

Molar volume measurements for $P \neq 0$ have been made by Dwyer *et al.* (1965) to $P \simeq 340$ bar with corrections by Younglove (1968); Krause (1978) has made measurements to $P \simeq 2$ kbar. Values will be given in the following paragraphs.

As discussed earlier the EOS can be determined from a single isotherm and a series of selected isochoric measurements. The most convenient isotherm is that measured at 4.2 K since there is a negligible difference between 4.2 and $T = 0$ for the $J = 0$ species. The most accurate isotherms were measured from 0.4 to 25 kbar by Anderson and Swenson (1974) on n-H_2 and n-D_2 by the piston displacement method. This technique provides values of P vs V/V_r where V_r is a reference volume. To take $V_r = V_0$, the measurements were extrapolated to $P = 0$. Silvera *et al.* determined the 4.2 isochore for $P < 340$ bar and found differences from the extrapolated curve. They also compared to other existing data in the literature (Driessen *et al.*, 1979) and found that a better overall consistency could be obtained by refitting the data of Anderson and Swenson. This yielded a larger reference volume for p-H_2.[14] They also corrected the Anderson and Swenson data for quadrupolar pressures to present EOS data for o-D_2. Their results are shown in Figs. 42 and 43 for $P-V$ and B_m-V. In these figures the points represent values of P_0 vs V and B_m vs V calculated by Silvera and Goldman (1978) using self-consistent phonon theory and the H_2-H_2 isotropic potential given in Eq. (3.11).

[14] C. A. Swenson (private communication) states that the Anderson–Swenson isotherm is in good agreement with the low-pressure isotherm of Krause (1978) when he uses Krause's value of $V_0 = 23.25$ cc/mole.

The 4.2 K isotherm can be represented with a Birch relation

$$P(V) = Y^5 \sum_{n=1}^{2} B_n (Y^2 - 1)^n , \tag{7.11}$$

where $Y = (\bar{V}_0/V)^{1/3}$. Values of the constants are given in Table XII.

Driessen *et al.* used isochoric measurements to provide $P-V-T-C_1 = 0$ data to 2 kbars and used a reasonable extrapolation to 25 kbars. Closely tabulated values are given for P, V, B_m, and T_{melt} along with tables for obtaining values at arbitrary C_1. We provide some selected values of P vs V at 4.2 K for $J = 0$ species in Table XIII.

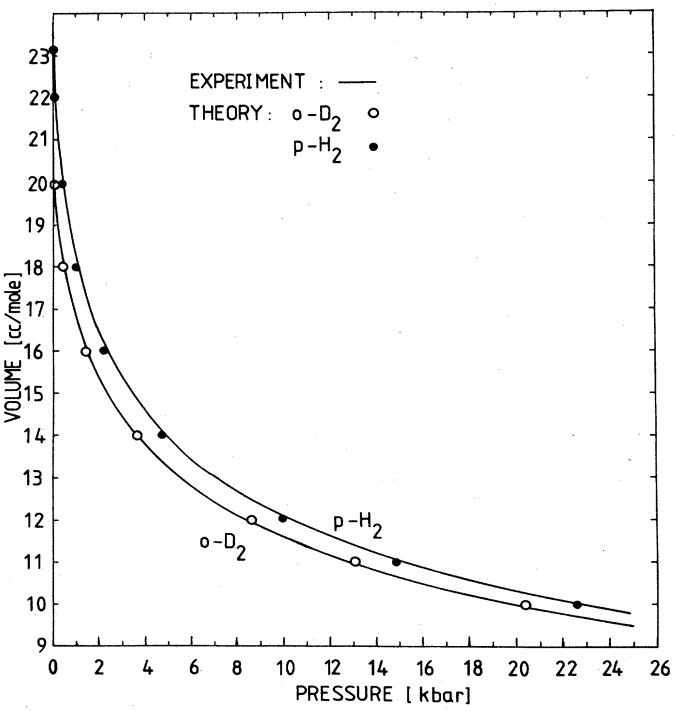

FIG. 42. Pressure volume relation at $T = 0$ K for para H_2 and ortho D_2 (from Silvera and Goldman, 1978).

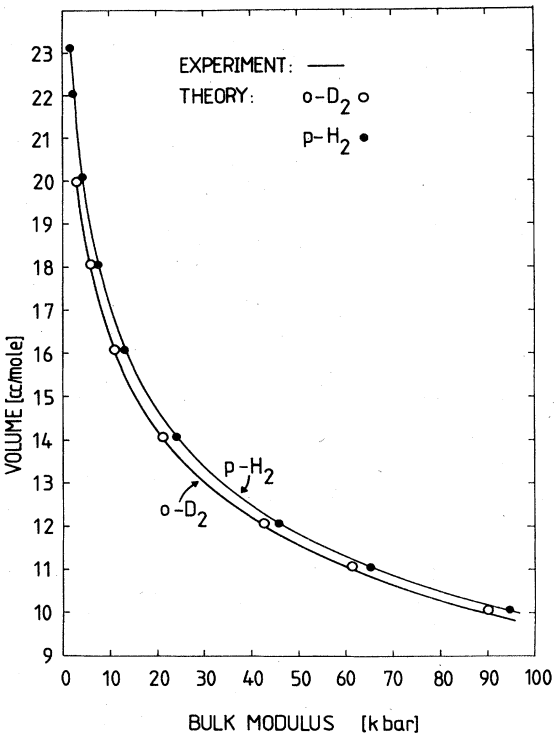

FIG. 43. Bulk modulus versus volume at $T=0$ K for para H_2 and ortho D_2 (from Silvera and Goldman, 1978).

For higher pressure accurate data does not exist for the solid hydrogens. A number of shock and explosive compression experiments have been performed (see discussion by Ross, 1974); however, the error limits are quite large, samples are severely heated, and in some cases only the volume is measured and the pressure is determined from calculations using model potentials. Since many-body forces are expected to play an important role at high densities and their density dependence is not well understood, model potentials do not allow a reliable extrapolation of the EOS data from ~10^4 bars to ~10^6 bars (corresponding roughly to ~10 cc/mole to ~2 cc/mole). However, extrapolation to ~10^5 bars can probably be done without serious error.

B. The sublimation energy

Very few measurements are available for the lattice or sublimation energy per particle. This was measured by Clusius and Bartholomé (1935) near the triple point for D_2, and by Simon (1923) for H_2. The $T=0$ K value is calculated, using thermodynamic relations. Schnepp (1970) found that the data used for the $T=0$ calculation were questionable and corrected those with modern values. A linear extrapolation (Silvera and Goldman, 1978) to give values corresponding to $J=0$ solids yielded −89.8 K/molecule for p-H_2 and −132.8 K/molecule for o-D_2. The sublimation energy is an important piece of information that has been used extensively in the determination of the isotropic intermolecular potential. Etters *et al.* (1975) calculated −88.76 K/mol for H_2 at $P=0$; Silvera and Goldman (1978) found −85.5 K/mol for H_2 and −132.3 K/mol for D_2 in fitting their potential which was discussed earlier.

TABLE XII. Constants for the Birch relation, Eq. (7.11).

	B_1	B_2	V_0
Species\units	bar	bar	cc/mole
p-H_2	2786.8	6 334.4	23.14
o-D_2	4766.5	10 101	19.95

C. Isochoric pressure dependence on temperature

In a beautiful series of measurements Meyer and coworkers (Jarvis *et al.*, 1966, 1968; Ramm *et al.*, 1969) were able to directly measure the quadrupolar pressure P_Q in H_2 and D_2. They measured $(\partial P/\partial T)_V$ as a function of concentration and temperature at pressures slightly greater than zero. From Eqs. (7.4b) and (7.5) we have

$$V\left(\frac{\partial P}{\partial T}\right)_V = \gamma_L C_{VL} + \gamma_Q C_{VQ} . \tag{7.12}$$

At low temperatures, as the lattice contributions are frozen out, (7.12) will be dominated by the EQQ term. Quadrupolar pressures are of the order of $10\text{-}10^2$ bars (see Fig. 40). Using a capacitance strain gauge, they measured ΔP with a sensitivity of 2×10^{-5} bar and an accuracy of 0.1 bar. Examples of the measurements are shown in Fig. 44. In Fig. 44a we see that by holding an H_2 sample at constant temperature and volume and allowing it to convert, the pressure changes. Fig. (44b) shows the effect of temperature. A large jump in P is observed at the phase transition. This has already been shown in Fig. 27 where this technique was used for studying the phase line. With the use of the bulk modulus the $P\simeq0$ volume changes as a function of C_1 can be calculated, $\Delta V=(V/B)\Delta P$. This has been used in Fig. 41 in the determination of volumes relative to the $J=0$ molar volumes.

TABLE XIII. P-V values at $T=4$ K for $J=0$ species of H_2 and D_2.

Volume	Pressure	
(cc/mole)	H_2	D_2
23.15	0	···
23	12	···
22	112	···
21	253	···
20	448	···
19.95	···	0
19	718	183
18	1 094	462
17	1 617	868
16	2 351	1 457
15	3 392	2 318
14	4 885	3 583
13	7 060	5 468
12	10 290	8 321
11	15 199	12 730
10	22 877	19 732
9.5	28 329	24 746

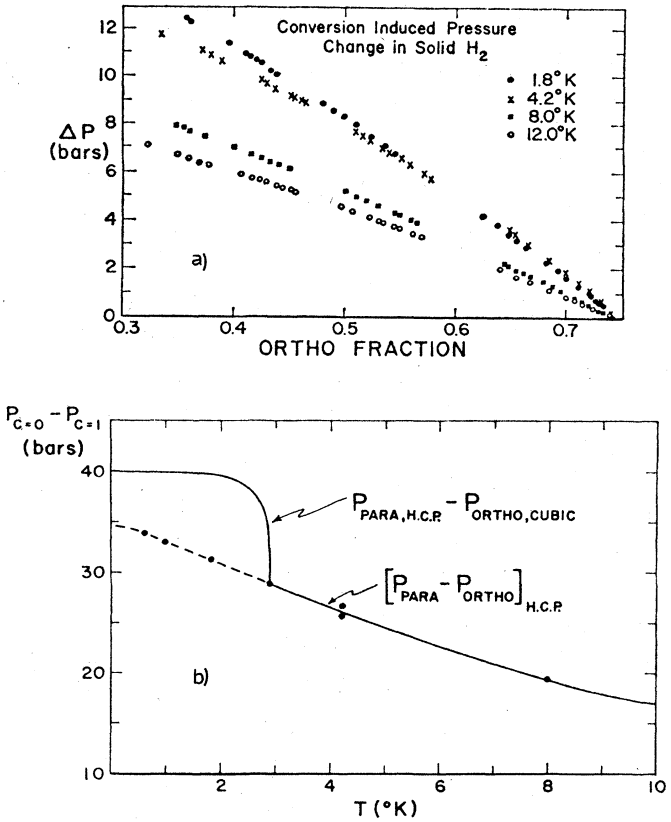

FIG. 44. The quadrupolar pressure in H_2 as determined from $(\partial P/\partial T)_V$ measurements. (a) Pressure change as a function of ortho concentration. (b) Quadrupolar pressure as a function of temperature found by extrapolation to ortho concentration $C=1$ (after Jarvis *et al.*, 1969).

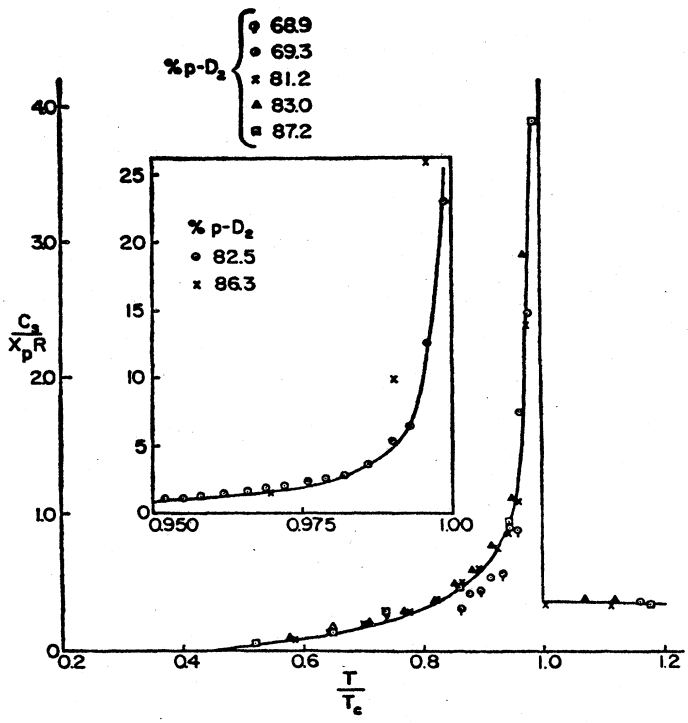

FIG. 45. Heat capacities of para-rich deuterium in the vicinity of the order disorder transition temperature (after Grenier and White, 1964).

D. Heat capacity

Specific heat measurements provided some of the initial indications that interesting phenomena occurred in the hydrogens at low temperature due to the quenching of the molecular angular momentum. Hill and Ricketson (1954) and Ahlers and Orttung (1964) have studied nominally normal H_2. Grenier and White (1964) have studied the phase transition in enriched D_2 and White (1976) has studied the ordered state of D_2 to $T \sim 0.6$ K as a function of concentration.

The λ anomaly due to the orientational ordering at $P=0$ is shown in Fig. 45. The temperature of the λ peak indicates the critical temperature of ordering; in Fig. 46, from the concentration dependence of the specific heat, we see the decrease in T_c with decreasing C_1 and its disappearance at relatively high C_1. Ahlers and Orttung (1964) studied the temperature and density dependence of the isochoric specific heat, C_1, to 15.9 cc/mole. In the vicinity of the λ anomaly, they observed 2 and even 3 peaks in some measurements, indicative of a very complicated phase transition. To our knowledge no other experiments have detected phenomena corresponding to these secondary peaks; we assume that they are related to some property of their apparatus and should not be taken too seriously without further systematic study or confirmation.

Theoretically, Nakamura (1955) analyzed the orientational part of the specific heat measurements of Hill and Ricketson. The specific heat was fitted with a T^{-2} law giving reasonable agreement with experiment but a somewhat too low value of Γ_{eff}. Later Berlinsky and Harris (1970) calculated the coefficients of terms up to T^{-5} in the high-temperature expansion of C_V. They were able to get good agreement with experiment for $k_B T/\Gamma \gtrsim 8$ by using a Padé approximant.

For a low concentration of $J=1$ molecules there is also a large number of low-temperature measurements of specific heat. Ahlers (1964) and Krause (1978) have made isochoric studies of H_2 at several densities. Other measurements at constant P have been made by Hill and Lounasmaa (1959, H_2 and D_2), Gonzales *et al.* (1957, D_2), Roberts and Daunt (1972, H_2 and D_2; 1974, D_2 to 0.6 K), Roberts *et al.* (1976, D_2), and Grenier and White (1964, HD). The observations for $C_1 \lesssim 0.04$ are characterized by three principal parts: (1) a lattice contribution, (2) a Schottky term arising from the isolated $J=1$ pairs of molecules (see energy levels, Fig. 12) with a maximum at $T \simeq 1.4$ K, and (3) a second Schottky term, probably due to the energy levels of next nearest neighbor $J=1$ molecules as determined by EQQ interactions. For a higher concentration, triples (energy levels are given by Miyagi, 1968) and larger clusters of $J=1$ molecules begin to contribute significantly. In addition, in H_2 the specific heat measurements are sensitive to clustering due to the rotational diffusion discussed earlier. Measurements of the specific heat have not yet been carried out at very low temperatures to study the "quadrupolar-glass" phase.

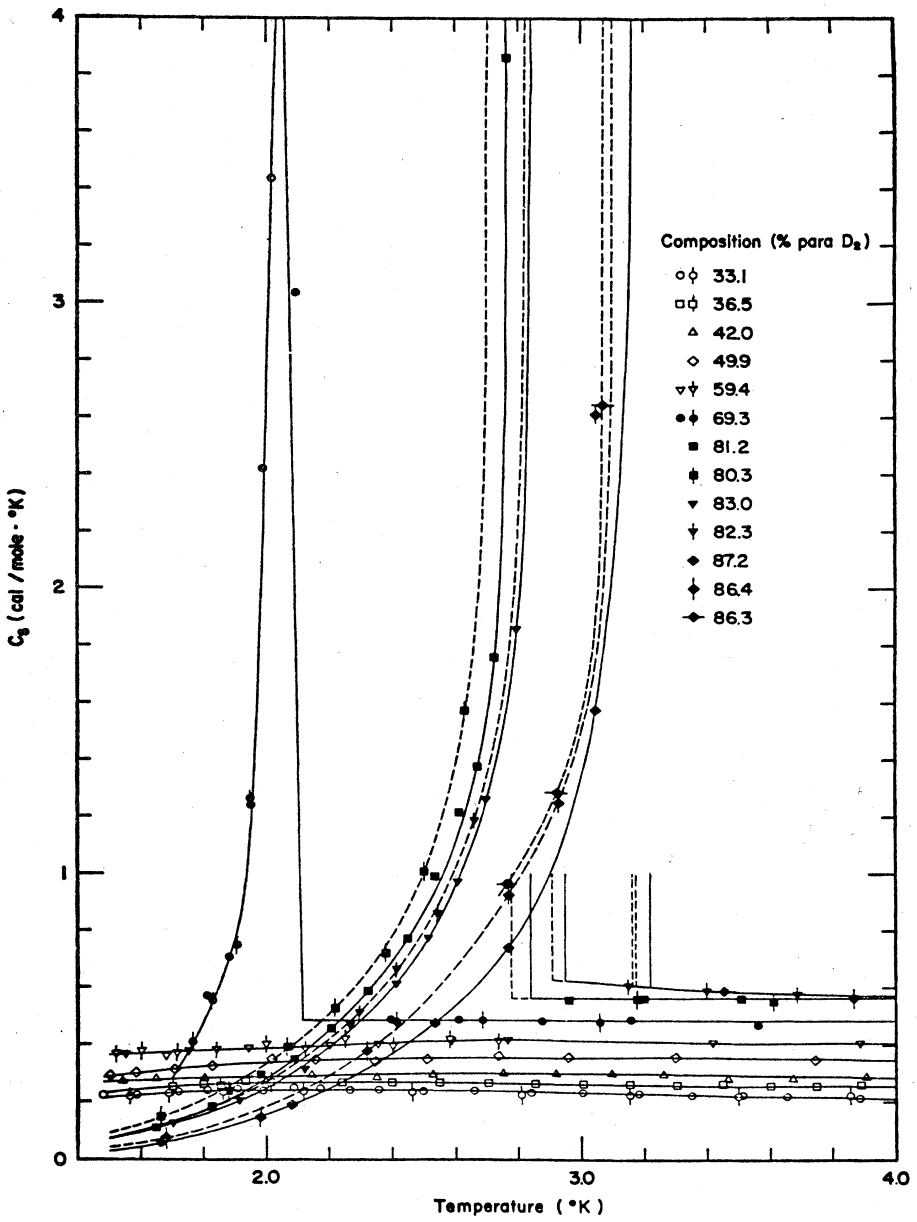

FIG. 46. Heat capacity of deuterium for several para concentrations (after Grenier and White, 1964).

In Fig. 47 we show the specific heat of D_2 with 3.5% p-D_2 from Roberts and Daunt (1974); Fig. 48 shows the orientational part of the specific heat for three p-D_2 concentrations measured to 150 mK (Roberts *et al.*, 1976). The solid lines are based upon the energy level diagram of isolated pairs as was first suggested by Nakamura (1955) and has been discussed and extended by Orttung (1962) and Roberts *et al.* The analyses yield reasonably accurate values of Γ_{eff}. Roberts *et al.* suggest that the deviations of the theory from experiment at low C_1 and low T may be due to the crystalline field splitting of isolated $J=1$ molecules. With this assumption their analysis yields a value of $|V_c|/k_B = 0.087$ K for the splitting between the $J_z = \pm 1$ doublet, and $J_z = 0$ singlet.

By subtracting off the orientational part of the specific heat the lattice contribution can be isolated and can be accurately represented by a Mie-Grüneisen-Debye model. In Fig. 49 we show the results of Krause (1978) for the lattice specific heat of para H_2.

E. Long-wavelength properties: Debye temperature and elastic constants

The Debye temperature [see Eq. (7.7b)] is important in characterizing the lattice dynamical properties of the solid. The Debye model is a simple continuum model which can successfully approximate many properties of the solid. The Debye temperature defines an effective maximum phonon frequency ω_D in the solid:

$$\theta_D \equiv \hbar\omega_D/k_B .$$

Here θ_D can be calculated in terms of the long-wave-

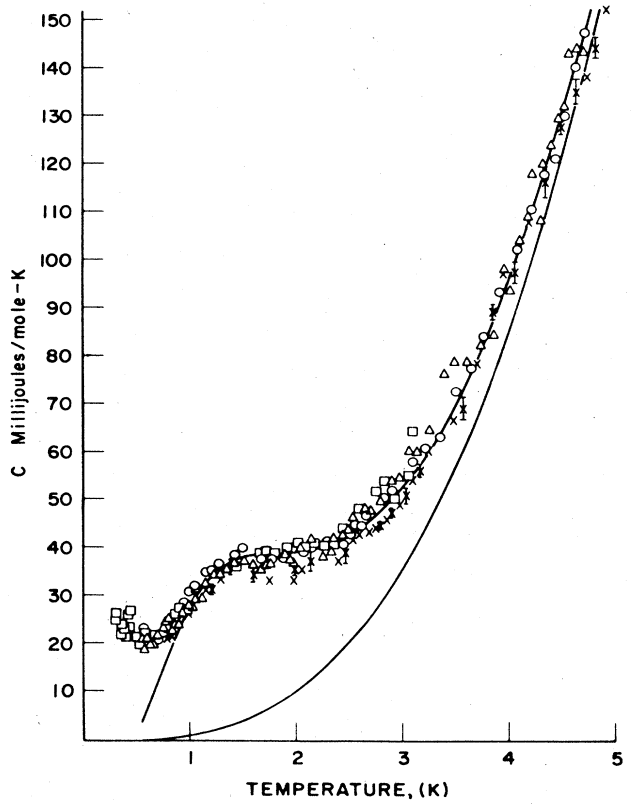

FIG. 47. Specific heat versus temperature of 3.5% para D_2. The points represent experimental data, the lower full curve represents the lattice specific heat only (after Roberts and Daunt, 1974).

length (small k) properties of the solid; experimentally it can be directly determined in specific heat measurements (which were listed in the previous section) as well as from neutron scattering (Nielsen and Bjerrum-Møller, 1971) untrasonic measurements (Bezuglyi and Minyafaev, 1967, 1968; Wanner and Meyer, 1973: n-H_2 and n-D_2) and Brillouin scattering (Thomas *et al.*, 1978: p-H_2). These measurements also provided elastic constants.

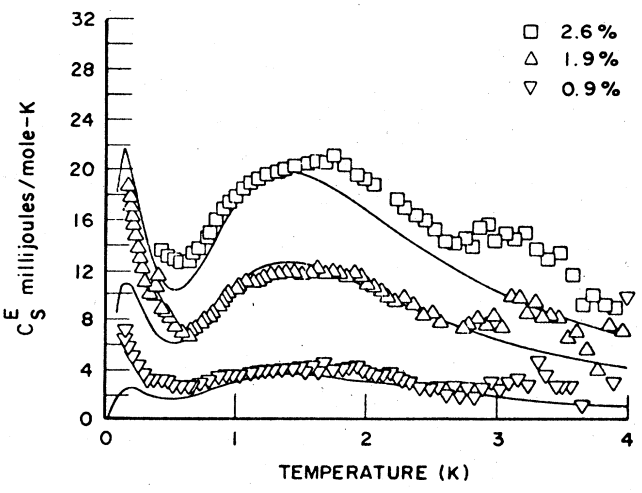

FIG. 48. Orientational part of the specific heat as a function of temperature of solid D_2 for three para concentrations. The drawn lines are from theory (after Roberts *et al.*, 1976).

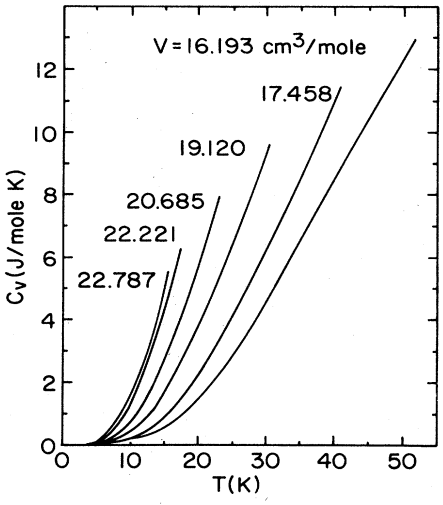

FIG. 49. The lattice specific heat as a function of temperature for several molar volumes of para-hydrogen (after Krause, 1978).

We have taken the average of six measurements in H_2 and six in D_2 corresponding nominally to the hcp $J=0$ species at 4.2 K, and find $\theta_D = 120.3 \pm 3$ K for H_2, and 109.4 ± 1.5 K for D_2; there is only one measured value for HD: 110 ± 3 K. Ahlers (1963) and Krause (1978) have measured the density dependence of θ_D, as shown in Fig. 50. The solid lines are self-consistent phonon calculations of Goldman (1979a). Ahlers and Krause as well as Hill and Lounasmaa (1959) have studied the temperature dependence of θ_D, with results shown in

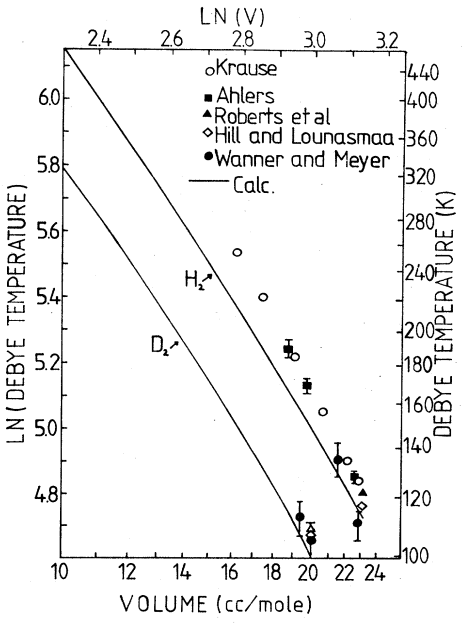

FIG. 50. Density dependence of the Debye temperature in para H_2 and ortho D_2. The lines represent theoretical calculations of Goldman (after Goldman, 1979).

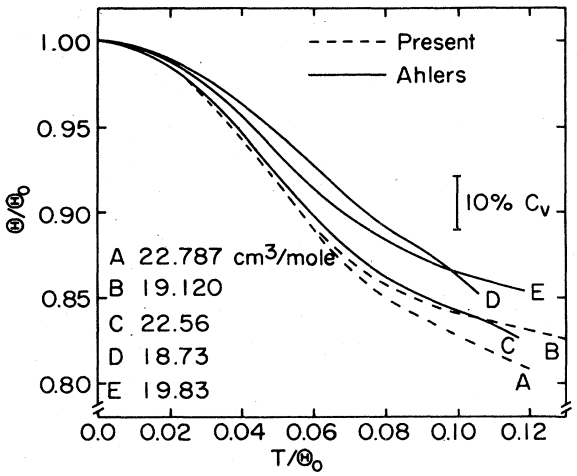

FIG. 51. Temperature dependence of the Debye temperature in para H_2 normalized to the value at $T=0$ K for several densities (after Krause, 1978).

Fig. 51. Driessen *et al.* (1979) tabulate θ_D to high pressure; their value corresponds to high-temperature average values.

The elastic constants in hcp hydrogen have also been calculated by Goldman (1979). His results are shown, along with experimental values, in Fig. 52.

F. Thermal conductivity

The thermal conductivity of the crystalline hydrogens depends dramatically on the $J=1$ content. To our knowledge it has only been measured in the hcp phase. Measurements have been made by Hill and Scheidmesser (1958, H_2: $0.005 < C_1 < 0.72$), Bohn and Mate (1970, H_2: $0.002 < C_1 < 0.05$), Constable and Gaines (1973, HD), Huebler and Mate (1978, H_2: $0.2 < C_1 < 0.7$), and Gorodilov *et al.* (1978, D_2: $0.22 < C_1 < 0.30$). Ebner and Sung (1970) have presented a theory for the effect of $J=1$ impurities, a general discussion of thermal conductivity processes is also given by Constable and Gaines.

The thermal conductivity, K, in H_2 is shown in Figs. 53 and 54 for a series of concentrations and in HD for $T < 1$ K (Fig. 55) and extrapolated to the case of no impurities (H_2, D_2). Similar results are found in D_2 as a function of concentration. An enormous variation of more than 200 in the peak value of K is seen with variation of C_1. This data is for the hcp phase. Presumably the high C_1 samples of Huebler and Bohn were never cycled into the ordered state and back, which would create fcc-hcp mixtures.

The total thermal resistance W can be written as a sum of several contributions:

$$W = pT^{-3} + bT^{1.5} + dT^n e^{-\theta_D/\beta T} + W_{C_1}. \tag{7.13}$$

The first term arises from boundary scattering and is dependent on the size and nature (single crystal or polycristalline) of the sample. The second term arises from point defect scattering and the third from phonon scattering by umklapp processes (θ_D is the Debye temperature). The last term is the thermal resistance due to $J=1$ molecules in a lattice of $J=0$ molecules. Ebner and Sung calculated the effect of $J=1$ molecules by assuming that the rotational substates of the $J=1$ molecule allow for an additional scattering mechanism due to a two-phonon Raman mechanism. The theory is in qualitative agreement with experiment. They predicted $W_{C_1} \sim C_1^2 T^{-2}$ for $C_1 < 0.1$. The concentration dependence seems to be borne out by the measurements of Bohn and Mate, although the temperature dependence is closer to T^{-3}. The HD samples of Constable and Gaines also contained H_2 and D_2 impurities enabling them to compare to the theory for W_{C_1}. They see an anomalously large value of W_{C_1} at low temperatures, which they suggest arises from one-phonon processes within the model of Ebner and Sung.

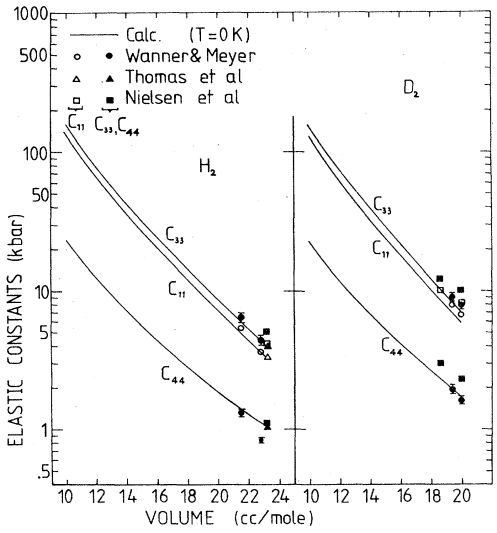

FIG. 52. Elastic constants in H_2 and D_2 as a function of molar volume. The lines are calculations of Goldman (after Goldman, 1979).

VIII. THE TRANSLATIONAL GROUND STATE AND RENORMALIZED INTERACTIONS

In this section we discuss the translational properties of solid hydrogen in the ground state. Hydrogen is a quantum solid,[15] i.e., a solid in which the molecules of the ordered array undergo large rms displacements or zero-point motion (ZPM) about their equilibrium lattice sites. Since the dynamical energy is of the same order as the static lattice energy, these crystals must be treated quantum-mechanically and so have earned their name. The fact that the ZPM is large would not present a difficulty in the theoretical treatment of these solids if the interaction potential were harmonic; it is the highly anharmonic nature of the real isotropic potentials that creates great difficulties in the theory.

Fortunately the coupling between the rotational and translational motions in H_2 are very weak (Mertens and Biem, 1972). As a consequence we can treat the orien-

[15] A number of excellent reviews on quantum solids exist. See, for example, Horner (1974), Koehler (1974), Guyer (1969).

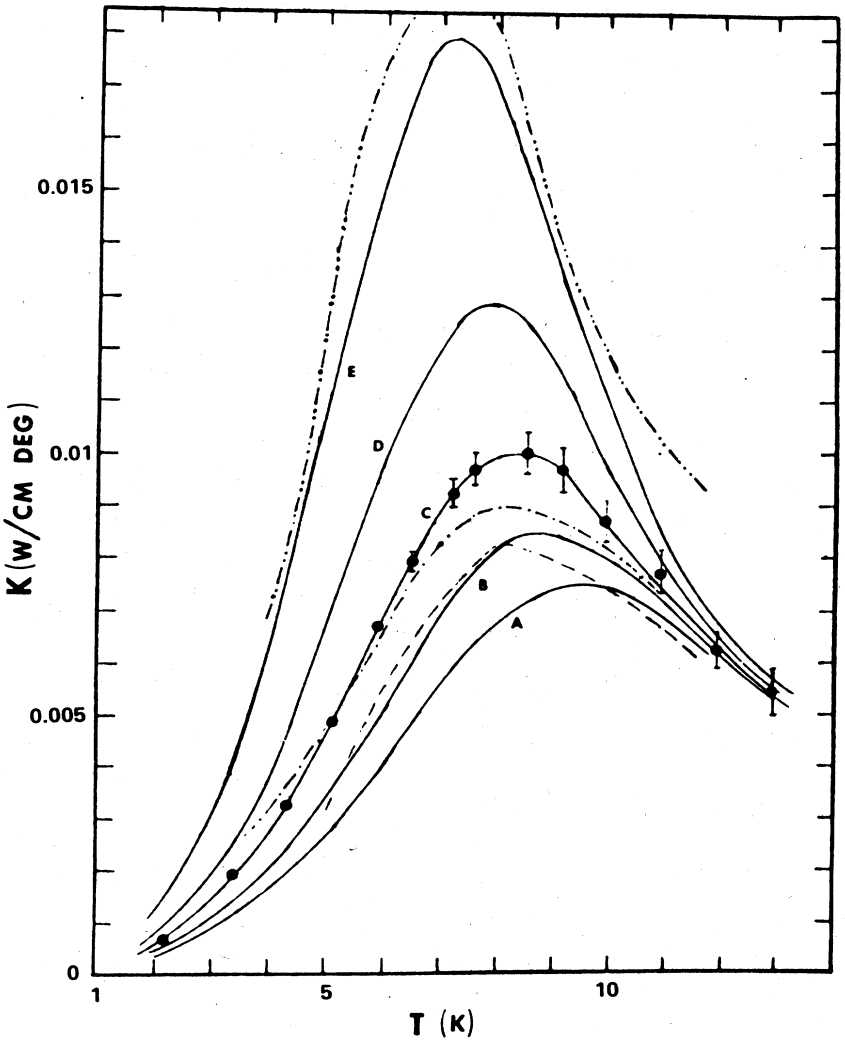

FIG. 53. Thermal conductivity of hydrogen at constant o-H_2 concentration versus temperature. a) Ortho concentrations A-E, 0.70, 0.60, 0.50, 0.40, 0.30, respectively (after Huebler and Bohn, 1978).

tational and translational degrees of freedom of the ground state independently. As we saw in Sec. VI, for $c_0 \sim 1$, the anisotropic part of the interaction potential led to an orientationally ordered state. The main effect of the anisotropy on the ground state is to determine the orientational structure. Other than that the effect of the anisotropy on the ground state energy or the phonon energies is ~1% and can be ignored or treated perturbatively (Jochemsen *et al.*, 1978; Silvera *et al.*, 1979). Thus we can approximate the interaction potential by its isotropic part. This approximation is essentially exact for even J species at low pressure.

In the following section we shall examine the current theories used in the study of the ground state properties. We shall see that an understanding of the quantum crystal behavior hinges on our knowledge of the pair distribution function.

The ground-state translational properties of the hydrogens have been studied by Etters and Danilowitz (1973), Mertens (1972), Krumhansl and Wu (1972), Bruce (1972), Pollock *et al.* (1972), Ostgaard (1972), Anderson *et al.* (1976, 1977) and Goldman (1979b). This list is incomplete.

A. The ground state

The ground state of a crystal can be determined, given the Hamiltonian

$$H=\frac{-\hbar^2}{2m}\sum_i^N \nabla^2(i)+\phi(\{r_i\}) , \tag{8.1}$$

where ϕ is a sum over all pair interactions [Eq. (3.1)],

$$\phi=\frac{1}{2}\sum_{i,j}[(\phi_I(i,j)+\phi_A)]\simeq\frac{1}{2}\sum_{i,j}\phi_I(i,j) ,$$

and $\{r_i\}$ means the set of position vectors of all particles. We can see the role of the kinetic energy from the quantum law of corresponding states. By taking $\phi_I(i,j)$ in the form of the Lennard-Jones potential, Eq. (3.7), and rewriting Eq. (8.1) in terms of reduced energy units, using the well depth ϵ as the unit, we find

$$H=-\frac{1}{2}\lambda^2\sum_i \nabla_i^2+\frac{1}{2}\sum_{i\neq j} v(i,j) , \tag{8.2}$$

where $r \to r/\sigma$ and $\phi_I(i,j)=\epsilon v(i,j)$. Here $\lambda=\hbar/\sigma\sqrt{m\epsilon}$ is the de Boer quantum parameter. Its value is given for several atoms in Table XIV. We see that the lighter the

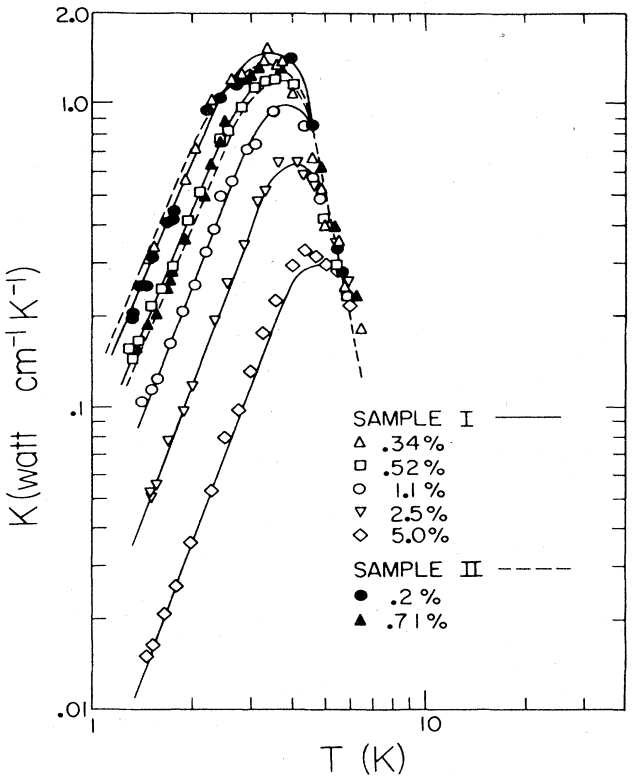

FIG. 54. Thermal conductivity of hydrogen at constant o-H_2 concentration vs. temperature for low-ortho concentrations (after Bohn and Mate, 1970).

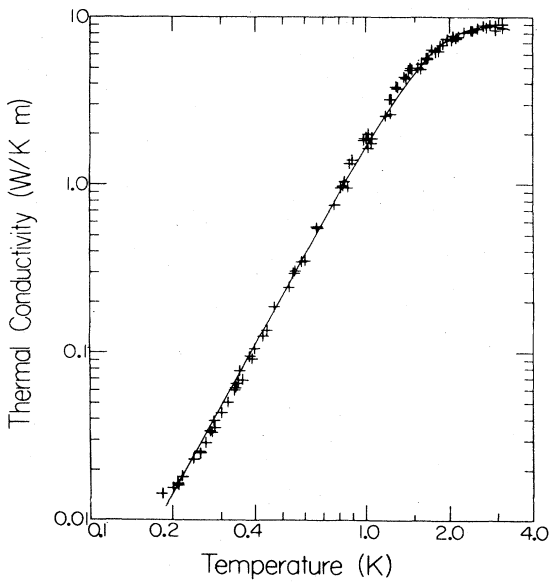

FIG. 55. The $J=1$ independent thermal conductivity versus temperature in HD (after Constable and Gaines, 1973).

atom and the shallower the potential (smaller ϵ), the larger is λ^2. As λ^2 grows, the kinetic energy plays a growing role in determining the total energy of the crystal at $T=0$ K, as seen from Eq. (8.2).

It is illuminating to study the quantum solid in terms of the usual Born–van Kármán force constants approach (Guyer, 1969). Then the potential ϕ is expanded in a Taylor series and we retain only the harmonic term w_h:

$$H_h=\frac{-\hbar^2}{2m}\sum_i^N \nabla^2(i)+\frac{1}{2}\sum_{i,j} w_h^{\alpha\beta}(i,j)u_\alpha(i)u_\beta(j)\,, \tag{8.3a}$$

$$w_h^{\alpha\beta}(i,j)=(\nabla_\alpha(i)\nabla_\beta(j)\phi)_{\{R_i\}}\,, \tag{8.3b}$$

where u_i is the displacement of particle i from its equilibrium position, R_i-r_i. This Hamiltonian can be solved exactly; the ground-state wave function is a correlated Gaussian:

$$|\psi_h)_{cg}=[(2\pi)^{3N}\det A]^{-1/4}\exp\left[-\frac{1}{4}\sum A^{-1}_{\alpha\beta}(ij)u_\alpha(i)u_\beta(j)\right]\,, \tag{8.4}$$

where

$$\frac{\hbar^2}{4m}A^{-2}(i,j)=w_h(i,j)\,. \tag{8.5}$$

The phonon frequencies are found by diagonalization of the dynamical matrix and are proportional to the square root of the force constants, Eq. (8.3b).

De Wette and Nijboer (1965) studied the phonon spectra of rare gas solid lattices and found that for a lattice such as that of H_2 at zero pressure the phonon frequencies are imaginary, implying a total breakdown of the Born-van Kármán approximation. On the other hand long-lived translational excitations with well defined k vectors and (except for a few points in the Brillouin zone) rather conventional phonon dispersion relations have been observed in H_2 by neutron scattering (Nielsen, 1973). The problem with the harmonic theory for H_2 was that the frequencies were determined by evaluating the force constants, w_h, using an L-J potential evaluated at the x-ray determined lattice parameter. However, the mean position of the molecule is far away from the minimum of the potential due to its neighbors. As a consequence the single particle well has a hump as in Fig. 56, so that the curvature, or force constants, are negative!

In quantum solids the particles occupy a volume in space related to the amplitude of the zero-point motion (not the hard core). This is so large that if the crystal did not distort there would be strong overlap of the repulsive hard cores. The crystal can lower its total energy by expanding, reducing the kinetic energy of localization at the expense of static energy. Only for very large mass will the particles be localized at the minimum of the potential well.

There are a number of problems with the simple

TABLE XIV. Lennard-Jones potential parameters and the quantum parameter λ^2.

Atom or molecule	ϵ[K]	σ[Å]	λ^2
^{3}He	10.2	2.56	0.241
^{4}He	10.2	2.56	0.182
H_2	37	2.92	0.076
D_2	37	2.92	0.038
Ne	35.6	2.74	0.0049
Ar	119.3	3.45	0.0027

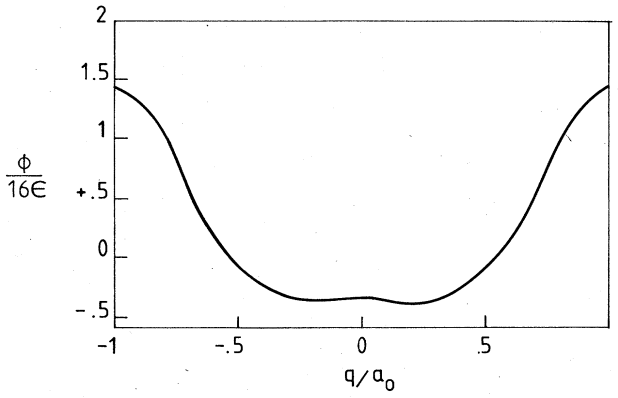

FIG. 56. The single particle potential of H_2 in an fcc lattice due to nearest neighbors with a Lennard-Jones potential. The zero-pressure lattice parameter, a_0, is used. The coordinate q represents a displacement of the central particle in the (1, 0, 0) direction and corresponds to one of the phonon displacements. Such a potential would clearly yield imaginary frequencies due to the negative curvature at $q=0$.

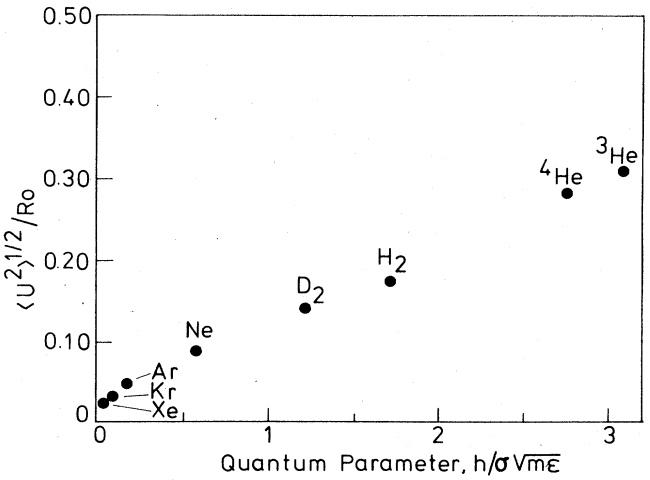

FIG. 57. The theoretical rms zero-point displacement amplitude relative to the nearest neighbor distances for a number of light solids.

Born-van Kármán theory. First of all, the expansion in u_i, usually terminated with the harmonic term, does not converge for quantum solids. Secondly, the derivatives of the potential, such as Eq. (8.3b), are evaluated at a point in space rather than being averaged over the motion of the particles. This averaging could, in a sense, average out the unpleasant effects of the hump in Fig. 56. It would also be appealing if the neighbors had the same motion as the central atom, i.e., the problem were solved self-consistently. Finally, the Born–van Kármán approach does not allow for short-range correlations of the molecules. In a real crystal short-range correlations must be present so that the relative motion of neighboring atoms minimizes overlap of the hard cores.

The self-consistent phonon approximation (scp) removes all but the last objection in H_2. In the scp, the exact Hamiltonian, Eq. (8.1), is replaced by an exactly solvable harmonic Hamiltonian

$$H_{\rm scp}=\frac{-\hbar^2}{2m}\sum_i^N \nabla^2(i)+\frac{1}{2}\sum_{i,j} w_{\rm scp}^{\alpha\beta}(i,j)u_\alpha(i)u_\beta(j)\,. \tag{8.6}$$

A variational principle applied to minimize H (Werthamer, 1976) determines the force constant:

$$w_{\rm scp}(i,j)=\langle\psi_{\rm cg}|\nabla(i)\nabla(j)\Phi\,|\psi_{\rm cg}\rangle \tag{8.7}$$

where $|\psi_{\rm cg}\rangle$ is defined just as in Eqs. (8.4), (8.5) with $w_h \to w_{\rm scp}$. This provides the desired self-consistency and averages the force constants over the zero-point motion. This is identical to averaging the force constants over the pair distribution function, (pdf), $g(i,j)$:

$$W(i,j)=\int g(i,j)\nabla(i)\nabla(j)\Phi d^3r_{ij}\,, \tag{8.8}$$

where

$$g(i,j)=\int \psi^*\psi\, dr_1\ldots\ldots dr_n/dr_i dr_j/\langle\psi|\psi\rangle. \tag{8.9}$$

If the many-body wave function $|\psi\rangle$ is a correlated Gaussian, then $g(i,j)\equiv g^{\rm cg}(i,j)$ is also a correlated Gaussian with a tensor width $\langle\,|(u_i-u_j)(u_i-u_j)|\,\rangle_{\rm scp}$ describing the zero-point motion. Calculations of the rms width of the pdf have been performed for a number of quantum solids. In Fig. 57 we show the particle localization defined as the rms longitudinal zero-point amplitude divided by the lattice constant, $\langle u^2\rangle^{1/2}/R_0$, vs. the quantum parameter for several solids. The calculations are by Etters and Danilowitz (1973) for helium, and by Goldman (1968, and unpublished) for the remaining points. The value of 0.18 for H_2 agrees well with the value determined by neutron scattering (Nielsen, 1973). It is also interesting to note that increasing density deepens the effective single particle potential well in the solid and localizes the particle. In Fig. 58 we show further results of Goldman (unpublished) where localization is plotted as a function of molar volume. The corresponding pressures can be found in Table XIII.

Although the scp can describe a number of properties of solid H_2 and D_2 quite well, especially when corrected

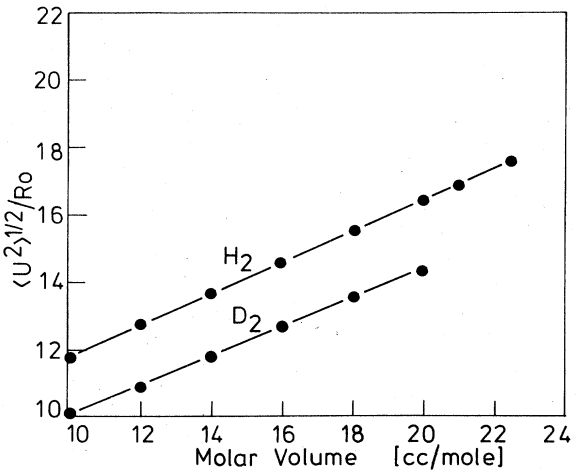

FIG. 58. The theoretical rms zero-point displacement amplitude relative to the nearest neighbor distance as a function of molar volume for H_2 and D_2.

for quartic and cubic anharmonicities, it does not deal at all with the short-range correlations. This is a particularly severe problem for helium and was first dealt with by Nosanow (1966) and generalized by Koehler (1967). Here, in place of using a correlated Gaussian as a variational ground-state wave function, one uses

$$|\psi_{\mathrm{srcg}}\rangle = \prod_{i,j} f(|r_i - r_j|)\,|\psi_{\mathrm{cg}}\rangle \tag{8.10}$$

where $f(r)$ is a Jastrow function or pair short-range correlation function. The Jastrow function has the property that it goes to zero as the particles approach each other and goes to 1 as $r \to \infty$. Commonly used functions for $f(r)$ have been $e^{-k\phi(ij)}$, where ϕ is the pair potential and $f(r) \sim \exp[-k/r_{ij}]$. The constant k must be determined variationally.

A variational principle can now be applied to the ground-state energy using Eq. (8.10) to provide expressions for the pdf, energy, etc. The difficulty that this theory has encountered is that the many-body integrals can no longer be evaluated as was the case for scp, and the convergence of cluster expansions is questionable. Etters and Danilowitz (1973) did avoid these problems for ground-state properties in helium and hydrogen, using a noncorrelated Gaussian formalism. Pollack *et al.* (1972) have examined this problem with the Monte Carlo technique.

In hydrogen the accurate calculation of renormalized interactions, to be discussed in the following section, requires a wave function or pdf, including short-range correlations. Horner (1974) reformulated the lattice dynamical problem by assuming a form for $g(r)$ from which he calculated the lattice properties, rather than starting with a variational wave function, and thus he avoided the problem of the cluster expansion. He took the pdf to be of the form

$$g(r) = g^{\mathrm{cg}}(r) f(r)(a + b \cdot r + c \cdot rr) \tag{8.11}$$

where g^{cg} is a correlated Gaussian, and $f(r)$ is a Jastrow function. For short-range $f(r) = |\psi(r)|^2$, where $\psi(r)$ is the solution of the pair Schrödinger equation, $(-\hbar^2/2m\nabla^2 + \phi(r))\psi = 0$; when the solution $\psi = \psi_{\max}$, $f(r)$ is set equal to $|\psi_{\max}|^2$ for all larger values of r.

The polynomial in Eq. (8.11) serves to preserve the zeroth, 1st and 2nd moments of distribution:

$$\int d^3r g(r) = 1\,, \tag{8.12a}$$

$$\int d^3r r g(r) = R\,, \tag{8.12b}$$

$$\int d^3r (r - R_{ij})(r - R_{ij}) g(r) = \langle u_{ij} u_{ij} \rangle\,. \tag{8.12c}$$

Equation (8.12a) preserves normalization and (8.12b) the density of the lattice. The third constraint preserves the width of the distribution, which ensures internal consistency of the phonon spectrum. Horner proposed that these constraints would be sufficient to determine the crystal properties, and there was little remaining freedom to change $g(r)$.

Goldman (1979b) has recently examined the Horner approach for H_2, with some generalization. He finds that there is indeed still freedom for modification of

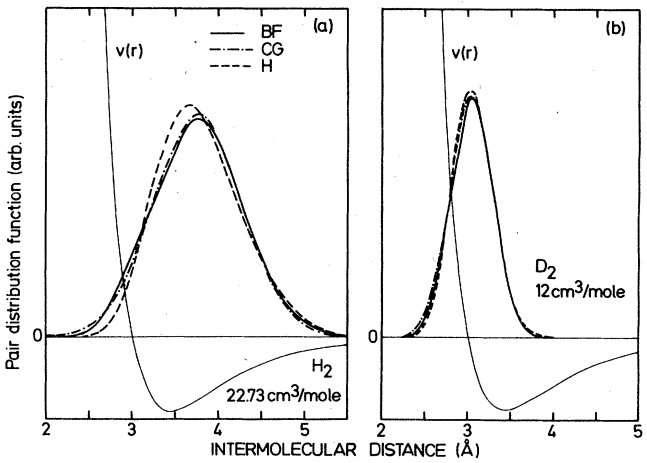

FIG. 59. Pair distribution functions along the pair axis in H_2 and D_2 at two different densities according to several theories: cg, correlated Gaussian; H, Horner; BF, Bruckner-Frohberg. All three distributions have the same zeroth, first, and second moments. The distributions are shown relative to the pair potential of Silvera and Goldman (after Goldman, 1979).

$g(r)$, in particular in the form of $f(r)$ which he arrives at by use of a Brueckner-Frohberg (BF) equation. His results, using the potential, Eq. (3.11), are shown in Fig. 59. Although the correlated Gaussian, the Horner pdf, and the pdf using the BF equation to determine $f(r)$ are all quite similar, the differences, in particular in the hard core region of the potential, give significant differences in the renormalizations.

B. Static renormalization of interactions

We have already seen that the zero-point motion in the solid can have a drastic effect on potential parameters. Whereas the Born–van Kármán force constants, Eq. (8.3b), give imaginary frequencies for H_2, the renormalized force constants, Eq. (8.7) give reasonable values. Similarly the zero-point motion has an important effect on the anisotropic interactions in the solid. The effective or renormalized interactions can differ significanly from interactions evaluated at separations of molecules corresponding to the x-ray determined lattice constant, R_0.

Potentials such as the EQQ interaction, derivable from a solution of Laplace's equation, are unaffected by spherically symmetric pdf's. Harris (1970) considered such interactions for an asymmetric distribution arising from a single particle Gaussian wave function with a Jastrow factor. He showed that the EQQ interaction averaged over the ground translational state maintains the same tensor transformation properties but is reduced in strength by a factor ξ_{54}:

$$\langle H_{\mathrm{EQQ}}(R_{12}) \rangle = \int g(R_{12}) H_{\mathrm{EQQ}}(R_{12}) d^3R_{12} = \xi_{54} H_{\mathrm{EQQ}}(R_0) \tag{8.13}$$

where, in general,

$$\xi_{mn} = \sqrt{4\pi/2n+1}\,\langle [Y_n^0(\Omega_{12})/(R_{12}/R_0)^m] \rangle\,. \tag{8.14}$$

As a result, we see from Eq. (8.13) and (3.17) that zero-

TABLE XV. Renormalization constant ξ_{54} as defined in Eq. (8.14). Calculations are by Goldman (1979) for an fcc lattice.

Molar volume [cc/mole]	ξ_{54} H_2	D_2
22.73	0.944	···
22	0.947	···
21	0.950	···
20	0.952	···
19.87	···	0.968
19	0.955	0.970
18	0.957	0.972
16	0.962	0.974
14	0.966	0.977
12	0.969	0.979
10	0.972	0.980

point motion averaging effectively renormalizes the EQQ coupling constant, giving us $\langle\Gamma\rangle=\xi_{54}\Gamma_0$, as in Eq. (3.19). Harris found a value of $\xi_{54}=0.93$ for H_2 at zero pressure. Noolandi and van Kranendonk (1969) showed that even if the Jastrow function $f(r)=1$, then assymetry in $g^{\alpha\beta}(r)$ due to the translational symmetry of a lattice would be sufficient to yield $\xi_{54}\simeq 0.95$. Although one would expect both of these effects to give a value for ξ_{54} of 0.85–0.90, recent refinements have indicated that, for H_2, the renormalization $\xi_{54}\sim 0.90$–0.95. Goldman (unpublished) found $\xi_{54}=0.905$ for H_2 using a Jastrow wavefunction formalism and about the same value with a Horner approach. Luryi and van Kranendonk (1979) have used a Debye model, with Horner's constraints, to calculate renormalization factors. Goldman (1979b) found $\xi_{54}=0.944$ for zero-pressure H_2 using a modified Horner approach. We believe these results, which are given for selected molar volumes in H_2 and D_2 in Table XV, are the most reliable values available.

Renormalization factors ξ_{nm} can be greater or smaller than 1. For exponential radial dependences, motional averaging can increase the effective strength of the interaction by factors 2–10. Another class of functions that often arises that must be "renormalized" are interactions squared, for example,

$$\langle|H_{EQQ}|^2\rangle=\sum_m\langle|H_{EQQ}|m\rangle\langle m|H_{EQQ}|\rangle\,.$$

These functions arise in perturbation theory, calculation of spectral intensities, etc. We stress here that

$$\langle|H_{EQQ}|^2\rangle\neq\xi_{54}^2|H_{EQQ}(R_0)|^2\,.$$

Renormalization of these functions can result in values a factor ~2 larger than the unrenormalized quantity.

IX. CONCLUDING REMARKS

In the preceding pages I have tried to provide an extensive picture of the properties of the solid hydrogens along with a compilation of useful data. Much of our current knowledge is based on studies of the excitation spectra of these solids, using probes such as NMR, neutron scattering, Raman and infrared spectroscopy, etc. In a future article I shall review the excitations in the hydrogens which in turn is most easily understood in terms of the picture developed here in part I.

ACKNOWLEDGMENTS

I would like to thank V. V. Goldman and A. Lagendijk for stimulating discussions and comments. I also thank J. Van Kranendonk for a number of comments on the manuscript.

REFERENCES

Ahlers, G., 1964, J. Chem. Phys. **40**, 3123.
Ahlers, G., and W. H. Orttung, 1964, Phys. Rev. **133**, 1642A.
Ahlrichs, R., R. Penco, and G. Scoles, 1976, Chem. Phys. **19**, 119.
Amstutz, L. I., H. Meyer, S. M. Meyers, and D. C. Rorer, 1969, Phys. Rev. **181**, 589.
Amstutz, L. I., J. R. Thompson, and H. Meyer, 1968, Phys. Rev. Lett. **21**, 1175.
Anderson, A. B., J. C. Raich, and R. D. Etters, 1976, Phys. Rev. B **14**, 814.
Anderson, A. B., J. C. Raich, and L. B. Kanney, 1977, Phys. Rev. B **15**, 5804.
Anderson, M. S., and C. A. Swenson, 1974, Phys. Rev. B **10**, 5184.
Barnes, R. G., P. J. Bray, and N. Ramsey, 1954, Phys. Rev. **94**, 893.
Bauer, W., W. Lantzsch, J. P. Toennies, and K. Walaschewski, 1976, Chem. Phys. **17**, 19.
Bell, R. J., and I. J. Zucker, 1976, in *Rare Gas Solids*, edited by M. L. Klein, and J. A. Venables (Academic, New York), p. 151.
Bender, C. F., and H. F. Schaefer, 1972, J. Chem. Phys. **57**, 217.
Berkhout, P. J., and I. F. Silvera, 1977, Communications on Physics **2**, 109.
Berkhout, P. J., 1978, Ph.D. Thesis, University of Amsterdam, unpublished.
Berkhout, P. J., J. Th. Minneboo, and I. F. Silvera, 1978, J. Low Temp. Phys. **32**, 401.
Berlinsky, A. J., and A. B. Harris, 1971, Phys. Rev. B **4**, 2808.
Berlinsky, A. J., and W. N. Hardy, 1973, Phys. Rev. B **8**, 5013.
Berlinsky, A. J., 1975, Phys. Rev. B **12**, 1482.
Berlinsky, A. J., and A. B. Harris, 1970, Phys. Rev. A **1**, 878.
Birnbaum, A., and J. D. Poll, 1969, J. Atmos. Sci. **26**, 943.
Bloom, M., 1957, Physica **23**, 767.
Bohn, R. G., and C. F. Mate, 1970, Phys. Rev. B **2**, 2121.
Bostanjoglo, O., 1965, Z. Phys. **187**, 44.
Bostanjoglo, O., and R. Kleinschmidt, 1967, J. Chem. Phys. **46**, 2004.
Bruce, T. A., 1972, Phys. Rev. B **5**, 4170.
Bulatova, R. F., and V. S. Kogan, 1964, Soy. Phys.-JETP **19**, 575.
Buzerak, R. F., M. Chan, and H. Meyer, 1977, J. Low Temp. Phys. **28**, 415.
Chandrasekharan, V., and R. D. Etters, 1978, J. Chem. Phys. **68**, 4933.
Clusius, K., and E. Bartholomé, 1935, Z. Phys. Chem. (Leipzig) **B30**, 237.
Cochran, W. T., and J. R. Gaines, 1979, preprint, to be published.
Coll, C. F., and A. B. Harris, 1970, Phys. Rev. B **2**, 1176.
Coll, C. F. III, and A. B. Harris, 1971, Phys. Rev. B **4**, 2781.
Coll, C. F. III, and A. B. Harris, and A. J. Berlinsky, 1970, Phys. Rev. Lett. **25**, 858.
Constable, J. H., and J. R. Gaines, 1971, Solid State Commun. **9**, 155.
Constable, J. H., and J. R. Gaines, 1973, Phys. Rev. B **8**, 3966.
Cook, G. A., R. F. Dwyer, O. E. Berwaldt, and H. E. Nevins,

1965, J. Chem. Phys. **43**, 1313.
Cremer, E., and M. Polanyi, 1933, Z. Phys. Chem. (Leipzig) **B21**, 459.
Cullen, J. R., D. Mukamel, S. Shtrikman, L. C. Levitt, and E. Callen, 1972, Solid State Commun. **10**, 195.
Cunningham, C. M., D. S. Chapin, and H. L. Johnston, 1958, J. Am. Chem. Soc. **80**, 2283.
Curzon, A. E., and A. J. Mascall, 1965, Br. J. Appl. Phys. **16**, 1301.
Deal, W. J., 1972, Int. J. Quantum Chem. **6**, 593.
DeWette, F. W., and B. R. A. Nijboer, 1965, Phys. Lett. **18**, 19.
Depatie, D. A., and R. L. Mills, 1968, Rev. Sci. Instrum. **39**, 105.
Dondi, M. G., U. Valbussa, and G. Scoles, 1972, Chem. Phys. Lett. **17**, 137.
Driessen, A., J. A. de Waal, and I. F. Silvera, 1979, J. Low Temp. Phys. **34**, 255.
Durana, S., and J. P. McTague, 1975, J. Low Temp. Phys. **21**, 21.
Dwyer, R. F., G. A. Cook, O. E. Berwaldt, and N. E. Nevins, 1965, J. Chem. Phys. **43**, 801.
Ebner, C., and C. C. Sung, 1972, Phys. Rev. A **5**, 2625.
Etters, R. D., and R. L. Danilowitz, 1973, Phys. Rev. A **8**, 1698.
England, W., J. C. Raich, and R. D. Etters, 1976, J. Low Temp. Phys. **22**, 213.
Eyring, H., J. Walter, and G. E. Kimball, 1944, *Quantum Chemistry* (Wiley, New York), p. 72.
Farkas, L., 1933, Ergeb. Exakten Naturwiss. **12**, 163.
Farkas, A., 1935, "Orthohydrogen, Parahydrogen, and Heavy Hydrogen", (Cambridge University, Cambridge, England).
Farrar, J. M., and Y. T. Lee, 1972, J. Chem. Phys. **57**, 5492.
Felsteiner, J., 1965, Phys. Rev. Lett. **15**, 1025.
Felsteiner, J., Z. Friedman, and J. A. Sussman, 1972, Phys. Rev. B **6**, 2491.
Felsteiner, J., and Z. Friedman, 1973, Phys. Rev. B **8**, 3996.
Felsteiner, J., D. B. Litvin, and J. Zak, 1971, Phys. Rev. B **3**, 2706.
Gaines, J. R., A. Mukherjee, and J. -C. Shi, 1978, Phys. Rev. B **17**, 4188.
Gallup, G. A., 1977a, J. Chem. Phys. **66**, 2252.
Gallup, G. A., 1977b, Mol. Physics **33**, 943.
Gates, J. V., P. R. Ganfors, B. A. Fraas, and R. O. Simmons, 1978, J. Phys. (Paris) (Suppl. 8), Vol. 1, C6-103.
Gates, J. V., P. R. Ganfors, B. A. Fraas, and R. O. Simmons, 1979, Phys. Rev. B **19**, 3667.
Giaque, W. F., and H. L. Johnston, 1928, J. Am. Chem. Soc. **50**, 3221.
Goldman, V. V., 1968, Phys. Rev. **174**, 1041.
Goldman, V. V., 1975, in *Proceedings of the Low Temperature Physics Conference 14*, M. Krasius and M. Vuorio, eds., Helsinki (North-Holland, Amsterdam), Vol. 4, p. 411.
Goldman, V. V., 1976, J. Low Temp. Phys. **24**, 297.
Goldman, V. V., 1979a, J. Low Temp. Phys. **36**, 521.
Goldman, V. V., 1979b, Phys. Rev. **B**, accepted for publication.
Gonzales, O. D., D. White, and H. L. Johnston, 1957, J. Phys. Chem. **61**, 773.
Goodwin, R. D., and H. M. Roder, 1963, Cryogenics **3**, 12.
Gorodilov, B. Ya., I. N. Krupskii, and V. G. Manzhelli, 1978, Sov. J. Low Temp. Phys. **3**, 1562.
Gray, C. G., 1967, Can. J. Phys. **46**, 135.
Grenier, G., and D. White, 1964, J. Chem. Phys. **40**, 3015.
Grilly, E. R., 1953, Rev. Sci. Instrum. **24**, 72.
Gush, H. P., and J. Van Krenendonk, 1966, Can. J. Physics **40**, 1461.
Guyer, R. A., 1969, Solid State Phys. **123**.
Haas, W. P., N. J. Poulis, and J. J. W. Borleffs, 1961, Physica **27**, 1037.
Hardy, W. N., and A. J. Berlinsky, 1975, Phys. Rev. Lett. **34**, 1520.
Hardy, W. N., A. J. Berlinsky, and A. B. Harris, 1977, Can. J. Phys. **55**, 1150.
Hardy, W. N., and J. R. Gaines, 1967, Phys. Rev. Lett. **19**, 1417.
Hardy, W. N., I. F. Silvera, K. N. Klump, and O. Schnepp, 1968a, Phys. Rev. Lett. **21**, 291.
Hardy, W. N., I. F. Silvera, and J. P. McTague, 1968b, Phys. Rev. Lett. **22**, 297.
Hardy, W. N., I. F. Silvera, and J. P. McTague, 1971, Phys. Rev. Lett. **26**, 127.
Hardy, W. N., I. F. Silvera, and J. P. McTague, 1975, Phys. Rev. B **12**, 753.
Harrick, N. J., and N. F. Ramsey, 1952, Phys. Rev. **88**, 228.
Harris, A. B., 1968, Solid State Commun. **6**, 149.
Harris, A. B., 1970, Phys. Rev. B **1**, 1881.
Harris, A. B., A. J. Berlinsky, Solid State Commun. **24**, 159.
Harris, A. B., A. J. Berlinsky, and W. N. Hardy, 1977, Can. J. Phys. **55**, 1180.
Harris, A. B., A. J. Berlinsky, and H. Meyer, 1973, Phys. Rev. B **7**, 4720.
Herzberg, G., and L. L. Howe, 1959, Can. J. Phys. **37**, 636.
Herzberg, G., and A. Monfils, 1960, J. Mol. Spectrosc. **5**, 482.
Hill, R. W., and O. V. Lounasmaa, 1959, Philos. Mag. **37**, 785.
Hill, R. W., and W. A. Rickelson, 1954, Philos. Mag. **45**, 277.
Hill, R. W., and B. Schneidmesser, 1958, Z. Phys. Chem. Neue Folge **16**, 257.
Hirschfelder, J. O., C. F. Curtiss, and R. B. Bird, 1954, Molecular Theory of Gases and Liquids (John Wiley and Sons, New York).
Holian, B. L., 1978, Phys. Rev. **18**, 4780.
Homma, S., and H. Nakano, 1975, Prog. Theor. Physics **54**, 19.
Horner, H., 1974, in *Dynamical Properties of Solids*, edited by G. K. Horton and A. A. Maradudin (North-Holland, Amsterdam), Vol. 2, Chap. 8.
Huebler, J. E., and R. G. Bohn, 1978, Phys. Rev. B **17**, 1991.
Husa, D. L., and J. G. Daunt, 1978, Phys. Lett. A**65**, 354.
Ishimoto, H., K. Nagamine, and Y. Kimura, 1973, J. Phys. Soc. Jpn. **35**, 300.
Ishimoto, H., K. Nagamine, Y. Kimura, and H. Kumagai, 1976, J. Phys. Soc. Jpn. **40**, 312.
James, H., 1968, Phys. Rev. **167**, 862.
James, H., 1970, Phys. Rev. B **2**, 2213.
James, H. M., and J. C. Raich, 1967a, Phys. Rev. **162**, 649.
James, H. M., and J. C. Raich, 1967b, Phys. Rev. **162**, 649.
Jarvis, J. E., H. Meyer, and D. Ramm, 1969, Phys. Rev. **178**, 1461.
Jarvis, J., D. Ramm, and H. Meyer, 1967, Phys. Rev. Lett. **18**, 119.
Jaszuński, M., E. Kochanski, and P. Siegbahn, 1977, Mol. Phys. **33**, 139.
Jochemsen, R., 1978, Ph.D. Thesis, University of Amsterdam, unpublished.
Jochemsen, R., A. J. Berlinsky, F. Verspaandonk, and I. F. Silvera, 1978, J. Low Temp. Physics **32**, 185.
Jochemsen, R., V. V. Goldman, and I. F. Silvera, 1979, J. Low Temp. Phys. **36**, 243.
Karl, G., and J. D. Poll, 1967, J. Chem. Phys. **46**, 2944.
Keesom, W. H., J. de Smedt, and H. H. Mooy, 1930, Commun. Kamerlingh Onnes Lab., Univ. Leiden **19**, 2090.
Kelly, H. P., 1970, Phys. Rev. A **1**, 274.
Ketchin, V. V., A. J. Likhter, Yu. M., Parlyuchenko, L. Z. Ponizovskii, and A. N. Utyzh, 1977, Zh. Eksp. Teor. Fiz. **72**, 345.
Kim, Y. S., and R. G. Gordon, 1974, J. Chem. Phys. **61**, 1.
Kim, Y. S., and R. G. Gordon, 1975a, Phys. Rev. A**11**, 796; Kim, Y. S. and R. G. Gordon, 1975b, Phys. Rev. A**11**, 804.

Knaap, H. F. P., and J. J. M. Beenakker, 1961, Physica **27**, 523.
Kochanski, E., B. Roos, P. Siegbahn, and M. H. Wood, 1974, Theor. Chim. Acta **32**, 151.
Koehler, T. R., 1967, Phys. Rev. Lett. **18**, 654.
Koehler, T., 1974, *Dynamical Properties of Solids*, edited by G. K. Horton and A. A. Maradudin, (North-Holland, Amsterdam), Vol. II, Chap. 1.
Kogan, V. S., 1963, Sov. Phys.-Usp. **5**, 951.
Kogan, V. S., A. S. Bulatov, and L. F. Yakimenko, 1964, Sov. Phys.-JETP **19**, 107.
Kogan, V. S., B. G. Lazarev, and R. F. Bulatova, 1957, Sov. Phys.-JETP **4**, 593.
Kogan, V. S., B. G. Lazarev, and R. F. Bulatova, 1960, Sov. Phys.-JETP **10**, 485.
Kogan, V. S., B. G. Lazarev, R. P. Ozerov, and Zhdanov, 1961, Sov. Phys.-JETP **13**, 718.
Kolos, W., and C. J. J. Roothaan, 1960, Rev. Mod. Phys. **32**, 219.
Kolos, W., and L. Wolniewicz, 1964a, J. Chem. Phys. **41**, 3663.
Kolos, W., and L. Wolniewicz, 1964b, J. Chem. Phys. **41**, 3674.
Kolos, W., and L. Wolniewicz, 1965, J. Chem. Phys. **43**, 2429.
Kolos, W., and L. Wolniewicz, 1966a, J. Chem. Phys. **45**, 509.
Kolos, W., and L. Wolniewicz, 1966b, J. Chem. Phys. 45, 515.
Kolos, W., and L. Wolniewicz, 1967, J. Chem. Phys. **46**, 1426.
Kolos, W., and L. Wolniewicz, 1968, J. Chem. Phys. **49**, 404.
Kolos, W., and L. Wolniewicz, 1974, Chem. Phys. Lett. **24**, 457.
Krause, J. K., 1978, Ph.D. Thesis, Iowa State University, unpublished.
Krause, J. K., and C. A. Swenson, 1979, Solid State Commun. **31**, 833.
Krumhansl, J. A., and S. Y. Wu, 1972, Phys. Rev. B **5**, 4155.
Langhoff, P. W., R. G. Gordon, and M. Karplus, 1971, J. Chem. Phys. **55**, 2126.
Le Roy, R. J., 1971, J. Chem. Phys. **54**, 5433.
Lee, R. J., and J. C. Raich, 1972, Phys. Rev. B 5, 1591.
Luryi, S., and J. Van Kranendonk, 1979a, Can. J. Phys. **57**, 307.
Luryi, S., and J. Van Kranendonk, 1979b, Can. J. Phys. **57**, 136.
Luryi, S., and J. Van Kranendonk, 1979c, Can. J. Phys. **57**, 933.
Luryi, S., J. Van Kranendonk, and J. Noolandi, 1977, Phys. Rev. Lett. **38**, 418.
MacAdam, K. B., and N. F. Ramsey, 1972, Phys. Rev. A **6**, 898.
Manzhelli, V. G., B. G. Udovidchenko, and V. B. Esel'son, 1973, JETP Lett. **18**, 16.
Manzhelli, V. G., B. G. Udovidchenko, and V. B. Esel'son, 1975, Sov. J. Low Temp. Phys. **1**, 384.
Margenau, H., 1943, Phys. Rev. **64**, 385.
Margenau, H., and N. R. Kestner, 1971, *Theory of Intermolecular Forces* (Pergamon, Oxford).
McKellar, A. R. W., and T. Oka, 1978, Can. J. Phys. **56**, 1315.
McMahan, A. K., H. Beck, and J. A. Krumhansl, 1974, Phys. Rev. A **9**, 1852.
Megaw, H., 1939, Philos. Mag. **28**, 129.
Mertens, F. G., 1972, Z. Phys. **250**, 1.
Mertens, F. G., and W. Biem, 1972, Z. Phys. **250**, 273.
Meyer, W., 1976, Chem. Phys. **17**, 27.
Meyer, H., F. Weinhaus, B. Maraviglia, and R. L. Mills, 1972, Phys. Rev. B **6**, 1112.
Milenko, Ju., Ja., and R. M. Sibileva, 1974, Ukrainian J. of Phys. **19**, 2008.
Milenko, Ju., Ja., and R. M. Sibileva, 1975, Sov. J. Low. Temp. Phys. **1**, 382.
Michels, A., W. de Graaff, and C. A. Ten Seldam, 1960, Physica **26**, 393.
Mills, R. L., 1978, J. Low Temp. Phys. **31**, 423.
Mills, R. L., and E. R. Grilly, 1956, Phys. Rev. **101**, 1246.
Mills, R. L., D. H. Liebenberg, J. C. Bronson, and L. C. Schmidt, 1977, J. Chem. Phys. **66**, 3076.
Mills, R. L., D. H. Liebenberg, and J. C. Bronson, 1978, J. Chem. Phys. **68**, 2663.
Mills, R. L., and A. F. Schuch, 1964, Phys. Rev. Lett. **15**, 722.
Mills, R. L., J. L. Yarnell, and A. F. Schuch, 1973, *Proceedings of the Low Temperature Physics Conference 13*, Boulder (Plenum, New York), Vol. II, p. 202.
Miyagi, H., 1968, Prog. Theor. Phys. **40**, 1448.
Miyagi, H., and T. Nakamura, 1967, Prog. Theor. Phys. **37**, 641.
Motizuki, K., 1957, J. Phys. Soc. Jpn. **12**, 163.
Motizuki, K., 1962, J. Phys. Soc. Jpn. **17**, 1192.
Motizuki, K., and T. Nagamiya, 1956a, J. Phys. Soc. Jpn. **11**, 93.
Motizuki, K., and T. Nagamiya, 1956b, J. Phys. Soc. Jpn. **11**, 654.
Mucker, K. F., P. M. Harris, D. White, and R. A. Erickson, 1968, J. Chem. Phys. **49**, 1922.
Mucker, K. F., S. Talhouk, P. M. Harris, and D. White, 1966, Phys. Rev. Lett. **16**, 799.
Mulder, F., and A. van der Avoird, 1977, private communication.
Mulder, F., A. van den Avoird, and P. E. S. Wormer, 1979, Mol. Physics **37**, 159.
Nagai, O., and T. Nakamura, 1960, Prog. Theor. Phys. **24**, 432.
Nakamura, T., 1955, Prog. Theor. Phys. **14**, 135.
Nakamura, T., 1970, Progr. Theor. Phys. Supp. **46**, 343.
Nakamura, T., and H. Miyagi, 1970, Progr. Theor. Phys. **44**, 833.
Ng, K., W. J. Meath, and A. R. Allnatt, 1976, Mol. Phys. **32**, 177.
Niebel, K. F., and J. A. Venables, 1974, Proc. Roy. Soc. **A336**, 365.
Nielsen, M., 1973, Phys. Rev. B **7**, 1626.
Nielsen, M., and H. Bjerrum-Møller, 1971, Phys. Rev. B **3**, 4383.
Nielsen, M., W. Ellenson, S. Shapirow, and K. Carneiro, 1975, Sov. J. Low Temp. Phys. **1**, 371.
Noolandi, J., 1970, Can. J. Phys. **48**, 2032.
Noolandi, J., and J. Van Kranendonk, 1969, Phys. Lett. **30A**, 258.
Noolandi, J., and J. Van Kranendonk, 1970, Can. J. Phys. **48**, 675.
Nosanow, L. H., 1966, Phys. Rev. **146**, 120.
Omar, M. H., and Z. Dokoupil, 1962, Physica **28**, 461.
Orlikowski, T., and L. Wolniewicz, 1974, Chem. Phys. Lett. **24**, 461.
Orttung, W. H., 1962, J. Chem. Phys. **36**, 652.
Ostgaard, E., 1972, J. Low Temp. Phys. **8**, 479.
Oyarzun, R., and J. Van Kranendonk, 1971, Phys. Rev. Lett. **26**, 646.
Oyarzun, R., and J. Van Kranendonk, 1972, Can. J. Phys. **50**, 1494.
Pauling, L., 1930, Phys. Rev. **36**, 430.
Pedroni, P., M. Chan, R. Schweiz, and H. Meyer, 1975, J. Low Temp. Phys. **19**, 537.
Pedroni, P., F. Weinhaus, and H. Meyer, 1974, Solid State Commun. **14**, 279.
Petzinger, K. G., and D. J. Scalapino, 1973, Phys. Rev. B **8**, 266.
Poll, J. D., and G. Karl, 1966, Can. J. Phys. **44**, 1467.
Poll, J. D., and L. Wolniewicz, 1978, J. Chem. Phys. **68**, 3053.

Pollock, E. L., T. A. Bruce, G. V. Chester, and J. A. Krumhansl, 1972, Phys. Rev. B **5**, 4180.
Raich, J. C., and K. Albert, 1979, Sol. State Commun. **30**, 125.
Raich, J. C., A. B. Anderson, and W. England, 1976, J. Chem. Phys. **64**, 5088.
Raich, J. C., and R. D. Etters, 1968, J. Phys. Chem. Solids **29**, 1561.
Raich, J. C., and R. D. Etters, 1972, J. Low Temp. Phys. **6**, 229.
Raich, J. C., and H. M. James, 1966, Phys. Rev. Lett. **16**, 173.
Raich, J. C., and L. B. Kanney, 1977, J. Low Temp. Phys. **28**, 95.
Ramm, D., H. Meyer, and R. L. Mills, 1970, Phys. Rev. B **1**, 2763.
Ramsey, N. F., 1956, *Molecular Beams* (Clarendon, Oxford), p. 172.
Reif, F., and E. M. Purcell, 1953, Phys. Rev. **91**, 631.
Roberts, R. J., and J. G. Daunt, 1970, Phys. Lett. **33A**, 353.
Roberts, R. J., and J. G. Daunt, 1972, J. Low Temp. Phys. **6**, 97.
Roberts, R. J., and J. G. Daunt, 1974, J. Low Temp. Phys. **16**, 405.
Roberts, R. J., E. Rojas, and J. G. Daunt, 1976, J. Low Temp. Phys. **24**, 265.
Roffey, B. F., S. A. Boggs, and H. L. Welsh, 1974, Can. J. Phys. **52**, 2451.
Rollin, B. V., and E. Watson, 1955, in *Conf. de Physique des Basses Temp.* (Paris), 474.
Rose, M. E., 1957, *Elementary Theory of Angular Momentum* (Wiley, New York).
Ross, M., 1974, J. Chem. Phys. **60**, 3634.
Rotenberg, M., R. Bivins, N. Metropolis, and J. K. Wooten, Jr., 1959, *The 3-J and 6-J Symbols* (MIT, Cambridge, Mass).
Rulis, A. M., and G. Scoles, 1977, Chem. Phys. **25**, 183.
Sandler, Y. L., 1954, J. Phys. Chem. **53**, 58.
Schaefer, J., and W. Meyer, 1979, J. Chem. Phys. **70**, 344.
Schmidt, F., 1974, Phys. Rev. B **10**, 4480.
Schnepp, O., 1970, Phys. Rev. A **2**, 2574.
Schuch, A. F., and R. L. Mills, 1966, Phys. Rev. Lett. **16**, 616.
Schuch, A. F., R. L. Mills, and D. A. Depatie, 1968, Phys. Rev. **165**, 1032.
Schweitzer, R., S. Washburn, and H. Meyer, 1978, Phys. Rev. Lett. **40**, 1036; [**41**, 913 (E)].
Schweitzer, R., S. Washburn, and H. Meyer, 1979, preprint.
Sharma, S. K., H. K. Mao, and P. M. Bell, 1979, preprint.
Silver, D. M., and R. M. Stevens, 1973, J. Chem. Phys. **59**, 3378.
Silvera, I. F., 1975, *Proceedings of the 14th Int. Conf. on Low Temp. Physics* (North-Holland, Amsterdam), edited by M. Krusius and M. Vuorio, p. 123.
Silvera, I. F., 1978, in *Correlation Functions and Quasiparticle Interactions in Condensed Matter*, edited by J. W. Halley (Plenum, New York), p. 612.
Silvera, I. F., P. J. Berkhout, and L. M. Van Aernsbergen, 1979, J. Low Temp. Phys. **35**, 611.
Silvera, I. F., A. Driessen, and J. A. de Waal, 1978, Phys. Lett. A **68**, 207.
Silvera, I. F., and V. V. Goldman, 1978, J. Chem. Phys. **69**, 4209.
Silvera, I. F., W. N. Hardy, and J. P. McTague, 1969, Discuss. Faraday Soc. **48**, 54.
Silvera, I. F., W. N. Hardy, and J. P. McTague, 1971, Phys. Rev. B **4**, 2724.
Silvera, I. F., and R. Jochemsen, 1979, Phys. Rev. Lett. **43**, 377.
Silvera, I. F., and M. Nielsen, 1976, Phys. Rev. Lett. **37**, 1275.
Simon, F., 1923, Z. Phys. **15**, 307.
Simon, F., K. Mendelssohn, and M. Ruhemann, 1930, Naturwissenschaften **18**, 34.
Simon, F., M. Ruhemann, and W. A. M. Edwards, 1929, Z. Phys. Chem. B **6**, 331.
Sivardière, J., 1972, Phys. Rev. B **5**, 2094.
Smith, G. W., and R. M. Housley, 1960, Phys. Rev. **117**, 732.
Smith, G. W., and C. F. Squire, 1958, Phys. Rev. **111**, 188.
Souers, P. C., 1979, Lawrence Livermore Laboratory report UCRL-52628.
Spain, I. L., and S. Segall, 1971, Cryogenics **11**, 26.
Srivistava, I. B., and A. K. Barua, 1965, Indian J. Phys. **35**, 722.
Stewart, F. S., N. R. Davidson, and W. T. Simpson, 1965, J. Chem. Phys. **42**, 3175.
Stewart, J. W., 1956, J. Phys. Chem. Solids **1**, 146.
Stoicheff, B. P., 1957, Can. J. Phys. **35**, 730.
Sullivan, N. S., 1976a, J. Phys. (Paris) **37**, 981.
Sullivan, N. S., 1976b, J. Phys. (Paris) Lett. **37**, L-209.
Sullivan, N. S., and M. Devoret, 1978, J. Phys. (Suppl. **8**), Vol. 1, C6-92.
Sullivan, N. S., M. Devoret, B. P. Cowan, and C. Urbina, 1978, Phys. Rev. B **17**, 5016.
Sullivan, N. S., and R. V. Pound, 1972a, Phys. Letters **39A**, 23.
Sullivan, N. S., and R. V. Pound, 1972b, Phys. Rev. A, 1102.
Sullivan, N. S., H. Vinegar, and R. V. Pound, 1975, Phys. Rev. B **12**, 2596.
Tang, K. T., and J. P. Toennies, 1977, J. Chem. Phys. **66**, 1496.
Tapia, O., and G. Bessis, 1972, Theor. Chim. Acta **25**, 130.
Thakkar, A. J., 1977, Chem. Phys. Lett. **46**, 453.
Thomas, P. J., S. C. Rand, and B. P. Stoicheff, 1978, Can. J. Phys. **56**, 1494.
Van Kranendonk, J., 1960, Can. J. Phys. **38**, 240.
Van Kranendonk, J., and G. Karl, 1968, Rev. Mod. Phys. **40**, 531.
Van Kranendonk, J., and V. Sears, 1966, Can. J. Phys. **44**, 313.
Victor, G. A., and A. Dalgarno, 1969, J. Chem. Phys. **50**, 2535.
Victor, G. A., and A. Dalgarno, 1970, J. Chem. Phys. **53**, 1316.
Vinegar, H. J., J. J. Byleckie, and R. V. Pound, 1977, Phys. Rev. B **16**, 3016.
Waech, T. H., and R. B. Bernstein, 1967, J. Chem. Phys. **46**, 4905.
Wanner, R., and H. Meyer, 1973, J. Low Temp. Phys. **11**, 715.
Weinhaus, F., and H. Meyer, 1972, Phys. Rev. B **7**, 2974.
Weinhaus, F., S. M. Meyers, B. Maraviglia, and H. Meyer, 1970, Phys. Rev. B **3**, 626.
Werthamer, N. R., 1976, in *Rare Gas Solids*, edited by M. L. Klein and J. A. Venables (Academic, New York).
White, D., 1976, Chem. Phys. **14**, 301.
White, D., and E. N. Lassettre, 1960, J. Chem. Phys. **32**, 72.
Woolley, H. W., R. B. Scott, and F. G. Brickwedde, 1948, NBS Journal Res. **41**, 379.
Yarnell, J. L., R. L. Mills, and A. F. Schuch, 1974, Sov. J. Low Temp. Phys. **1**, 366.
Younglove, B. A., 1968, J. Chem. Phys. **48**, 4181.
Zandee, L., and J. Reuss, 1977, Chem. Phys. **26**, 345.